An Experimental and Computational Investigation of Pressurised Anaerobic Digestion

Thesis submitted in accordance with the requirements of the University of Chester for the degree of Doctor of Philosophy by Zhixuan Liang

January 2021

Declaration

The material being presented for examination is my own work and has not been submitted for an award of this or another HEI except in minor particulars which are explicitly noted in the body of the thesis. Where research pertaining to the thesis was undertaken collaboratively, the nature and extent of my individual contribution has been made explicit.

Acknowledgements

I would like to thank my family, friends, and especially my supervisor Professor Steve Wilkinson team for their continued support throughout this journey. I would also like to thank David Morris from Autichem for building the bioreactors for most of my experiments. Further thanks to Dr. Mayo Osundeko and Dr. Jon Pittman from University of Manchester for helping to identify the species of the pondweed.

Abstract

The aim of this work is to gain a greater understanding of the effect of headspace pressure on biogas production from anaerobic digestion. This is important to improve the energy content of the biogas *i.e.,* increase the methane content and therefore reduce the need for upgrading to scrub out carbon dioxide. In addition, headspace pressure can potentially be used to provide energy for mixing and gas sparging, thereby removing the need for mechanical agitation.

In this work, an existing computational model was adapted to investigate its prediction of the variation of biogas production as headspace pressure is increased above atmospheric. The simulation results were accompanied with experimental work using periodic venting of sealed laboratory bottles. The headspace pressure was inferred from the weight loss during venting to atmosphere.

In addition, a fully instrumented, pressurised digestor system was designed and constructed in which headspace pressure could be measured directly. Experiments were conducted with headspace pressures of up to 3.4 barg. The biogas that accumulated in the headspace during the digestion process was sampled periodically to determine its composition. The results showed that biogas produced at higher pressures has a higher methane content. A mass balance for the headspace sampling process, which assumed no gas was released from the liquid during sampling, was compared to experimental measurements. This led to the discovery that the effective Henry's constant for the solubility of carbon dioxide could be an order of magnitude lower in digestate than the known value for pure water.

Both the adapted model and the laboratory-scale experiments showed that as the headspace pressure increases, the production rate of biogas decreases. The adapted model also gives slightly higher methane content for higher pressure. The model was then used to estimate the specific growth rates of bacteria used in the laboratory-scale experiments and the agreement was not good, which indicates further changes to the model are needed.

The results show that the rate of biogas production reduces as the headspace pressure increases but the rate of decrease is not very steep. This same trend was also displayed for yeast fermentation, which was also studied as another model process for pressurised biological gas production. The variation of the rate of CO_2 evolution with pressure was also used to infer the concentration of dissolved CO_2 within the fermenting yeast cells.

Finally, turning attention back to anaerobic digestion processes for energy, it is encouraging that at the relatively modest elevation of pressure required for sparging to give mixing (less than 0.5 barg), the reduction in biogas evolution is small. This small penalty might therefore be offset in a production scale system by the reduced costs of mixing and increased methane content of the biogas.

Table of Contents

List of Figures

List of Tables

Abbreviations

ABR	anaerobic baffled reactor
ADM1	anaerobic digestion model No. 1
AEBR	anaerobic expanded-bed reactor
AFBR	anaerobic fluidised-bed reactor
AM2	two-reaction model
AMBR	anaerobic migrating blanket reactor
ASBR	anaerobic sequencing batch reactor
ATP	adenosine triphosphate
BOD	biological oxygen demand
CAPEX	capital costs
COD	chemical oxygen demand
F:M ratio	food to microorganism ratio
GAC	granular activated carbon
GHGs	greenhouse gases
GWP	global warming potential
HRT	hydraulic retention time
MAD	microalgae anaerobic digestion model

MathML	mathematical markup language
MBR	membrane bioreactor
ML	maximum likelihood
MLSS	mixed liquor suspended solids
MP	maximum parsimony
MSA	multiple sequence alignment
NJ	neighbour-joining
NPV	net present value
ODEs	ordinary differential equations
OLR	organic loading rate
OPEX	operating and maintenance costs
P&ID	piping and instrumentation diagram
PCA	principal component analysis
PSA	pairwise sequence alignment
PSA	pressure swing adsorption
RAxML	randomized accelerated maximum likelihood
SBGN	systems biology graphical notion
SBML	systems biology markup language

SBR	aerobic sequencing batch reactor
SBW	systems biology workbench
SRT	solid retention time
TS	total solid
UASB	upflow anaerobic sludge blanket
UPGMA	unweighted pair group method using arithmetic averages
USB	upflow sludge blanket
VFAs	volatile fatty acids
VS	volatile solids

1.*Introduction*

1.1. Research Background

This project is concerned with improving the efficiency of biomethane production as a sustainable alternative to fossil fuels.

1.1.1. Global Warming Caused by Fossil Fuels

As the global economy is growing at a significant rate, this will lead to an increase in energy demand around the globe, regardless of the amount of effort that has been made to increase the efficiency of energy use (Johansson *et al*., 1993). There is continued use of fossil fuels - a finite energy source, as well as deforestation and modern agriculture (livestock and cultivation of crops) that are causing the release of an unprecedented amount of greenhouse gases (GHGs) such as carbon dioxide (CO_2), nitrous oxide (N_2O) and methane (CH_4) into the atmosphere. These are the leading causes of climate change and the energy crisis we face today (Intergovernmental Panel on Climate Change [IPCC], 2014). Resolving these issues has become the predominant challenge and will have unbearable consequences if they are not resolved in timely manner.

According to Brander (2012), CO_2 is considered the most common GHG emitted from all human activities. In 2010, the total anthropogenic emissions of GHG were 52 gigatonnes of CO_2-equivalent per year ($GtCO_2$-eq/yr) (IPCC, 2014), 72% of which was CO_2, 20% was CH_4, 5% was N_2O and 2.2% was fluorinated gases

(F-gases) covered under the Kyoto Protocol (IPCC, 2014). Table 1.1 shows the atmospheric lifetime and global warming potential (GWP) of the 3 most common greenhouse gases. The “atmospheric lifetime” of a greenhouse gas refers to the approximate amount of time it will take an atmospheric pollutant from the anthropogenically-increased concentration to return to its natural concentration as a result of it being converted to another chemical compound. GWP is an index indicating the amount of warming a gas can cause over a 100-year period. Since CO_2 is the most common GHG, its index value is 1. GWP for other GHGs is the number of times more warming they can cause compared to CO_2 for the same amount of gas. For example, 1 kg of N_2O can cause 298 times more warming than 1 kg of CO_2 over a 100-year period, therefore, its GWP is 298 (Montzka, Dlugokencky & Butler, 2011).

Table 1.1 – Global warming potential and atmospheric lifetime of the 3 most common greenhouse gases (Jacobson, 2005; Montzka, Dlugokencky & Butler, 2011).

Greenhouse Gas	Atmospheric Lifetime (years)	Global Warming Potential (GWP)
CO_2	30 – 95	1
CH_4	9	25
N_2O	120	298

Burning fossil fuels release GHGs such as CO_2, CH_4 and N_2O (Everett, Boyle, Peake, & Ramage, 2012). Of all the greenhouse gases, carbon dioxide is overall the largest contributor because of its sheer volume. The vast majority of the

emissions are coming from the combustion of fossil fuels. Recent evidence (British Petroleum and BP Amoco [BP], 2018) shows that, in 2017, the primary energy consumption of the globe was 13511 million tonnes of oil equivalent (Mtoe). Among all the sources, fossil fuels were the highest contributors at 85.2%. Within fossil fuel, oil was the largest contributor, at approximately 34.2%, followed by coal at 27.6% then natural gas at 23.4%. The other sources were nuclear, hydroelectricity and renewables, as they made up the rest of 14.8% of the remaining primary energy consumption (British Petroleum and BP Amoco [BP], 2018).

1.1.2. Other Issues Related to the Use of Fossil Fuels

Using energy at the existing rate is leading to the rapid depletion of fossil fuels and will ultimately result in complete exhaustion (Ritchie & Roser, 2017). The exhaustion of fossil fuels will remove valuable chemical feedstocks, which will require new process routes to be developed. Another problem caused by burning fossil fuels is pollution. Sulphur dioxide (SO_2) is also a part of the flue gas generated from the combustion of coals, which is the cause of acid rain and breathing problems for living creatures. A study by Bowen and Irwin in 2008 showed that the content of sulphur within all grades of coal is 0.4 – 4.0% by weight. This results in the presence of sulphur dioxide in flue gas if the coal is not purified before combustion.

1.1.3. Anaerobic Digestion as a Sustainable Energy Option

As a result of the aforementioned problems, it is essential to find sustainable energy sources that can take the place of fossil fuels as soon as possible. There are several alternative technologies that are sustainable, for instance, solar power, wind power, biomass, geothermal power, wave and tidal power are all viable options (York, 212). They have all been developed to counter and relieve the severity of climate change. However, they all have various degrees of limitations that are affecting their overall contribution to the total energy consumption, such as being constrained by geography. Solar power, for example, would not be a viable option for the UK's energy needs because of the limited amount of direct sunlight received every year, while wave and tidal power would of course not be suitable option for Switzerland and Austria because they are land-locked countries.

Energy from biomass and waste are considered as one of the prevailing future energy sources because they are essentially limitless and can be used to continuously generate power. With regard to this, there have been steady developments in applications of anaerobic digestion. There are five types of biomass and waste suitable for anaerobic digestion: (1) energy crops and inedible residues form food crops, (2) waste oils and animal fat, (3) manure, (4) organic fraction of municipal solid waste and (5) sewage sludge (Apples *et al*., 2011).

Recent studies (Apples, *et al*., 2011; Mao, Feng, Wang & Ren, 2015; Mir, Hussain & Verma, 2016) have shown that even though anaerobic digestion with biomass and waste is a developed and extensively employed technology, there is still plenty of room for improvements for overall efficiency, reducing operation costs and increasing its added value. One way of raising its energy density is by increasing its methane content so it can be introduced to the natural gas grid.

1.1.4. Advantages of Pressurised Anaerobic Digestion

A study by Hayes, Isaacson, Pfeffer and Liu in 1990 showed that CO_2 is 40 to 60 times more soluble than CH_4 in water under digestion conditions. Therefore, if the digestion process occurs in a reactor above atmospheric pressure, the amount of CO_2 dissolved in digestate increases as the pressure accumulated in headspace increases due to Henry's law.

In this work, therefore, we investigate higher pressures to increase biogas methane content. This is in contrast to previous studies for *in situ* methane enrichment (Hayes *et al*., 1990) in which the pressure is kept close to atmospheric, but the digestate is circulated through a bubble column in which CO2 is stripped out of the digestate using an inert gas stream such as nitrogen. Although this concept of non-pressurised *in situ* methane enrichment technology was first proposed nearly 30 years ago (Hayes *et al*., 1990), this technology

remains at the stage of modelling and pilot scale until now (Nordberg *et al*., 2012).

Fully developing the pressurised anaerobic digestion process could bring a multitude of benefits to anaerobic digestion and the biogas upgrade process. Firstly, it can produce biogas with high methane content directly from the sources and reduce the necessity of post-production upgrading process. Secondly, when combined with an identical reactor or a bellows to recycle the biogas in headspace, it can provide essential mixing for the culture to enhance the digestion process. Such mixing by sparging with headspace biogas avoids the additional energy, capital and maintenance costs associated with conventional mechanical agitation systems. Furthermore, the recycling of biogas into the fermenter afforded by pressurised operation has been shown to give higher productivity, one possible mechanism for this being that higher levels of CO_2, which is an intermediate in the formation of CH_4, drives the equilibrium in the forward direction (Al-mashhadani, Wilkinson & Zimmerman, 2016).

With the aforementioned advantages, this technology could make anaerobic digestion a more cost-effective option as a renewable energy source.

1.2. Hypothesis and Objectives

The hypothesis of this project is that the pressurised anaerobic digestion process can produce biogas with higher CH_4 content. Higher CH_4 removes the necessity for biogas upgrading and facilitates its direct injection into the natural gas grid. The objectives of this project are listed below:

1. To adapt an existing mathematical model to simulate the anaerobic digestion process above atmospheric pressure with periodic venting.
2. To perform laboratory-scale experiments of anaerobic digestions to study the effects of headspace pressure on biogas production with various headspace volumes and venting frequencies.
3. To compare the adapted model with the experimental data to identify if and where adapted models need to be modified to better represent pressurised systems.
4. To perform glucose and yeast fermentation at various headspace pressures to study the effects of headspace pressure on CO_2 production rate. The reason for studying glucose yeast fermentation is because it is a similar process to anaerobic digestion, but the gas is produced more quickly.
5. To design and fabricate an instrumented bioreactor for pressurised anaerobic digestion and study how headspace pressure affects biogas composition.

1.3. Contribution of This Work

The contributions of this project are as follows:

1. The first systematic study into the variation of biogas production with headspace pressure (albeit rather modest pressures – up to 3.4 barg).
2. The adaptation of an existing computational model and parameter elimination.
3. The development and validation of a bench scale system for pressurised fermentation studies.
4. The phylogenetic identification of the algal feedstock used in this project to the family level.

1.4. Structure of the Thesis

Chapter 2 reviews the literature on anaerobic digestion process and critically outlines the advantages and disadvantages of anaerobic digestion. It also describes some typical anaerobic digestion treatment processes, upgrading technologies and the importance of mixing to the process. It contains a review of some established mathematical models of anaerobic digestion model, which are adapted within this project. Finally, some recently published research work on yeast fermentation and phylogenetic analysis to identify the species of feedstock is covered. Chapter 3 discusses the computational modelling strategy and resources along with the equipment, methods and the analytical procedures for each experiment. Chapter 4 demonstrates the results from the experiments

performed and discusses the implications of those results. Chapter 5 concludes the project, summarising the key findings and gives recommendations for future work.

2. *Literature Review*

In this chapter, I provide a comprehensive review of literature relevant to this thesis including methods for biogas upgrading (removal of CO_2) and mathematical modelling of anaerobic digestion.

2.1. Anaerobic Digestion

2.1.1. Historical Perspective

The natural decomposition of organic matter producing a flammable gas was first reported by Van Helmont in the 17th century (Tietjen, 1975, cited in Abbasi, Tauseef & Abbasi, 2012, p. 11). During 1804-1808, John Dalton and Humphry Davy determined that methane was the main gas produced by anaerobic digestion of farmyard manure. In 1859, the first anaerobic digestion plant was built at a leper colony in Bombay, India (Monnet, 2003). Then, in 1895, this technology was further developed in a wastewater treatment facility, where the biogas produced during the process was recovered and used to power streetlamps in Exeter, England (Bond & Templeton, 2011).

Table 2.1 is a list of advantages and disadvantages of anaerobic digestion compared to aerobic digestion.

Table 2.1 – Advantages and disadvantages of anaerobic digestion compare to aerobic digestion (Tchobanoglous, Burton, & Stensel, 2003).

Advantages	***Disadvantages***
Requires less energy than aerobic digestion	Requires longer start up time to develop necessary biomass inventory
Requires fewer nutrients than aerobic digestion	May require alkalinity addition
Requires smaller reactor volume than aerobic digestion	May require further aerobic digestion treatment process to achieve discharge requirement
Produces potential energy methane (CH_4)	Cannot remove phosphorus and biological nitrogen
Produces less biological sludge than aerobic digestion	May be more susceptible to the adverse effect of lower temperatures on reaction rates
Elimination of off-gas air pollution	The existence of toxic substances makes it sensitive to upsets
Rapid response to substrate if not fed for a long period of time.	Has the potential to produce corrosive gases and odours

The anaerobic digestion process, also known as the anaerobic fermentation and oxidation process, is employed primarily for the treatment of wastewater sludge while reducing odour, pathogen concentration and the mass of solid organic

waste that requires further processing simultaneously (Peng *et al*., 2020). Nevertheless, demonstrations of utilisations for dilute waste streams have been illustrated and are becoming more ordinary.

The advantages of anaerobic digestion over aerobic digestion are summarised in Table 2.1 and include lower biomass yield and the fact that biological conversion of organic matter in the absence of oxygen as an electron acceptor produces energy that can be recovered in the form of methane.

2.1.2. Key Operating Parameters

Retention time is the time taken to complete the digestion of organic matter and it is associated with microbial growth rate (Mao, Feng, Wang, & Ren, 2015). Hydraulic retention time (HRT, τ) is the amount of time wastewater stayed in the digester, whereas solid retention time (SRT) is defined as the average time solid particles stay in the reactor (Ligero, de Vega & Soto, 2001). In order to achieve efficient conversion of complex organic matter to CH_4 and CO_2, the population of bacteria in the digester must be concentrated with adequate quantity. The bacteria must have a sufficient retention time to allow substrate decomposition and to prevent bacteria from washing out (Mao *et al*., 215).

Currently, the majority of the anaerobic digestion processes are operating at mesophilic conditions (typically at 35°C). However, when working with high-fibre organic substrates at HRT lower than 20 days, thermophilic conditions (typically 55°C) yield better results (Moset, Poulsen, Wahid, Højberg, & Møller, 2015). For

high-strength industrial wastewater treatments, anaerobic fermentation has proved to be more cost-effective compared to aerobic digestion by savings in reactor volume, nutrient addition and energy inputs (Tchobanoglous *et al*., 2003). However, since its quality of effluent is not as good compared to the one obtained from aerobic digestion process, an anaerobic digestion process is usually followed by an aerobic digestion process or used as a pre-treatment step prior to discharge to a domestic collection system.

2.1.3. Biochemistry of Anaerobic Digestion

There are four fundamental steps involved in the entire anaerobic digestion process: (1) hydrolysis, (2) fermentation (also known as acidogenesis), (3) acetogenesis and (4) methanogenesis. Figure 2.1 is the schematic diagram of the four key stages of the anaerobic digestion process.

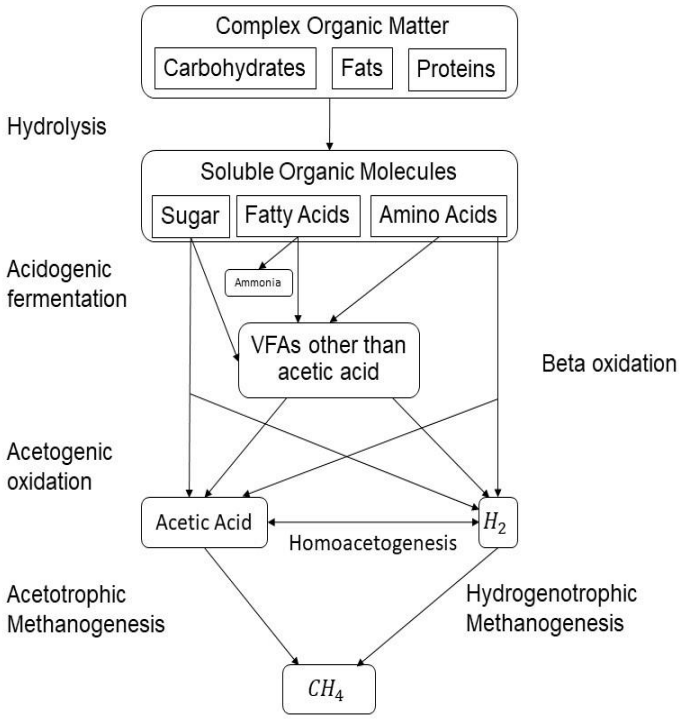

Figure 2.1 – Schematic diagram of the 4 steps of anaerobic digestion process (adapted from Kangle et al., 2012).

Hydrolysis is the first step for anaerobic digestion processes (Abdelgadir *et al*., 2014). This is a crucial step because polymers cannot be directly utilised by fermentative microorganisms (Kangle, Kore, Kore & Kulkarni, 2012). In this step, complex insoluble organic matter is converted to soluble organic molecules by hydrolytic enzymes. For instance, cellulose is converted to sugars or alcohols by cellulase, proteins to amino acids or peptides by proteases, lipids to long-chain fatty acids by lipases, and polysaccharides to monosaccharides by amylases. Hydrolysis reactions are as follows (Abdelgadir *et al*., 2014):

$$Lipids \rightarrow Fatty\ Acids$$

$$Polysaccharides \rightarrow Monosaccharides$$

$$Protein \rightarrow Amino\ Acids \qquad Eqn\ 2.1$$

$$C_{24}H_{40}O_{20} : H_2O + 3H_2O \rightarrow 4C_6H_{12}O_6$$

The second step is acidogenesis, (also known as fermentation). In this step, products from the first step are further decomposed to hydrogen (H_2), CO_2, acetate, ammonia, volatile fatty acids (VFAs) such as propionic acid (CH_3CH_2COOH) and butyric acid ($CH_3CH_2CH_2COOH$), acetic acid (CH_3COOH), lactic acid ($C_3H_6O_3$) and ethanol (C_2H_5OH) by facultative and anaerobic bacteria (Abdelgadir *et al*., 2014; Kangle *et al*., 2012). In an equilibrated system, the majority of the organic matter is decomposed to readily available substrates (H_2, CO_2 and acetic acid), which will skip the third step (acetogenesis) and directly be utilised methanogens in the final step (methanogenesis). However, a significant amount of substrate (approximately 30%) is converted into VFAs or alcohols (Kangle *et al*., 2012). Equations 2.2, 2.3 and 2.4 demonstrate three typical acidogenesis reactions where glucose is converted to acetic acid, ethanol and propionate respectively (Abdelgadir *et al*., 2014).

$$C_6H_{12}O_6 + 2H_2O \rightarrow 2CH_3COOH + 2CO_2 + 4H_2 \qquad Eqn\ 2.2$$

$$C_6H_{12}O_6 \rightarrow 2CH_3COOH + 2CO_2 \qquad Eqn\ 2.3$$

$$C_6H_{12}O_6 + 2H_2 \rightarrow 2CH_3COOH + 2H_2O \qquad Eqn\ 2.4$$

The next step is acetogenesis, where products formed (VFAs and alcohols) during acidogenesis are further degraded to H_2, CO_2 and acetic acid. A portion of the sugar skips acidogenesis and is directly converted to acetic acid. Equations

2.5, 2.6 and 2.7 represents the conversion of ethanol, propionate and glucose to acetate respectively (Abdelgadir *et al*., 2014; Kangle *et al*., 2012).

$$CH_3CH_2OH + 2H_2O \rightarrow CH_3COO^- + 2H_2 + H^+ \qquad Eqn\ 2.5$$

$$CH_3CH_2COO^- + 3H_2O \rightarrow CH_3COO^- + H^+ + HCO_3^- + 3H_2 \qquad Eqn\ 2.6$$

$$C_6H_{12}O_6 + 2H_2O \rightarrow 2CH_3COOH + 2CO_2 + 4H_2 \qquad Eqn\ 2.7$$

The final step is methanogenesis, where H_2 and acetate are converted to CH_4 and CO_2 by different methanogenic bacteria, because no single species can decompose all the available substrates (Kangle *et al*., 2012). This step is performed by a collection of organisms known as methanogens, including *Methanobacterium*, *Methanobacillus*, *Methanococcus* and *Methanosarcina* (Abdelgadir *et al*., 2014). In this step, CH_4 is formed in two ways, hydrogenotrophic methanogenesis and acetotrophic or aceticlastic methanogenesis (Kangle *et al*., 2012). Hydrogenotrophic methanogenesis utilises H_2 as the electron donor and CO_2 as electron acceptor to produce methane (Eqn 2.8). Acetotrophic methanogenesis converts acetic acid to carbon dioxide and methane (Eqn 2.9). Their respected reactions are as follows (Abdelgadir *et al*., 2014):

$$CO_2 + 4H_2 \rightarrow CH_4 + CO_2 \qquad Eqn\ 2.8$$

$$CH_3COOH \rightarrow CH_4 + CO_2 \qquad Eqn\ 2.9$$

2.1.4. Anaerobic Digestion for Biological Treatment of Liquid Effluents: Pros and Cons

In modern industry, the anaerobic digestion process is a popular method for waste treatment from a variety of sources. This process has numerous benefits and drawbacks, which must be examined in detail and comprehended completely, so that its potential can be maximised as well as made economically viable when it is implemented. The advantages and disadvantages versus aerobic treatment processes were introduced earlier and are now considered in more detail (Stuart, 2006).

2.1.4.1. Advantages:

2.1.4.1.1. Extensive Resources

The feedstock for anaerobic digestion is usually some form of waste. This can be collected from domestic/municipal waste, sewage waste, agricultural waste and food production residues, unless it is biomass purposely produced to utilise as feedstock, for example, energy crops and microalgae (Mao *et al*., 215).

2.1.4.1.2. Valuable Products

Anaerobic digestion can produce a variety of useful products. The first and most obvious product is the methane-rich biogas, which is a renewable alternative source of energy to fossil fuels for heat and power production. This methane-rich biogas has great potential because it is renewable and widely recognised as a replacement to fossil fuels. The second product is the organic fertiliser, another

final product of anaerobic digestion (digestate), which can be an alternative to chemical fertiliser and agrochemicals (Tambone *et al*., 2010; Stuart, 2006). This organic fertiliser comes in two forms, fibre and liquor. Fibre can be extracted from solid residue and it is bulky. It contains plant nutrients and can be used to condition the soil (Stuart, 2006). Liquor is the liquid residue which contains various plant nutrients. It can be use as liquid fertiliser. Organic fertiliser is a promising product since it is cheaper than conventional chemical fertiliser, contains high nutrient content (N, P, K) and is more environmentally friendly (Tambone *et al*., 2010; Stuart, 2006). The last product is biochar. The digestate can be transformed into biochar, which can be utilised as soil enhancer or an adsorbent for purification of flue gas or wastewater (Inyang, Gao, Pullammanappallil, Ding & Zimmerman, 2010). Both uses of biochar have high potential but use as an adsorbent would be more preferable in this scenario because it would be easier to extract fibre to make soil enhancer.

2.1.4.1.3. Pollution Control

Rapid growth in the global population has drastically increased the discharge of domestic and agricultural wastes. Raw sewage and agricultural wastes are considered as hazardous pollution because bacteria which decomposes organic matters in waste also absorb oxygen from water. In some extreme cases, an excessive amount of oxygen is removed making it unsuitable for aquatic life and making it “dead”. Anaerobic digestion can reduce the biological oxygen demand (BOD) and chemical oxygen demand (COD) in effluents, hence, reducing the potential danger. Another concern for pollution is methane, which is a major

greenhouse gas when it is emitted to the atmosphere instead of collected. An efficient system for an anaerobic digestion process can maximise the methane production and collect it for electricity and heat production.

2.1.4.1.4. Pathogen Removal

Untreated sludge spread on land can potentially contain pathogenic microorganisms such as bacteria, viruses, protozoa and parasites (Irwin *et al*., 2017). They may cause infection to animals or crops, run-off into water and infect human. One benefit of using anaerobic digestion is to remove these bacteria. There are two types of anaerobic digestion: **Mesophilic Digestion** and **Thermophilic Digestion**. The digester is heated to 30-35°C and feedstock has a retention time of 15-30 days for mesophilic digestion. It is more robust but produces less biogas than thermophilic digestion (Kim, Ahn & Speece, 2002). For thermophilic digestion, the digester is heated to 55°C with retention time of 12-14 days. This offers better pathogen removal and higher methane production than mesophilic digestion (Kim *et al*., 2002). However, pasteurisation (heat treatment for 30 minutes at 70°C) is recommended to guarantee complete annihilation.

2.1.4.1.5. Odour Reduction

The spreading of raw slurries on land and decomposing of faecal matter has an unpleasant smell. This is usually caused by the release of compounds such as ammonia, volatile organic acids and sulphides. Anaerobic digestion can reduce odour from land-spreading by 50-60% (Hjorth *et al*., 2009).

2.1.4.1.6. Weed Seeds Elimination

Slurry obtained from anaerobic digestion can be used as organic fertiliser with negligible risk of spreading weed, thus, essentially removes all known weed seeds (Johansen *et al*., 2013).

2.1.4.1.7. Scalable Technology

Since the anaerobic digestion process does not require a 'critical mass' to be operational, reactors can be scaled to different sizes depending on the application, such as large municipal wastewater treatment plants or small onsite projects for disposal of faecal waste from farm animals (Mezzullo, McManus, & Hammond, 2013; De Dobbelaere, et al., 2015). Remote, rural and off-grid areas in developing countries can benefit from this (Kinyua, Rowse, & Ergas, 2016).

2.1.4.1.8. Developed Technology

Anaerobic digestion itself is not a new concept. People have been applying this technology for different purposes for centuries (He, Liu, Sadiq, Gu, & Zhang, 2017). Over the last 100 years, anaerobic digestion has been used to treat sewage sludge. Especially during the last three decades, more experiments have been done and much more experience has been obtained on anaerobic digestion of industrial wastewater and farm waste (Braber, 1995). The variety of treatment systems available, for instance, anaerobic sequencing batch reactor (ASBR) (Singh & Srivastava, 2011), upflow anaerobic sludge blanket (UASB) (Chong, Sen, Kayaalp & Ang, 2012) and anaerobic baffled reactor (ABR) (Barber & Stuckey, 1999), depending on the feedstock has also made anaerobic digestion an attractive option.

2.1.4.1.9. Economic Benefits

Anaerobic digestion facilities can produce heat and power at a significantly lower cost, allowing the plant to produce electricity to power itself. If an excessive amount of energy is produced, it can be sold off generating revenue. A recent study (Li, Jin, Zhang, O'Hara, & Mundree, 2017) investigated the economic performance of five anaerobic digestion processes under identical external conditions. They concluded that all of the five processes are operating with profit in net present value (NPV). Cooperative agricultural digesters can create onsite employment depending on the scale and process used. Anaerobic digestion can effectively remove COD content from effluents, which helps industries to reduce their running costs because they are charged according to the volume and COD content of waste.

2.1.4.1.10. Domestic Waste Recycling

Recent developments of anaerobic digestion technology (Mata-Alvarez, *et al*., 2000) in some European countries have added the organic portion of municipal waste to its list of feedstocks. This leads to reduction in volume of landfill waste and hence decreasing landfill gas methane emission.

2.1.4.2. Disadvantages

2.1.4.2.1. Sensitivity to Operating Conditions

In anaerobic digestion, most of the control is directly carried out by the microorganisms themselves. However, the reaction rates of individual sub-

processes can be easily affected by operation conditions such as temperature, pH, essential trace nutrients toxicants, HRT, SRT and organic loading rate (OLR) (Lohani & Havukainen, 2018; Abdelgadir, et al., 2014). Therefore, controlling and maintaining these conditions is crucial for optimal performance.

2.1.4.2.2. Fluctuating Loads

Anaerobic digestion is executed by a group of interactive microorganisms: Hydrolytic Bacteria, Acidogens, Acetogens and Methanogens. There is a delicate balance between these sub-groups and steady-state conditions are achieved over a period of a few months (Abdelgadir, et al., 2014). Recent studies (Mora, Lafuente, & Gabriel, 2020; Braz, Fernandez-Gonzalez, Lema, & Carballa, 2019; Li, Yang, Li, & Sun, 2018) showed that organic shock loads disrupt this delicate balance between microorganisms and eventually causing the failure of methanogenesis. Therefore, the concentration of COD in the influent must be cautiously monitored and carefully maintained at a constant level.

2.1.4.2.3. Comparatively Low COD Removal

In general, anaerobic digestion process can reduce organic pollution in the range of 84.5-923% (Hu, Kobayashi, Qi, Oshibe, & Xu, 2018), however, this is still not enough. Industries are normally charged based on the level of COD in their effluent. Therefore, a second step (normally aerobic digestion) is needed to achieve an acceptable level of COD removal.

2.1.4.2.4. Capital Investment

From a small on-site digester for a farm to a large industrial project, the high initial investment required to develop an anaerobic digester is usually the primary

obstacle to its implementation. This initial investment needed for a project is the sum of fixed and working capital (Sinnott, 2005, p. 244). Fixed capital is the total cost of getting the plant ready for start-up, which is a one-time only unrecoverable cost at the end of the project life other than the scrap value. It is paid to the contractors. It includes the following cost (Sinnott, 2005, p. 244):

1. Design, construction supervision and other engineering.
2. All the equipment and their installation.
3. All piping, control systems and instrumentation.
4. Buildings and structures.
5. Auxiliary facilities (*i.e*., utilities, land and civil engineering work).

Working capital is the further investment needed over the fix capital, to activate the plant and operate it until revenue is generated, which can be recovered at the end of project. This includes the cost of (Sinnott, 2005, p. 244):

1. Start-up.
2. Initial catalyst charges.
3. Raw materials and intermediates in the process.
4. Inventories for finished products.
5. Funds to cover customers' outstanding accounts.

There are two methods for estimating the capital cost, they are historical costs and step counting methods (Sinnott, 2005, p. 247). The historical costs method is a quick estimate of the capital costs of a project based on the information of the cost of previous projects using the same manufacturing processing. The

capital cost of a project regards to its capacity can be calculated with the following equation (Sinnott, 2005, p. 247):

$$C_2 = C_1(\frac{S_2}{S_1})^n \qquad Eqn\ 2.10$$

where $C_2 =$ capital cost of the project with capacity S_2, $C_1 =$ capital cost of the project with capacity S_1. The value of the index n is usually taken as 0.6, the well-known six-tenths rule, when the data available are not sufficient to calculate the index for the particular process.

The second method is step counting. This provides a quick, order of magnitude, estimation of the capital cost for a proposed project (Sinnott, 2005, p. 249). This method is based on a system in which the capital cost can be calculated by the number of significant processing steps in the overall process. The capacity and complexity of the process such as material of construction, produce and operating conditions are the ordinary factors included. For plant capacities under 60,000 tonnes per year:

$$C = 150{,}000\ N\ (Q/s)^{0.30} \qquad Eqn.\ 2.11$$

For plant capacity over 60,000 tonne per year:

$$C = 170\ N\ (Q/s)^{0.675} \qquad Eqn.\ 2.12$$

where C = capital cost in British pounds, N = number of functional units, Q = plant capacity, tonne per year, s = reactor conversion. Reactor conversion is defined as:

$$s = \frac{mass\ of\ desired\ product}{mass\ reactor\ input} \qquad Eqn.\ 2.13$$

2.1.4.2.5. Requirement of Expertise

For successful operation of an anaerobic digestion, a complete comprehension of the process is required. The delicateness of anaerobic digestion mentioned in section 2.1.2.2.1 and 2.1.2.2.2 implies that it cannot be treated as a 'black-box' process. For developed countries, employing people with essential skills will add to the running costs. In developing countries, the expertise required may be very hard to acquire or simply just not available.

2.1.4.2.6. Production of Hydrogen Sulphide

An enormously corrosive gas, hydrogen sulphide (H_2S), will be produced when sulphur is present in the waste feed. This requires the purchase of more robust, hence more expensive digesters.

2.1.4.2.7. Persistence of Heavy Metals

The presence of heavy metals or persistent organic pollutants within feedstock will be another problem for anaerobic digestion (Bożym, Florczak, Zdanowska, Wojdalski & Klimkiewicz, 2015; Levén, Nyberg, Korkea-aho & Schnürer, 2006). The process does not eliminate heavy metals, thus the only way to handle this situation is by making sure the feedstock is as clean as possible (Stuart, 2006).

2.1.4.2.8. Economic Viability

There are a lot of aspects to the anaerobic digestion process, this includes stabilisation, optimisation of the inorganic nutrient recycles, savings on synthetic fertilisers and sales of liquid fertiliser and compost. All of these features must be

utilised to their maximum potential in order to make anaerobic digestion an economical approach for renewable energy.

2.1.5. Operation and Design of Anaerobic Treatment Processes

A wide variety of wastewater can be treated utilising anaerobic digestion processes, Table 2.2 below provides some examples. There are various methods of utilising anaerobic digestion process for wastewater treatment depending on the type of wastewater and its characteristics, for instance, suspended growth, attached growth, sludge blanket and membrane separation. Anaerobic suspended growth system is where microorganisms are freely suspended in wastewater during the biological process and the settled biomass needs to be recycled (Lyberatos & Pullammanappallil, 2010, p. 411). Anaerobic attached growth system is where microorganisms attach and grow on the surface of packing material. The packing materials could be glass, coarse gravel, peat moss, ceramic, plastic, polysterene sheets, polyurethane foam cubes or fibrous carriers (Loupasaki & Diamadopoulos, 2013). The settled biomass does not require recycling. Anaerobic sludge blanket reactor is where wastewater influent is treated by passing through flocculent or granular sludge blankets (Oakley, *et al*., 2017). Membrane separation is used to separate the solids from liquid for treated wastewater. Membrane Bioreactor (MBR) can either be a membrane submerged internally in a conventional activated sludge system (Mirzoyan, *et al*.,

2010) or placed externally as the last stage of activated sludge process as replacement of clarifier or sedimentation tank (Brindle & Stephenson, 1996).

Table 2.2 – Examples of types of wastewater can be treated by anaerobic digestion processes (Tchobanoglous et al., 2003).

Alcohol distillation	Breweries	Chemical manufacturing
Dairy and cheese processing	Domestic wastewater	Fish and seafood processing
Landfill leachate	Pharmaceuticals	Pulp and paper
Slaughterhouse and meatpacking	Soft drink beverages	Sugar processing

There are a few reasons why anaerobic digestion processes are so appealing, especially for warm temperature and high strength wastewaters. Firstly, it saves energy because aeration is not a necessity. Secondly, the processes generate low solids. Thirdly, it requires fewer nutrients compared to an aerobic process because less biomass is produced (Abdelgadir, et al., 2014).

2.1.5.1. Suspended Growth Systems

Anaerobic suspended growth treatment is performed in an airtight reactor. It was initially designed in a similar fashion to an anaerobic sludge digester, which were early utilisations of anaerobic treatment for wastewater treatment and sludge

(McCarty, 2001). There are a few configurations that are commonly associated with suspended growth treatment, Figure 2.2 demonstrates three of them.

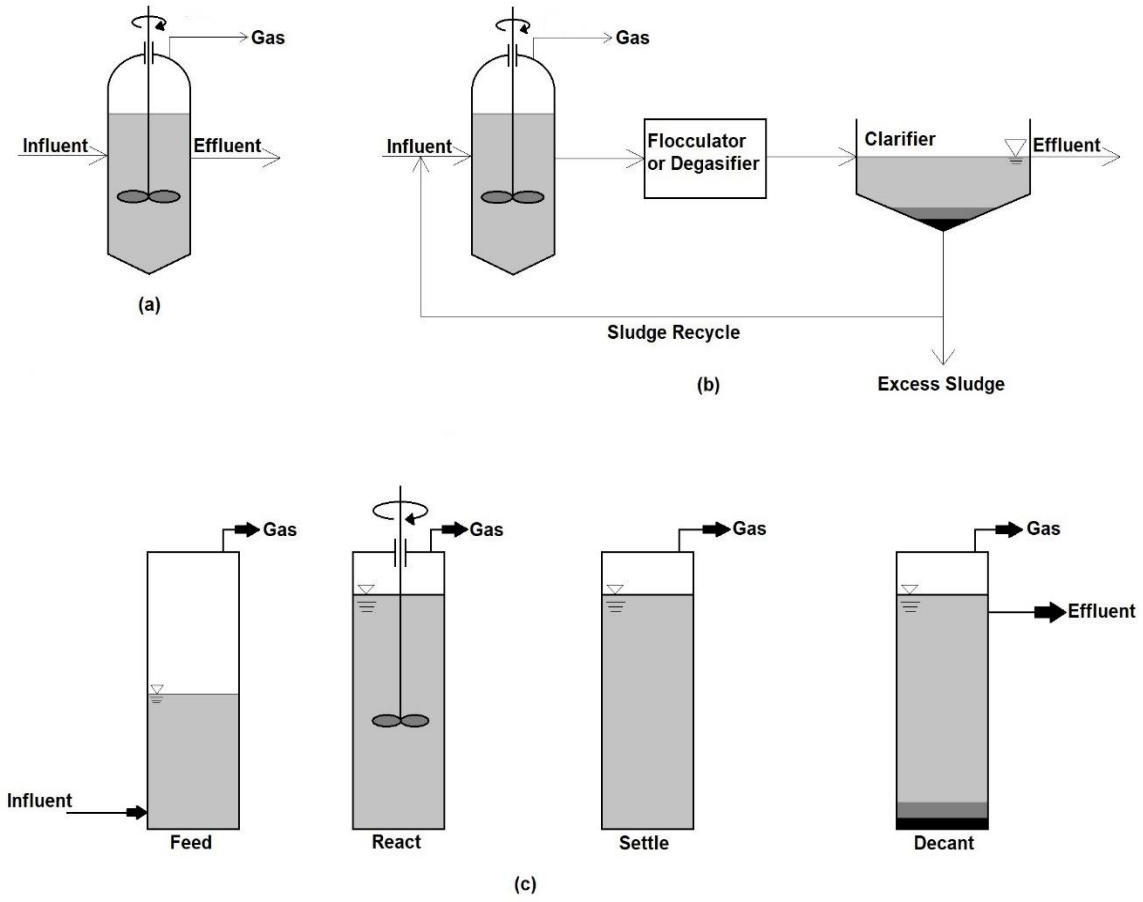

Figure 2.2 – Three typical configurations of anaerobic suspended growth treatment. (a) Complex-mix anaerobic digester, (b) Anaerobic contact reactor, (c) Anaerobic sequencing batch reactor (ASBR) (adapted from Tchobanoglous et al., 2003).

Figure 2.2 (a) illustrates the complete-mix anaerobic digester. It is one of the basic types of anaerobic digesters. It comprises a mix tank, a complete-mix digester with mixing and heating units and biogas recovery system. Pre- or post-digester solid separation is optional (RCM Digesters, 2013). The typical setup for

complete-mix digesters is usually round tanks above ground, heated and insulated. However, it can also be adapted to operate in a heated, covered and mixed earthen basin. Waste can be mixed by mechanical propellers, gas or liquid circulation (United States Environmental Protection Agency [EPA], 2015). This digester can be designed to improve volatile solids (VS) reduction with less regard for excess energy or to maximise biogas production as an energy source. The HRT is normally equivalent to the SRT for this type of digesters (Parkin & Owen, 1986).

Figure 2.2 (b) is the anaerobic contact process. It consists of a complete-mix anaerobic digester with suspended growth of biomass, a flocculator or degasifier, and a clarifier. There are numerous different designs of anaerobic contact process system depending on

1. The method of mixing utilised in the bioreactor,
2. The equipment for flocculator or degasifier,
3. The type of clarifier.

The mixing in the bioreactor is mostly performed by mechanical propellers, circulation of biogas or sludge (Kariyama, Zhai, & Wu, 2018). The flocculator or degasifier is equipped with a propeller and a vacuum pump and its objective is to remove biogas such as methane and carbon dioxide for a more efficient solid settlement process. The clarifier consists of a plate settling tank or a simple settling tank. The settled and thickened sludge within is then returned to the contact reactor or complete-mix reactor (Loganath & Senophiyah-Mary, 2020). This configuration overcomes the disadvantages of not recycling sludge found in

the complete-mix suspended growth process. By doing this, the process HRT can be differentiated from SRT and becomes shorter. Reduction in SRT leads to a decrease in volume of the anaerobic reactor. The general method to separate and thicken solids prior to sludge recycling is gravity separation. Nevertheless, poorly settled sludge can be produced easily, and substitute separation processes must be utilised or other methods must be applied to enhance the solid capture.

Figure 2.2 (c) shows the anaerobic sequencing batch reactor (ASBR) process. This is really similar to aerobic sequencing batch reactor (SBR) and can be considered to be a suspended growth process with the reaction and liquid-solids separation in the same reactor. The ASBRs process includes four steps: feed, react, settle, and decant (Loganath & Senophiyah-Mary, 2020). The feed step is adding additional substrate to the reactor. The feed volume depends on several aspects, for instance, preferred HRT, organic loading and the characteristics of settling sludge. The react step is the vital step in converting organic substrate to biogas. The time required for this step relies on a few factors, including the characteristics of the substrate and its strength, biomass concentration, mandatory quality of effluent and temperature of waste. In the settling step, the reactor acts as a clarifier and the mixing is turned off, allowing biomass solids separation (Sung & Dague, 1995). The reactor operates as a clarifier. The time required for settling the sludge is affected by several factors, for example, biomass settleability, the concentration of mixed liquor suspended solids (MLSS) in the reactor and the variable specific process loading rate (food to

microorganism ratio, F:M ratio). Biomass settleability usually ranges from 10 to 30 minutes (Sung & Dague, 1995). MLSS is a crucial parameter which alters the settling velocity as well as the ability to achieve a clear supernatant effluent for discharge. The decant step occurs after an adequate amount of solids separation has happened. The decant volume is usually the same as the feed volume from the previous feed step. The total volume to be decanted from each stage and the decanting rate determine the time required for the decant step. After the decant step is completed, the reactor is ready to be fed another batch of substrate for treatment.

Dague, McKinney and Pfeffer (1966) reported that anaerobic biomass flocculate in a similar manner compared to aerobic activated sludge and the F:M ratio was a critical parameter affecting anaerobic bioflocculation. Biomass flocculate better and quicker at low F:M ratios than high F:M ratios, which leads to low suspended solids in effluent from the reactor. A low F:M ratio can be achieved by reducing the food concentration (F) and/or increasing the mass of microorganisms (M). In a continuous feed, completely mixed system such as complete-mix or anaerobic contact process, the reactor operates at steady-state, which means food concentration in the reactor is constant. On the other hand, the food concentration is at its highest instantly after feeding in a batch fed system, then gradually declines as food is consumed by the microorganisms until the next batch is fed into the reactor, as demonstrated in Figure 2.3. In a batch fed system, the substrate concentration just before feeding gets lower than a continuous feed system at any time. Consequently, a batch fed system is able to

achieve biomass flocculation-granulation and solids separation more efficiently than continuously fed anaerobic contact process.

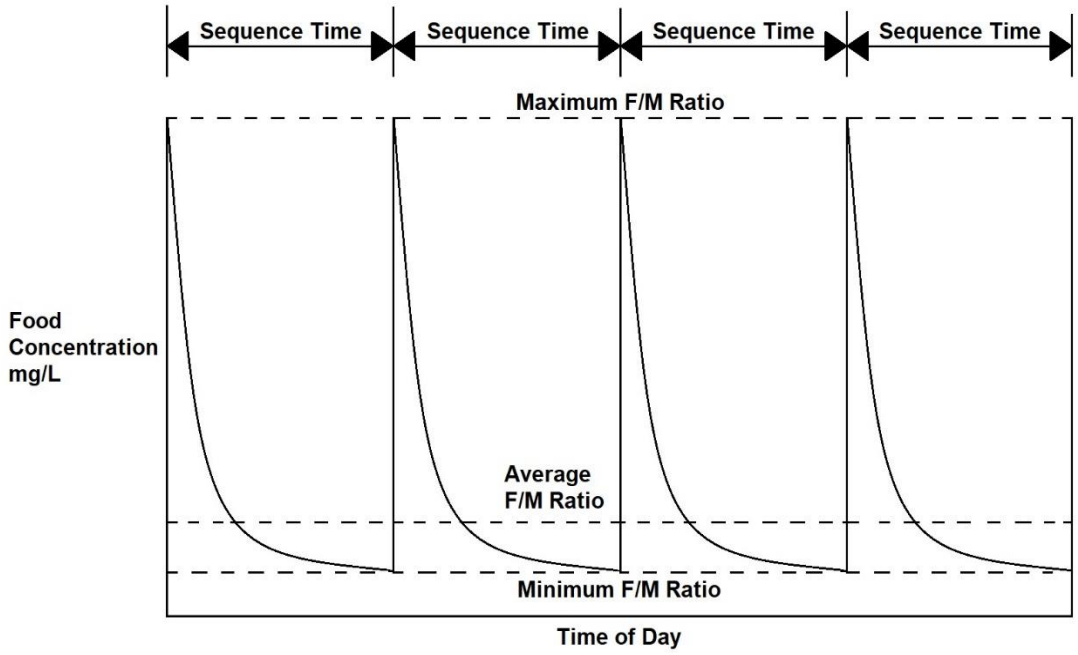

Figure 2.3 – Demonstration of F:M ratio and food concentration of a batch feeding system (adapted form Sung & Dague, 1995).

Early studies in the late 1930s on the effects mixing could have on anaerobic digestion concluded that it was crucial and reactors should have continuous mixing at an adequate intensity to guarantee uniform conditions throughout the reactor (Sung & Dague, 1995). However, in the 1970, a study focused on solids retention in suspended growth anaerobic processes, Dague, McKinney and Pfeffer (1970) reported that processes with overly intensified mixing have poor performance in solids separation and could shear the fragile anaerobic bioflocs. They also reported that intermittent mixing (2 minutes per hour) actually had

better overall performance for the reactors based on COD removal efficiency and improved biomass-solids separation.

Table 2.3 – Typical organic loading rates for anaerobic suspended growth at 30°C (Tchobanoglous et al., 2003).

Process	***Volumetric organic loading, kg COD/m^3·d***	***Hydraulic retention time τ, d***
Complete-mix	1.0 – 5.0	15 – 30
Anaerobic contact	1.0 – 8.0	0.5 – 5
Anaerobic sequence batch reactor	1.2 – 2.4	0.25 – 0.5

2.1.5.2. Anaerobic Sludge Blanket Reactors

The upflow anaerobic sludge blanket (UASB) reactor is believed to be advantageous in high-strength organic wastewater treatment due to its rich microbial diversity and high biomass concentration (Chan, Chong, Law, & Hassell, 2009; Daud, et al., 2018). The high biomass concentration suggests that great volumes or highly concentrated organic waste can be treated, and the pollutant transformation is rapid in condensed reactors. It was one of the most significant developments in anaerobic digestion treatment processes developed in the late 1970s in the Netherlands by Lettinga and his co-workers (Lettinga, *et al*., 1980). The separation device at the top of the reactor is known as a three-

phase separator, which allows the reactor to separate the mixtures of gas, water and sludge under high turbulence conditions. The UASB reactors resemble the upflow sludge blanket (USB) processes except for (Lettinga, *et al*., 1980):

1. Mechanical mixing and/or sludge recirculation are kept to a minimum level or even omitted completely.
2. A proper system for gas-solids separation is installed in the upper part of the reactor.

The basic concepts triggering the process are:

1. If physical and chemical conditions are beneficial to sludge flocculation and to the maintenance of a well flocculated sludge are provided, the anaerobic sludge can achieve and sustain excellent characteristics of settling.
2. A sludge blanket (bed) may be considered as a separate fluid phase with its own specific properties. A relatively stable phase is usually formed from a well-established sludge blanket and it is capable of tolerating rather strong agitating forces. Thus, a considerable amount of mixing energy is required for the redispersion of the sludge in liquid phase.
3. The washout of discrete sludge particles (flocs) released from the sludge blanket can be minimised by fabricating a dedicated quiescent zone within the reactor. It enables the sludge particles to flocculate, settle and/or to be entrapped in a secondary sludge blanket (position in the settling compartment).

The fundamental types of anaerobic sludge blanket processes are: (1) the initial UASB process and modification of initial design, (2) the anaerobic migrating blanket reactor (AMBR®), and (3) the anaerobic baffled reactor (ABR). Figure 2.4 is the schematic diagram of the UASB process and some alternations, (a) original UASB process, (b) UASB reactor with sedimentation tank and sludge recycle, and (c) UASB reactor with internal packing for mixed-film attached growth placed above the sludge blanket (Tchobanoglous et al., 2003).

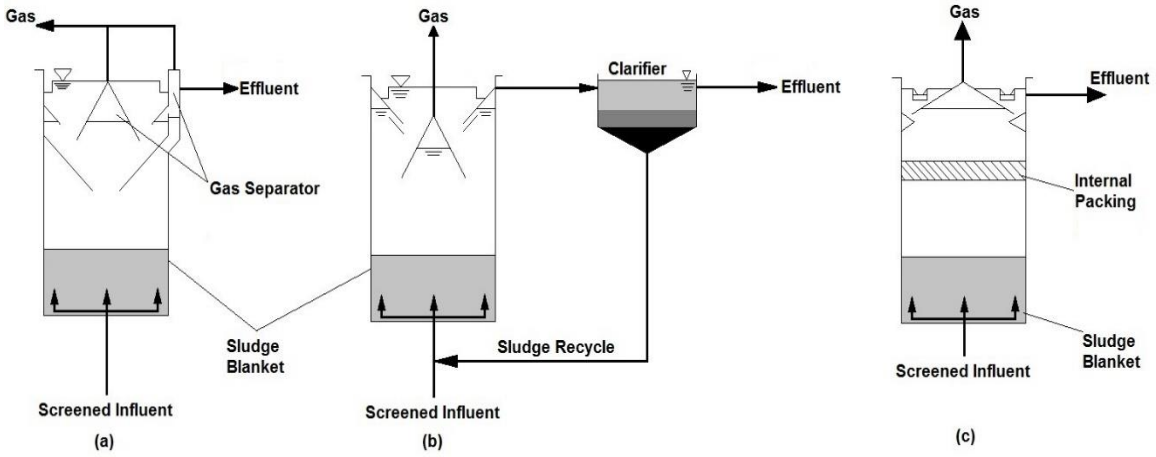

Figure 2.4 – Schematic diagram of the UASB process and some alternations. (a) Original UASB reactor, (b) UASB reactor with a clarifier and sludge recycle, (c) UASB reactor with internal packing (adapted from Tchobanoglous et al., 2003).

Figure 2.4 (a) demonstrates the basic UASB reactor. It consists of the reactor, sludge blanket settling at the bottom of the reactor, a three-phase separator that separates gas, liquid and solids, a biogas effluent and a liquid effluent. The wastewater enters the UASB reactor at the bottom and travels in an upflow fashion through the sludge bucket. The influent delivery system, the gas liquid

solids separator and the effluent withdraw design are the crucial elements of the UASB reactor design. As Figure 2.4 (b) illustrates the basic UASB reactor can be altered by adding a clarifier or adding a layer of packing material at top of the reactor as shown in Figure 2.4 (c). The alternations are aimed to improve the solid capture within the system as well as to avoid loss of the UASB reactor solids due to process disturbances or change in the UASB sludge blanket density and characteristics.

The UASB system is extremely reliant on its granulation process compared to other anaerobic technologies, for instance, anaerobic sequencing batch reactor, anaerobic filter and fluidised bed reactors. The core component for this technology is the anaerobic granular sludge. Sludge granules are multi species, highly concentrated microbial communities and none of the species in this granular ecosystem is able to decompose complex organic wastes individually. The main disadvantage of UASB reactor is the extremely long time it takes to start up, which normally takes 2 to 8 months for the anaerobic granular sludge to fully develop (Liu, *et al*., 2003; Daud, et al., 2018).

2.1.5.3. Anaerobic Baffled Reactors

Displayed in Figure 2.5 is the schematic diagram of anaerobic baffled reactor (ABR). An ABR comprises a tank with alternating hanging and standing baffles. Baffles are used to divide the tank into multiple compartments and guide the wastewater flow down into the settled sludge, and then in an upflow fashion into

the next compartment (SSWM, 2017). This increases the contact time of fresh wastewater entering the chamber with residual sludge which contains the microorganisms responsible for anaerobic digestion of organic compounds at the bottom and improves the treatment. Nevertheless, both remaining sludge and effluent need further treatment before they can be reused and properly discharged (SSWM, 2017). The compartmentalised design segregates the HRT from SRT, making it achievable for wastewater to be treated anaerobically within a few hours.

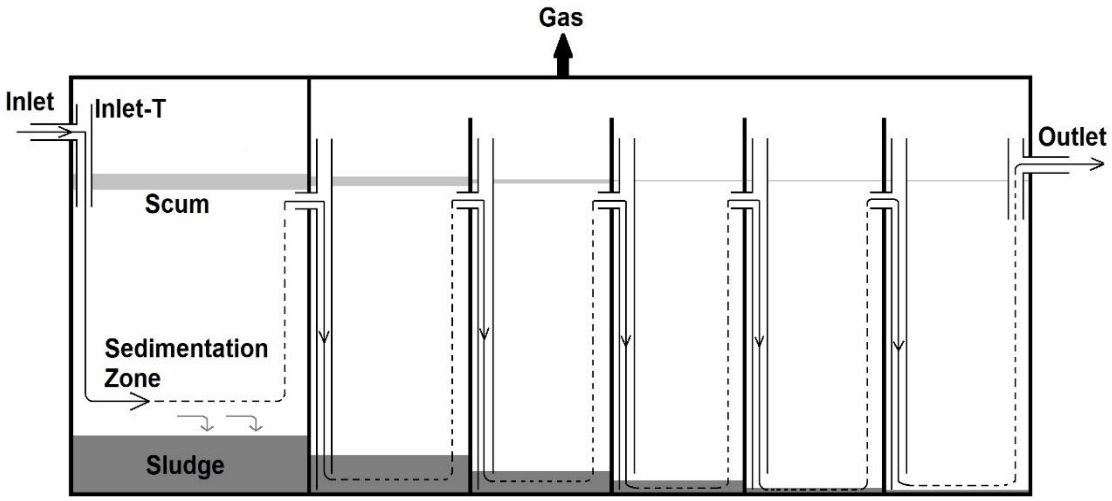

Figure 2.5 – Schematic diagram of anaerobic baffled reactor (ABR) (adapted from Tilley, et al., 2014).

ABRs combine the theories of moving bed reactors, Septic Tanks and UASB reactors. The main difference between AMBR, UASB reactors and ABR is the fact that it is not essential to have a floating sludge blanket. Furthermore, because some of the activated sludge that is washed out of one chamber is

trapped in the next one, it is not necessary to have effluent retention (SSWM, 2017).

Several modifications have been made in order to improve the performance of ABR, they are: (1) alterations to the baffle design, (2) hybrid reactors with a settler to capture and return solids, or (3) using packing in the upper section of each chamber to capture solids. The objectives for these modifications have been to increase solid retention capacity (Barber & Stuckey, 1999), to treat different wastewater with high solids content (Boopathy & Sievers, 1991) or to reduce capital costs. Figure 2.6 is a demonstration of the original ABR design and its modification.

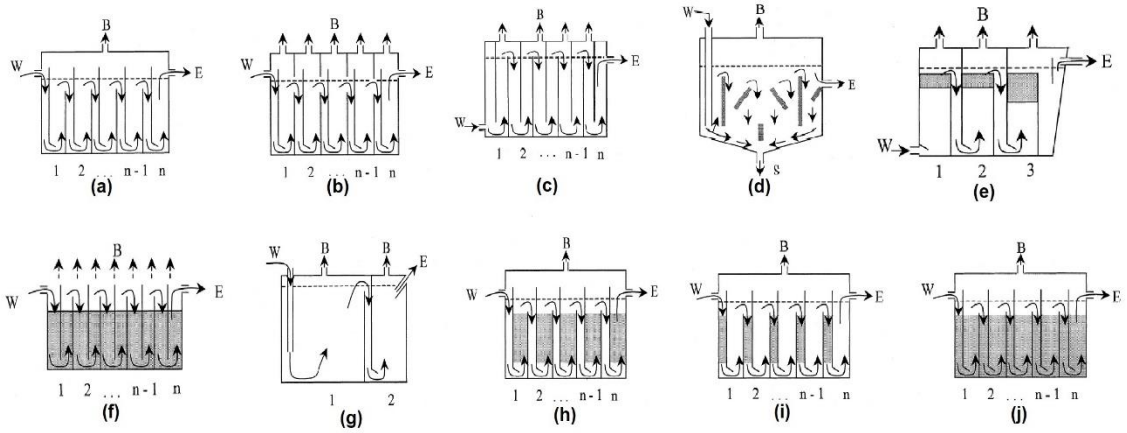

Figure 2.6 – Schematic diagram of original design of ABR and its modifications for performance improvement. (a) Single gas headspace, (b) Individual gas headspace, (c) Vertical, (d) Horizontal, (e) Hybrid with single zone, (f) Open top, (g) Enlarged first compartment, (h) Up-comers packing, (i) Down-comers packing, (j) Entire reactor packing. Key: W = Wastewater, B = Biogas, E = Effluent, S = Solids, (Shaded areas represent random packing) (taken from Barber & Stuckey, 1999).

Figure 2.6 (c) is the original design of an ABR even though Figure 2.6 (a) is the one that is generally recognised. Figure 2.6 (b and d-j) are the alterations that have been made to improve the reactor performance from the original design. It was reported by Barber and Stuckey (1999) that in 1983, Bachmann and the team studied the performance of some baffled reactors before and after narrowing the downflow chambers as well as slanting the bottom edge of baffles (Figure 2.6 (a)). The results demonstrated that the reactor's efficiency and methane production rates were increased but the methane content had decreased in the alternated design. Figure 2.6 (b) changed from single gas headspace to individual gas headspace for each compartment. In 1981, Fannin and the team added vertical baffles to a plug-flow reactor treating high solids sea kelp slurry (Figure 2.6(c)). This improved the ability of the reactor to maintain high populations of gradually growing methanogens (Barber & Stuckey, 1999).

The next noticeable modification to the design was made during the development of the first few hybrid designs by Tilche and Yang in 1987 (Figure 2.6 (e)) (Barber & Stuckey, 1999). The objective of these design alterations was to enhance solids retention for high strength wastewater treatment. Packings of randomly packed Pall rings were placed at the liquid surface of first two chambers, and then, a deeper and organised modular corrugated block with a high voidage in the third chamber (Barber & Stuckey, 1999). Pall ring is a Raschig ring with flaps cut from the wall thereof and bent inward. In addition, at least one tongue is cut from the flap and bent away from the flap but contained within the wall of the Raschig ring to increase the number of edges to disrupt the flow (United States

Patent No. US3266787A, 1966). Furthermore, the reactor was considerably larger than the previous designs, a solids settling chamber was merged at the final compartment. Solids carried out from the baffled reactor would accumulate in the settling chamber and then subsequently be recycled to the first chamber. High gas production from the first chamber would reduce the density of bioflocs, causing them to be afloat. However, they were retained as the consequence of packing. Each compartment was isolated and had independent gas production and individual measurement for gas composition within the chamber.

2.1.5.4. Other Anaerobic Reactor Types

In 1995, Angenent and Dague conducted a parallel study of UASB and ASBR systems (as cited in Angenent & Sung, 2001). The issues they discovered in those two processes were tackled by developing an innovative reactor known as the anaerobic migrating blanket reactor (AMBR), as displayed in Figure 2.7.

The original design of AMBR by Angenent and Sung (2001) is demonstrated in Figure 2.7 (b). It comprises a rectangular Plexiglas reactor divided into three compartments. Round openings are placed towards the bottom of two Plexiglas baffles dividing the chambers, which are used to establish adequate contact between substrate and biomass, minimise short circuiting of substrate and ensure migration of biomass. However, the headspace is not compartmentalised (Angenent & Sung, 2001). It is a baffled reactor with continuous feed and does not rely on feed distribution systems or intricate gas-solids-separation. There is

no necessity for effluent recycling either, however, intermittent and gentle mixing from the impellers is required in order to maintain sufficient contact between biomass and substrate. In an AMBR, influent horizontally flows into the reactor from one end and effluent leaves from the other end. Subsequently, the final compartment finishes up with lowest substrate concentration as well as low rate of substrate utilisation for microbes. As a result, the biogas production in this chamber will be low and will be able to serve as an internal sedimentation tank to prevent loss in biomass from the effluent (Tauseef, Abbasi, & Abbasi, 2013). The flow pattern along with the movement of biomass cause biomass to accumulate in the final compartment. Reversing the flow periodically can prevent excessive biomass accumulation in the final compartment. When the flow is reversed, the initial compartment is converted to final compartment and the final compartment is transformed into initial compartment. The reason to have three compartments in an AMBR is to prevent sudden disintegration of biomass floc when the flow is reversed. The middle compartment needs to be fed for a short period of time as well before reversing the flow (Tauseef, *et al*., 2013).

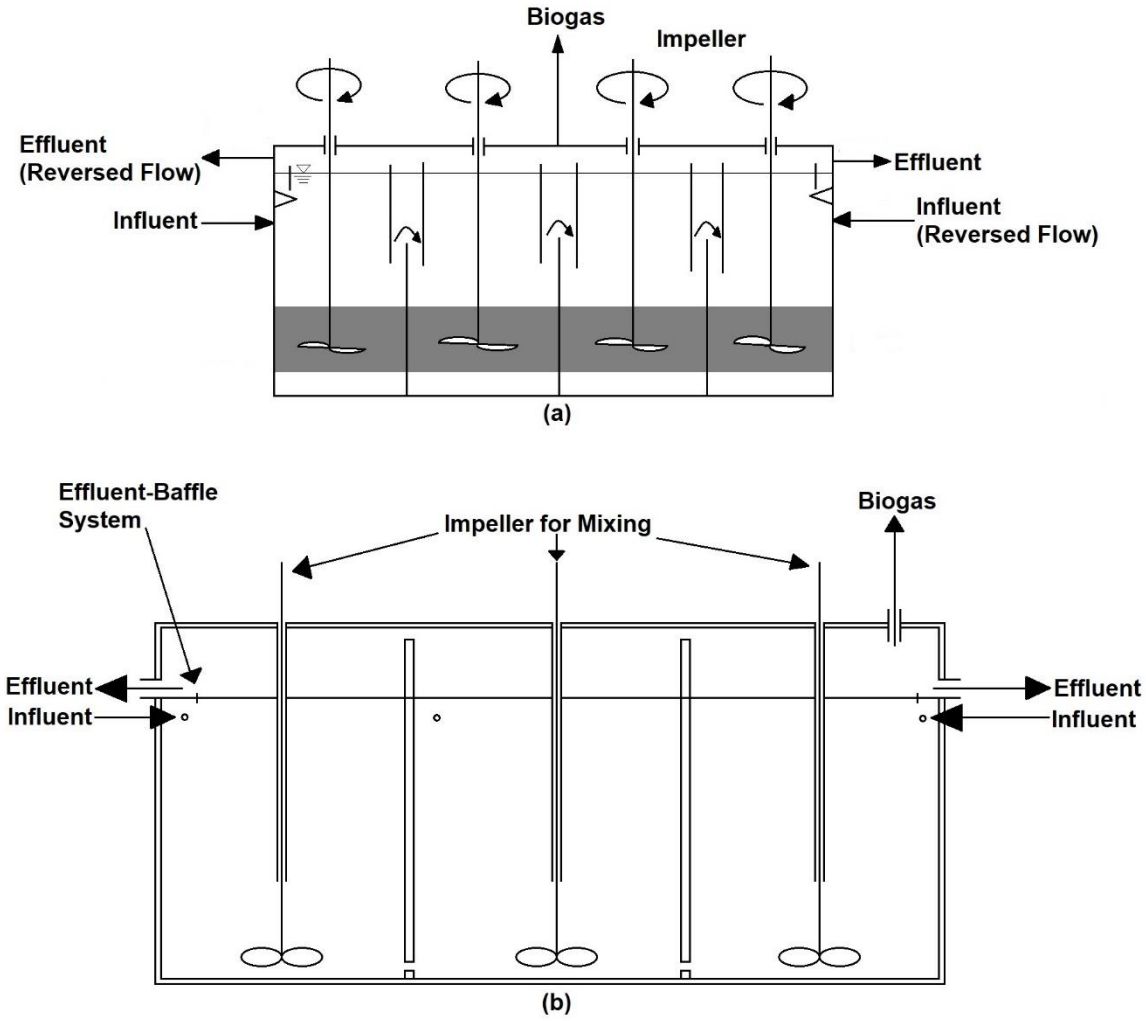

Figure 2.7 – Schematic diagram of two different designs of anaerobic migrating blanket reactor (AMBR) (adapted from Tchobanoglous et al., 2003; Tauseef, et al., 2013).

Different designs of attached growth upflow anaerobic filter reactors use different types of packing and degree of bed expansion. Figure 2.8 displays three types of attached growth upflow anaerobic filter processes.

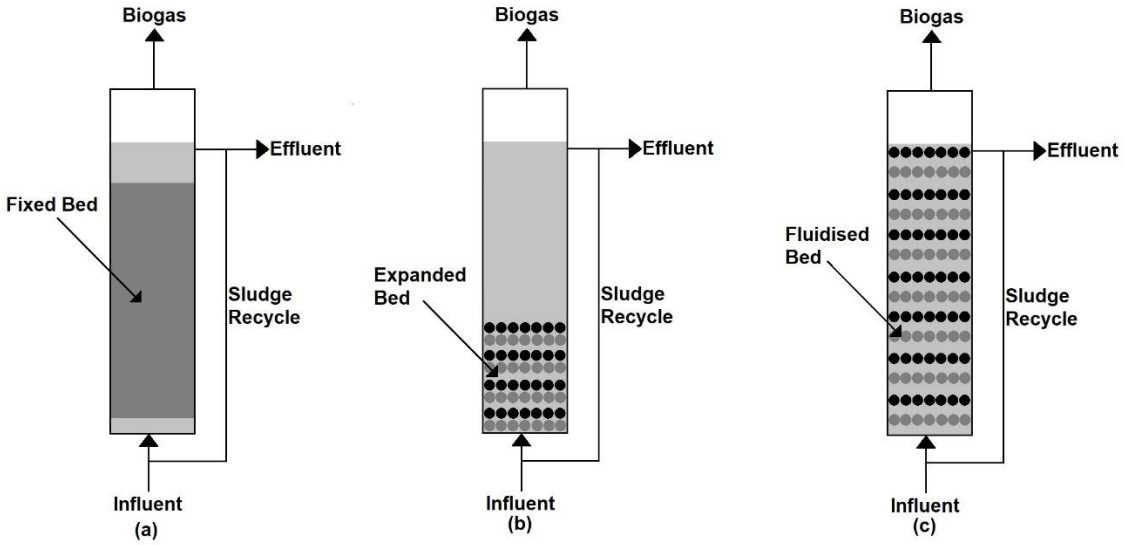

Figure 2.8 – Schematic diagram of attached growth upflow anaerobic filter reactors (adapted from Tchobanoglous et al., 2003).

Figure 2.8 (a) is an attached growth upflow anaerobic filter, fix-bed, packed bed or submerged filter reactor (Switzenbaum, 1983). It was first introduced by Young and McCarthy in 1969 for anaerobic treatment of domestic wastewater since UASB reactors only perform well with high strength, warm wastewater but not diluted, cool domestic wastewater (Jewell, *et al*., 1981). The packing is normally fixed for the entire depth. The packing materials can be plastic, stone, quartz, granite, sand, reticulated foam, polymers and granular activated carbon (GAC) (Chelliapan & Sallis, 2010). The reactor can be used for both upflow and downflow feed mode. Wastewater flows through the gaps between the biogrowth on the packing. Anaerobic packed bed reactors are used in cylindrical or rectangular tanks, full scale tanks are from 2 to 8 metres in diameter and 3 to 13 metres in height. The advantages of having a fully packed upflow anaerobic fix-

bed reactor is that it provides a quiescent zone at the inlet for dense biomass to accumulate, which is not easy to wash out. In addition, the reactor also offers large surface area which enables biofilm accumulation. Combining these two advantages ensures a shorter start-up time for the reactor because of the large amount of inoculum retained. If the shorter start-up time is not essential, then granule inoculum becomes preferable but not necessary to have because conventional municipal waste anaerobic sludge can be used (Chelliapan & Sallis, 2010).

Upflow attached growth anaerobic expanded-bed reactor (AEBR), (Figure 2.8 (b)) and attached growth anaerobic fluidised-bed reactor (AFBR), (Figure 2.8 (c)) are designed upon a similar fundamental concept: they are both derived from UASB. The reactor comprises an expandable column with a packing material of inert particles such as silica sand, alumina or activated carbon packing with a diameter from 0.2 to 0.5 mm, and a specific gravity of 2.65 (Tchobanoglous et al., 2003; Tauseef, *et al*., 2013; Switzenbaum, 1983). The inert particles serve as a support surface for microorganisms to grow and they are suspended by a rapid upflow of incoming wastewater. The difference between AEBR and AFBR is in the size of expansion. The expansion for AEBR is 15-25%, whereas the expansion for AFBR is 25-300% (Tauseef, *et al*., 2013). The smaller packing offers a greater surface area per unit volume which, in theory, supports a greater amount of biomass growth. These reactors run efficiently with feed that is soluble or contains easily degradable suspended materials such as whey, whey permeate, black liquor condensate and so on. In general, AEBR and AFBR are

more efficient than an anaerobic fix-bed reactor. The processes are capable of operating at higher removal efficiencies with higher loading rates and shorter retention time than an anaerobic fix-bed reactor.

2.1.6. Effects of Mixing

Mixing in anaerobic digester keeps the solid suspended and homogenises the incoming feed with the active microbial community inside the digester, avoids temperature and pH gradients, prevents foam, scum and crust formation, stratification and many more benefits (Lindmark, Thorin, Fdhila, & Dahlquist, 2014; Kariyama, Zhai & Wu, 2018). Different types of mixing equipment have been used in anaerobic digesters, such as mechanical, hydraulic and pneumatic mixing. A study (Lindmark et al., 2014) showed that during mesophilic anaerobic digestion of cattle manure, intermittent mixing improves performance compared to a continuously mixing system. Lindmark et al. (2014) also reported that duration or intensity of mixing does not make noticeable difference. However, increase in biogas production was reported (Lin & Pearce, 1991) when mixing duration was reduced from 45 min/h to 15 min/h. In addition, Rivard et al. (1990) reported that for high solids digestion of municipal solid waste (MSW), maximising OLR while minimising mixing intensities improves methane production where a minimum cost is preferable. High intensity was a waste of energy.

Traditionally, stirred tank digesters operate as continuous stirred tank reactors (CSTRs) and suppose to accrue all of the benefits ascribed above, multiple studies (Gómez, Cuetos, Cara, Morán & García, 2006; Rico, Rico, Muñoz, Gómez, & Tejero, 2011; Lindmark et al., 2014) reported that intermittent mixing reduces energy demand and maintenance cost as well as improves the biogas production compared to continuous mixing mode of a CSTR.

2.2. Biogas Upgrading Technologies

Currently, numerous biogas upgrading technologies have been developed, ranging from conventional absorption, pressure swing adsorption (PSA) and membrane separation to recent developments such as cryogenic upgrading, *in situ* methane enrichment and ecological lung (Petersson & Wellinger, 2009; Sun, *et al*., 2015; Ryckebosch, Drouillon and Vervaeren, 2011; Sahota et al., 2018).

2.2.1. Current Biogas Upgrading Technologies

2.2.1.1. Absorption

Physical or chemical absorption is when components of biogas diffuse into solvent by passing through the interfacial region. Physical absorption using water (water scrubbing) or organic physical solvent (physical scrubbing) as absorbent is one of them (Cozma, et al., 2013). When using water as solvent, pre-treatment to remove H_2S is usually recommended because H_2S dissolved in water is

corrosive. Raw biogas is pressurised to approximately 9 to 12 bar and then fed in from the bottom of the water scrubbing column flowing upwards while water is fed from the top as a counter current in a packed bed column packed with materials with high mass transfer coefficient. As a result of this, cleaned biogas leaves from the top of the column with increased methane content and pressurised water with dissolved gases leaves from the bottom. Dissolved gases in pressurised water are desorbed at atmospheric pressure or sometimes at 2 to 4 bar in a flash tank or a stripper and then recirculated (Sahota, et al., 2018). Using organic physical solvent is theoretically similar to using water as solvent (Petersson & Wellinger, 2009). Removal of H_2S before absorption process is also recommended because it is difficult to regenerate H_2S from solvent and it reduces the capacity for CO_2 absorption. Typical organic solvents are methanol and dimethyl ethers of polyethylene glycol (DMPEG). Spent solvents are then regenerated by depressurising and/or heating (Sahota, et al., 2018; Petersson & Wellinger, 2009). Figure 2.9 is the schematic diagram of absorption upgrading technology.

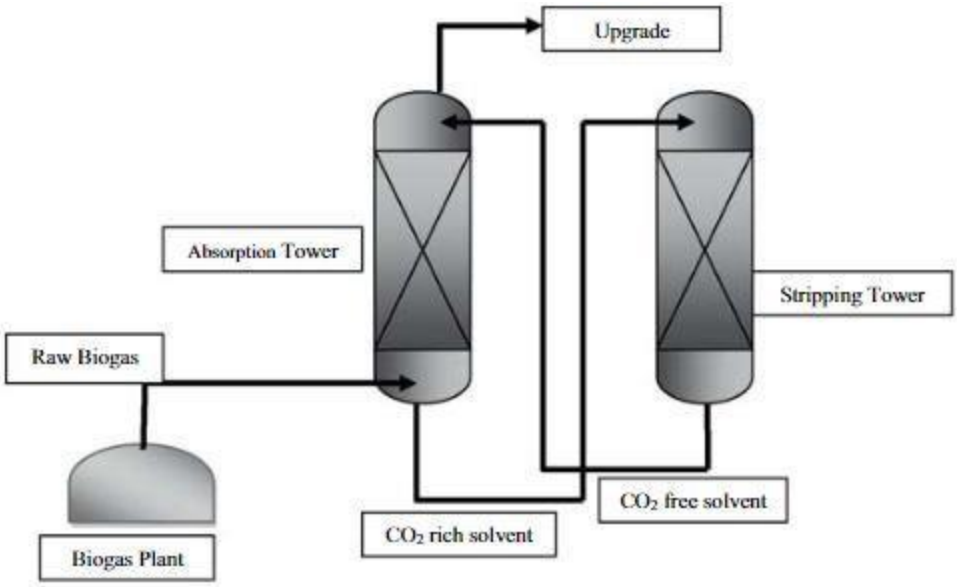

Figure 2.9 – A schematic diagram of absorption upgrading technology (taken from Sahota, et al., 2018).

Chemical absorption deviates from physical absorption in the chemical reaction between solvent and absorbed substances. In chemical absorption, amine-based solvents react chemically with H_2S and CO_2 so methane loss is as low as 0.1 – 0.2% (Sun, et al., 2015; Sahota, et al., 2018). Chemical absorption has a low pressure requirement compared to physical absorption, but regeneration of solvents require relatively high energy input (Kapdi, Vijay, Rajesh, & Prasad, 2005). Typical amine-based solvents are monoethanolamine (MEA), diglycolamine (DGA) and diethanolamine (DEA).

2.2.1.2. Adsorption

Classification of adsorption upgrading technologies are based on the regeneration methods of adsorbents. The typical methods for regenerating adsorbents are pressure swing adsorption (PSA), vacuum swing adsorption (VSA), temperature swing adsorption (TSA), electrical swing adsorption (ESA) and displacement desorption (Sahota, et al., 2018). Of all these technologies, PSA is the most commonly used because of low energy consumption, high efficiency, safety and design flexibility compared to other options (Miltner, Makaruk, & Harasek, 2017).

PSA and VSA are a sequence of four steps known as “Skarstrom cycle” that occurs in a column. The four steps are: feed, blowdown (or evacuation), purge and pressurisation (Grande, 2012). Plants using these technologies usually have four or more vessels working in parallel, so when adsorbing material is saturated, raw biogas can be fed to another vessel where adsorbing material is regenerated (Petersson & Wellinger, 2009). Pre-treatment for biogas is required to remove H_2S because adsorbents adsorb H_2S irreversibly. Columns filled with molecular sieve such as activated carbon, silicagel, alumina or zeolites under elevated pressure (around 8 bar) are used to separate CO_2, H_2O, N_2 and O_2 from biogas by adsorbed loosely in the cavities of the molecular sieve (dry gas for PSA process). Once the bed is saturated, the bed is depressurised to release gas with high CH_4 content. The adsorbing material is then regenerated by further depressurisation (PSA) or by putting it under vacuum (VSA) (Ryckebosch, et al., 2011). Figure 2.10 is a schematic diagram of PSA/VSA upgrading technology.

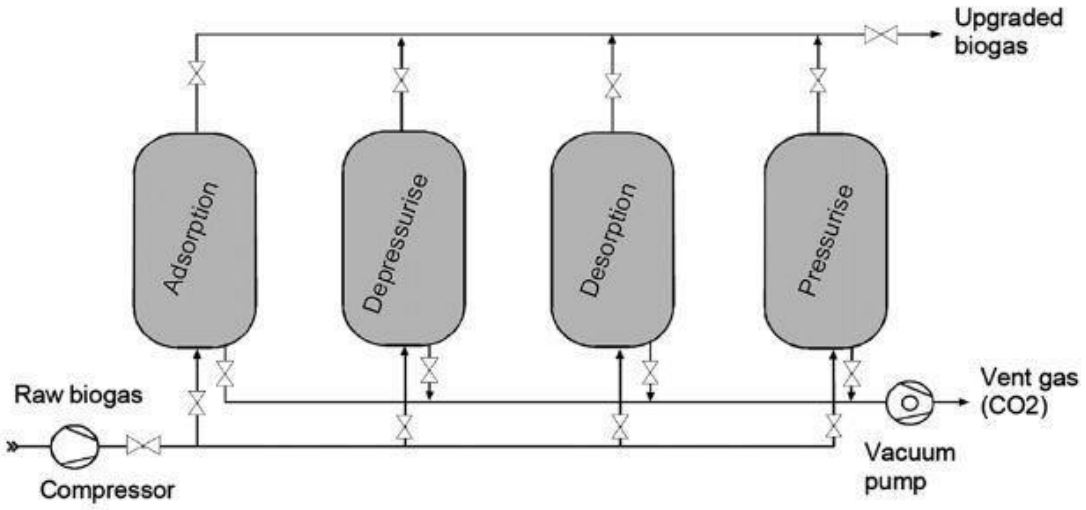

Figure 2.10 – A schematic diagram of PSA/VSA upgrading technology (taken from Ryckebosch, et al., 2011).

2.2.1.3. Membrane Separation

Membrane separation is a separating technology at the molecular scale (Sun, et al., 2015). There are two basic systems for membranes separation: (1) gas-gas separation and (2) gas-liquid separation (Ryckebosch, et al., 2011). For gas-gas separation, biogas is pressurised up to 36 bars and first needs to be treated to remove hydrocarbons, H_2S and oil vapour from compressors. Next, pre-treated biogas flow through the membranes, which are usually acetate-cellulose or hollow fibres bundled together, with CO_2 and remaining H_2S pass through to the permeate side while CH_4 is retained on the inlet side. Due to imperfection of the separation process, multi-stage process may be necessary (Ryckebosch, et al., 2011; Sun, et al., 2015). Waste gases from the first stage are recovered within the process to improve CH_4 capture while waste gases form the final stage is

either flared, used for heat production or captured catalytically (Patterson, Esteves, Dinsdale, & Guwy, 2011). The early designs produce off-gas containing up to 25% CH_4 while newer designs operating at 8 bars have far lower methane losses (Petersson & Wellinger, 2009). For gas-liquid separation, the crucial part is a micro porous hydrophobic membrane to separate gas phase from liquid phase. The molecules of the slight pressurised gas stream flowing in on one side, are diffused by the membrane and liquid flowing in counter current on the other side is able to absorb the CO_2. Liquid is prevented from flowing to gas side because of the pressure difference on two sides (Ryckebosch, et al., 2011). Typical absorbents used are $NaOH$ for H_2S or heat regenerative amine solutions for CO_2 (Patterson et al., 2011).

2.2.2. Emerging Biogas Upgrading Technologies

2.2.2.1. Cryogenic Separation

Cryogenic upgrading technology utilises the different physical properties of the gases to separate CH_4 from CO_2, N_2 and O_2. To avoid freezing and other problems, H_2O and H_2S need to be removed with pre-treatment (Sun et al., 2015). At atmospheric pressure, the boiling point for CH_4 is −160℃ and −78℃ is the de-sublimation point for CO_2 (Patterson et al., 2011). By progressively compressing and cooling raw biogas the CO_2 component can be selectively de-sublimed to a solid and separated individually. The process needs specialised low temperature equipment and consumes a large amount of energy equivalent

to 5 to 10% of the biomethane production. However, it shows great advantages in producing high purity CH_4 (>99%) and CO_2 (up to 98%) with low loss of CH_4 (normally <1%) (Sun et al., 2015; Sahota et al., 2018).

2.2.2.2. In situ Methane Enrichment

In situ methane enrichment process works based on the fact that CO_2 is more soluble in aqueous solutions than CH_4 . Sludge from the digester is taken out to a desorption column where it meets a counter flow of air or N_2. CO_2 dissolved in the sludge is desorbed and the sludge is then circulated back to the digestion chamber to absorb more CO_2. It is also possible to simultaneously remove H_2S and NH_4 which are both known to inhibit digestion through this process (Sun, et al., 2015; Petersson & Wellinger, 2009).

2.2.2.3. Ecological Lung

The ecological lung process utilises the same principle to remove CO_2 from biogas as humans removing CO_2 from their blood formed during respiration. The enzyme carboanhydrase is used to catalyse the reversible reaction

$$H_2O + CO_2 \leftrightarrow H^+ + HCO_3^-$$

This is used to remove CO_2 from biogas, then catalyse the reaction to convert bicarbonate (HCO_3^-) back to CO_2 and collect it (Petersson & Wellinger, 2009).

2.2.3. Energy Efficiency of Biogas Upgrading Technologies

The biogas upgrading technologies previously mentioned were compared in terms of energy efficiency (η), which is defined as follows (Sun, *et al*., 2015):

$$\eta = \frac{Energy_{upgraded\ gas}}{Energy_{raw\ gas} + Energy_{upgrading}}$$

In practice, the energy consumption by each biogas upgrading technology differs case by case. The loss of methane throughout the entire upgrading processes is the crucial parameter of all the parameters affecting the overall energy efficiency. Table 2.4 demonstrates the energy efficiency of numerous biogas upgrading technologies and other information. As Table 2.4 illustrates, there is no definite conclusion on which technology has the highest efficiency. The energy efficiency of *in situ* and microalgal photosynthesis are claimed to be significantly higher than others, but there is lack of detailed information to support these claims (Sun *et al*., 2015).

Table 2.4 – Example for energy efficiency of various biogas upgrading technologies (adapted from Sun et al., 2015).

Technology	**Energy Consumption (Electricity)**	**Efficiency (%)**	**Range of Efficiency (%)**	**Median (%)**	**Source**
Water Scrubbing	0.45 - 0.90 kW h/N m^3 cleaned gas	88.9 – 92.8	88.9 – 92.8	90.9	Plant and Supplier
Water Scrubbing + Regeneration	0.45 kW h/N m^3 cleaned gas	92.8	92.7 – 966.0	94.4	Plant and Supplier
Cryogenic Separation	0.8 – 1.54 kW h/N m^3 cleaned gas	86.4 – 92.5			Calculation
Physical Absorption	0.49 – 0.67 kW h/N m^3 cleaned gas	90.0 – 91.5			Plant + Literature
Chemical Absorption	0.3 kW h/N m^3 cleaned gas	88.5	88.5 – 97.7	93.1	Plant
PSA	0.3 – 1.0 kW h/N m^3 cleaned gas	84.8 – 90.4			Plant
Membrane	0.25 – 0.43 kW h/N m^3 cleaned gas	86.5 – 87.9			Plant + Literature

2.2.4. Cost of Biogas Upgrading Technologies

Similar to energy efficiency, the capital costs (CAPEX) or operating and maintenance costs (OPEX) of a specific biogas upgrading technology varies case by case. Table 2.5 provides some examples of CAPEX and OPEX of biogas upgrading technologies. For most of the plants in this figure, the costs of the building where the upgrading processed are located is not included.

As Table 2.5 demonstrates, the economies of scale imply lower CAPEX per unit of biogas for larger plant. Furthermore, the investment costs have not changed much since 2003 (Sun *et al*., 2015). The OPEX for a biogas upgrading plant mostly involves labour, utilities, chemical or water depending on the particular upgrading technology and maintenance methods. Despite the high efficiency, chemical absorption technologies have high OPEX, especially for larger plants because of oxidisation, degradation or loss of solvent. Cryogenic technologies have high OPEX because of the low efficiency of the thermodynamic cycle required to produce the low temperatures required.

Because of the lack of information on *in situ* biogas upgrading technology for energy efficiency and upgrading costs, it makes this project particularly important.

Table 2.5 – Example for Capital costs (CAPEX) and operation and maintenance costs (OPEX) of various biogas upgrading technologies (adapted from Sun et al., 2015).

Technology	**Yield (m^3/h)**	**CAPEX (€)**	**OPEX (€)**	**CAPEX (€/kW h)**	**OPEX (€, cent/kW h)**	**Source**
Water Scrubbing	660	2.5 M	–	644	–	Plant Data
Water Scrubbing + Regeneration	2000	2.6 M	0.4 M/yr.	219	0.37	Plant Data
Cryogenic Separation	161	0.9 M	0.4 M	960	4.80	Calculation
Physical Absorption	500	3.5 K/(m^3/h)	9.0/(m^3/h)	357	0.92	Plant + Literature
Chemical Absorption	500	3.5 K/(m^3/h)	11.2/(m^3/h)	357	1.15	Plant + Literature
PSA	500	3.7 K/(m^3/h)	9.2/(m^3/h)	377	0.92	Plant + Literature
Membrane	500	3.5 – 3.7 K/(m^3/h)	6.5 – 10.1/(m^3/h)	3667	0.67 – 1.05	Plant + Literature

2.3. Mathematical Modelling

2.3.1. Anaerobic Digestion Model No. 1 (ADM1)

Mathematical modelling is a central part of this work and we therefore discuss relevant previous models in this section. Anaerobic fermentation is one of the oldest biological process technologies employed by mankind. Its initial uses were mainly for beverage and food production (He, Liu, Sadiq, Gu, & Zhang, 2017). This technology has been utilised and developed over many centuries. Modelling for anaerobic digestion systems, on the other hand, has only been developed for the last few decades, including the well accepted anaerobic digestion model 1 (ADM1) by IWA (Batstone, *et al*., 2002). In addition to waste treatment, the major feature which increases the application of the anaerobic digestion process is a positive net energy production. The biogas produced by anaerobic digestion process could potentially displace usage of fossil fuels, thereby giving a direct reduction in greenhouse gas emissions. The benefits of having a generalised model for anaerobic digestion are listed below (Batstone, *et al*., 2002):

1. Model implementation for full scale plant design, operation and optimisation.
2. Can be used for further development work on process control and optimisation, aimed directly at application in full scale plants.
3. Can be used for additional model development and authentication studies to make results more compatible and comparable.

4. Can be used to assist the transfer of the technology from academic research to industry applications.

The anaerobic digestion process is acknowledged to be complicated, containing hundreds of species of bacteria. Combining anaerobic digestion with the cultivation of microalgae is a favourable alternative to producing methane using solar energy (Yang, et al., 2018; Hidaka, Takabe, Tsumori, & Minamiyama, 2017). However, due to its intrinsic complications, to design and operate such a combined system is a massive challenge. Currently the only study that has been dedicated explicitly to the modelling of anaerobic digestion of algal biomass is "*Modelling anaerobic digestion of microalgae using ADM1*" (Mairet *et al*., 2012). The model utilises Contois kinetics for the hydrolysis steps instead of first order kinetics used in ADM1 and it is a sufficient description of the anaerobic digestion of microalgae (Mairet, Bernard, Ras, Lardon & Steyer, 2011; Mairet *et al*., 2012). Because first order kinetics do not consider the bioavailability of the substrate, they are less suitable than Contois for simpler models with substrates such as microalgae.

The rate equation developed by Contois in 1959 (as cited in Wang & Li, 2014) incorporates an additional inverse relationship between microbial concentration and the saturable substrate term into the specific growth rate observed in a glucose-fed *Aerobacter aerogenes* culture (Wang & Li, 2014). The equation is demonstrated as follows:

$$\mu = \frac{\mu_{max} S}{K_C X + S} \qquad Eqn\ 2.14$$

where μ is the specific growth rate, μ_{max} is the maximum specific growth rate, S is the substrate concentration, K_C is a growth coefficient of the Contois function, X is the microbial concentration. Contois asserts the specific growth rate of a microbe is determined by both the microbial cell concentration and the limiting substrate concentration, as expressed by the classic Monod equation in Eqn 2.15 (Wang & Li, 2014).

$$\mu = \frac{\mu_{max} S}{K_s + S} \qquad Eqn\ 2.15$$

where K_s is the half-saturation coefficient.

Lyberatos and Skiadas (1999) pointed out that modelling of anaerobic digestion has been widely developed since the seventies, from simple models considering only one limiting reaction e.g. model by Graef and Andrews (as cited in Mairet *et al*., 2011) or two-reaction model, subsequently referred to as AM2 (Bernard, Hadj-Sadok, Dochain, Genovesi & Steyer, 2001) to more realistic representations (e.g. ADM1 from IWA). ADM1 depicts five steps of anaerobic digestion: disintegration, hydrolysis, acidogenesis, acetogenesis and methanogenesis. This model incorporates 19 biochemical reactions associated to 7 bacterial populations and consists of over 30 state variables (Mairet *et al*., 2011; Mairet *et al*., 2012). While ADM1 has been extensively used to depict the anaerobic digestion of numerous substrate (Batstone, Keller & Steyer, 2006; Parker, 2005), intuitive mathematical analysis is difficult due to its complexity. Thus, a simplified model which is also specifically developed for microalgae as feedstock is

required for a better understanding of anaerobic digestion processes as discussed in Chapter 2.3.2.

2.3.2. MAD Model as Simplification of ADM No.1

In this project, a model for anaerobic digestion of algal biomass, the Three-Reaction Model for the Anaerobic Digestion of Microalgae developed by Mairet and his co-workers (2012), named Microalgae Anaerobic Digestion model (MAD), was adapted using CellDesigner (Funahashi, *et al*., 2008). There are three reasons for using CellDesigner. First of all, CellDesigner is available for free. It can be downloaded from its official website free of charge. Secondly, CellDesigner has a user-friendly graphical notation system to make biochemical model development much easier. Models can be developed based on the process diagram using Systems Biology Graphical Notation (SBGN) and are stored using Systems Biology Markup Language (SBML). Models are then simulated and analysed through Systems Biology Workbench (SBW) (Funahashi, *et al.*, 2008). The key elements of SBGN are (Funahashi, *et al.*, 2008):

1. Allowing indication and interactions of various biological objects.
2. Being able to combine with other notations.
3. Being visually and semantically explicit.
4. Allowing conversions of graphical models into mathematical formulae for simulation and analysis by software tools.
5. Having software support to draw diagrams.

6. Making the notation scheme of SBGN freely available.

Lastly, an important reason is its compatibility. Since CellDesigner utilises SBML, each model exists as a single SBML text file which permits the exchange of data with other SBML compatible software.

This MAD model is a reduced dynamic model developed based on the experimental data acquired from anaerobic digestion of the freshwater microalgae *Chlorella vulgaris* over a period of 140 days (Mairet *et al*., 2012). The aim of the MAD model is to represent the crucial elements of the process accurately and match the variability from the experimental data set with the least number of reactions. The analysis to determine the minimum number of reactions required for the model, was performed using principal component analysis (PCA), which was summarised in the paper by Mairet *et al*. (2012). The experimental setup and conditions the MAD model are developed for is described in some detail below.

Figure 2.11 is a diagram for the experimental setup that was used to develop the MAD computational model. The system contains freshwater microalgae *Chlorella vulgaris*, strain CCAP211/11B (growing under non-limiting conditions) in a one litre tank continuous stirred anaerobic digester with 0.1 litre headspace. The operating temperature is maintained at 35 ℃ with no pH control. The gas-liquid transfer coefficient $k_L a$ is 5 d^{-1}. For the feed characteristics, the inert charge imbalance concentration (z_{in}) is 0.017 M, the pH value of influent (pH_{in}) is 9.6, inorganic carbon concentration (C_{in}) is 0.019 M, and the inorganic nitrogen

concentration (N_{in}) is 0.11 M. The feed was introduced as slugs, with an average organic loading of 1 $gCODL^{-1}d^{-1}$, while the same amount of reactor medium was removed each day in order to keep the constant liquid volume.

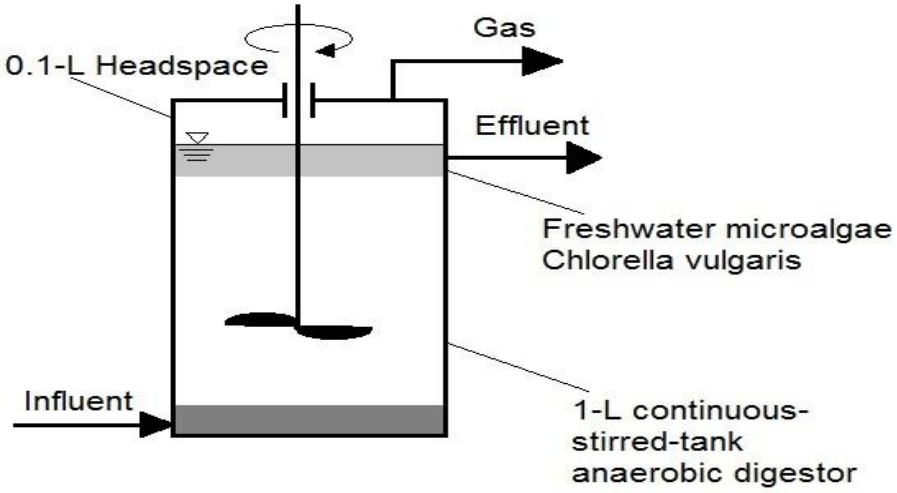

Figure 2.11 – The setup of the experiment for the MAD model (adapted from Mairet, et al., 2012).

As demonstrated in Figure 2.12, two groups of specific bacterial populations, symbolised by X_1 and X_2, decompose sugars and lipids (S_1) and proteins (S_2) of the algal biomass to VFAs (S_3) respectively, with the aid of ammonia NH_4^+, while inert (S_I) represents the undegradable fraction of algal biomass. Lastly, methanogenic population X_3 transforms the VFAs into methane.

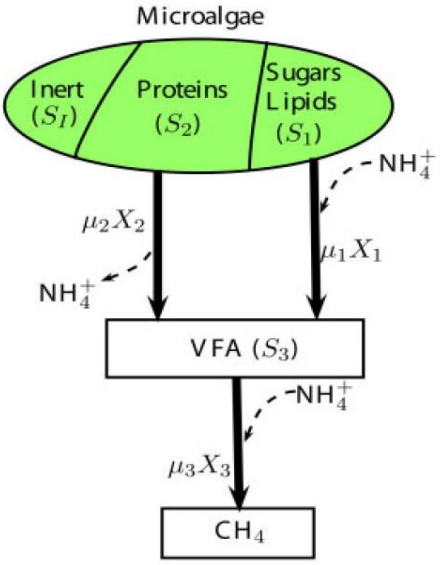

Figure 2.12 – The flow of COD and nitrogen for the anaerobic digestion of microalgae depict by the MAD model (taken from Mairet, et al., 2012).

2.3.2.1. Biological Reaction Pathway

Currently, the vast majority of anaerobic digestion models are a complicated representation of the system. This model, built using CellDesigner, is an adaptation of this Three-Reaction Model for the Anaerobic Digestion of Microalgae (Mairet, *et al*., 2012). The basic concept of this model is to simplify the current complicated models of anaerobic digestion to just three main reactions that are directly related to the production of the biogases carbon dioxide and methane while specifying algal biomass as the feedstock. The three biological reactions in the MAD model can be summarised as follows (Mairet, *et al*., 2012):

1. VFA production from hydrolysis-acetogenesis of sugar-lipids:

$$\alpha_1 S_1 + \alpha_2 NH_4^+ \xrightarrow{\mu_1(\cdot)X_1} X_1 + \alpha_3 S_3 + \alpha_4 CO_2 \qquad R_1$$

2. VFA and ammonium production from hydrolysis-acetogenesis of proteins:

$$\alpha_5 S_2 \xrightarrow{\mu_2(\cdot)X_2} X_2 + \alpha_6 S_3 + \alpha_7 NH_4^+ + \alpha_8 CO_2 \qquad R_2$$

3. Methane production via methanogenesis of the VFAs:

$$\alpha_9 S_3 + \alpha_{10} NH_4^+ \xrightarrow{\mu_3(\cdot)X_3} X_3 + \alpha_{11} CH_4^+ + \alpha_{12} CO_2 \qquad R_3$$

S_1 mainly consists of sugars and lipids and does not contain nitrogen. Meanwhile, S_2 is composed of proteins, which means it contains nitrogen. By using specific bacterial populations, denoted by X_1 and X_2, represented in R1 and R2, these two substrates are both degraded to volatile fatty acids (VFAs), represented as S_3. Lastly, as demonstrated in the AM2 model, a methanogenic population X_3 is used to convert the VFAs into methane. In order to maintain a low model complexity, the separation between lipids and sugars is not taken into consideration like ADM1. Finally, a small portion of microalgae is taken into account to produce inert substrate, represented as S_I, in agreement with batch experiment observations, but the data is not shown. In the following, S_i and X_i are expressed in $gCOD\ L^{-1}$ while CH_4, CO_2 and NH_4^+ are in $mol\ L^{-1}\ (M)$.

2.3.2.2. Charge Balance and pH

In order to determine the pH value in the digester, all the acid-base pairs are expected to be in equilibrium. Supposing the pH value is lower than 8, the concentration of carbonate ions CO_3^{2-} can be disregarded, and the concentration

of total inorganic carbon concentration, symbolised by C, then becomes the sum of the bicarbonate concentration HCO_3^- and dissolved carbon dioxide concentration CO_2. Considering the equilibrium constant $K_C = \frac{h[HCO_3^-]}{[CO_2]}$ for the pair HCO_3^-/CO_2, the bicarbonate concentration becomes:

$$[HCO_3^-] = \frac{K_C}{h + K_c} C \qquad Eqn. 2.16$$

with $h = [H^+]$.

Likewise, the distribution of the VFA between ionised VFA^- and non-ionised HVFA ($S_3 = [VFA^-] + [HVFA]$) and the total inorganic nitrogen between ammonium ions and free ammonia ($N = [NH_4^+] + [NH_3]$) leads to the following equations:

$$[VFA^-] = \frac{h}{K_{VFA} + h} S_3 \qquad Eqn. 2.17$$

$$[NH_4^+] = \frac{h}{K_N + h} N \qquad Eqn. 2.18$$

where $K_{VFA} = \frac{h[VFA^-]}{[HVFA]}$ and $K_N = \frac{[NH_3]}{[NH_4^+]}$, the dissociation constants for the pairs $VFA^-/HVFA$ and NH_3/NH_4^+. Supposing that the major component for VFAs is acetate, the equilibrium constant of acetate can be used for VFA; notice that the equilibrium constants for different VFA as butyrate and propionate are exceptionally close anyway.

The inert charge imbalance z, measured in M, is defined as follows:

$$z = \sum [Cat_I] - \sum [An_I] \qquad Eqn. 2.19$$

with Cat_I and An_I are those cations and anions which are not affected by the anaerobic digestion (Na^+, K^+, Cl^-, etc.), multiplied by their valencies. Then, charge balance leads to the next equation:

$$z + [NH_4^+] + h = [OH^-] + [HCO_3^-] + [VFA^-]/\widetilde{M}_{VFA} \qquad Eqn.\,2.20$$

with $\widetilde{M}_{VFA}$ represents the COD content of VFAs ($64\ gCOD\ mol^{-1}$ supposing pure acetate), and $[OH^-] = K_{H_2O}/h$. Substituting Eqn. 2.16, Eqn. 2.17 and Eqn 2.18 into Eqn. 2.20 and rearranging yields:

$$\frac{K_{H_2O}}{h} + \frac{K_C}{h + K_c}C + \frac{h}{K_{VFA} + h}\frac{S_3}{\widetilde{M}_{VFA}} - z - \frac{h}{K_N + h}N - h = 0 \qquad Eqn.\,2.21$$

which relates the $pH = (-log_{10}h)$ in the digester to the other state variables z, N, C and S_3.

In this work we did not control pH, indeed we had problems measuring pH which is a limitation of the experimental results presented in this thesis. However, since the spirit of this work is to develop low maintenance systems for mixing biogas upgrading, the lack of pH control could be seen to follow this philosophy.

2.3.2.3. Biological Reaction Kinetics

In the MAD model, the specific growth rate for reactions R_1 and R_2 of hydrolysis-acidogenesis are modelled as Contois Equation of Growth for the corresponding substrate.

$$\mu_i(S_i, X_i) = \overline{\mu}_i \frac{S_i}{S_i + K_{Si}X_i}, for\ i = 1{,}2 \qquad Eqn.\,2.22$$

For reaction R_3, Haldane function is used to model the methanogenesis specific growth rate and it is multiplied by an ammonia inhibition term (Mairet, *et al*., 2012).

$$\mu_3(S_3, NH_3) = \overline{\mu}_3 \frac{S_3}{S_3 + K_{S3} + S_3^2/K_{I3}} \frac{K_{I_{NH_3}}}{K_{I_{NH_3}} + NH_3} \qquad Eqn.\,2.23$$

The Haldane function, also known as Briggs-Haldane kinetics, can be derived assuming irreversible enzyme kinetics (Tzafriri & Edelman, 2004), i.e. it excludes the rapid equilibrium approximation from the Michaelis-Menten scheme.

2.3.2.4. Liquid-Gas Transfer

Considering all the methane produced is transferred to the headspace as a result of its very low solubility, the liquid-gas transfer rate of CH_4 (in mol L^{-1} d^{-1}) can be modelled as the following equation (Mairet, *et al*., 2012):

$$\rho_{CH_4} = \alpha_{11}\mu_3 X_3 \qquad Eqn.\,2.24$$

On the other hand, the liquid-gas transfer rate of CO_2 is modelled as the following equation (Mairet, *et al*., 2012):

$$\rho_{CO_2} = k_L a\left([CO_2] - K_{H,CO_2}P_{CO_2}\right) = k_L a\left(\frac{h}{K_C + h} - K_{H,CO_2}P_{CO_2}\right) \qquad Eqn.\,2.25$$

With P_{CO_2} is the partial pressure of CO_2 in the headspace, K_{H,CO_2} is Henry's constant for CO_2 and $k_L a$ is the liquid-gas transfer coefficient. The flow rate of biogas can be calculated by assuming an overpressure in the headspace (Mairet, *et al*., 2012):

$$q_{gas} = \max\left(0; k_p\left(P_{CH_4} + P_{CO_2} - P_{atm}\right)\right) \qquad Eqn.\,2.26$$

where k_p is a pipe resistance coefficient. Finally, the percentage of methane ($\%_{CH_4}$) in the biogas on a molar basis is simply determined from the following equation (Mairet, *et al*., 2012):

$$\%CH_4 = \frac{P_{CH_4}}{P_{CH_4} + P_{CO_2}} \qquad Eqn.\,2.27$$

2.3.2.5. Mass Balance in Liquid Phase

In a perfectly mixed reactor fed with microalgae categorised by their fractions of sugars-lipids β_1, proteins β_2 and inerts β_I respectively, the species concentration dynamics in the liquid phase are (Mairet, *et al*., 2012):

$$\dot{S}_1 = D(\beta_1 S_{in} - S_1) - \alpha_1 \mu_1 X_1 \qquad Eqn.\,2.28$$

$$\dot{S}_2 = D(\beta_2 S_{in} - S_2) - \alpha_5 \mu_2 X_2 \qquad Eqn.\,2.29$$

$$\dot{S}_3 = -DS_3 + \alpha_3 \mu_1 X_1 + \alpha_6 \mu_2 X_2 - \alpha_9 \mu_3 X_3 \qquad Eqn.\,2.30$$

$$\dot{X}_1 = (\mu_1 - D)X_1 \qquad Eqn.\,2.31$$

$$\dot{X}_2 = (\mu_2 - D)X_2 \qquad Eqn.\,2.32$$

$$\dot{X}_3 = (\mu_3 - D)X_3 \qquad Eqn.\,2.33$$

$$\dot{N} = D(N_{in} - N) - \alpha_2 \mu_1 X_1 + \alpha_7 \mu_2 X_2 - \alpha_{10} \mu_3 X_3 \qquad Eqn.\,2.34$$

$$\dot{C} = D(C_{in} - C) + \alpha_4 \mu_1 X_1 + \alpha_8 \mu_2 X_2 + \alpha_{12} \mu_3 X_3 - \rho_{CO_2} \qquad Eqn.\,2.35$$

$$\dot{z} = D(z_{in} - z) \qquad Eqn.\,2.36$$

$$\dot{S}_I = D(\beta_I S_{in} - S_I) \qquad Eqn.\,2.37$$

with S_{in}, N_{in}, C_{in} and z_{in} are concentrations of COD, inorganic nitrogen, inorganic carbon and inert charge imbalance in the feed respectively, D is the dilution rate which has dimensions of inverse time. It is instructive to illustrate the origin of the form of these equations from a general mass balance on each component. Consider the general mass balance for a liquid phase component:

$$accumulation = in - out + made - consumed$$

For inorganic carbon in the liquid phase, for example, the terms above are as follows where V_{liq} is the volume (in units of litres, L) of the liquid and Q is the volumetric flow rate into the digestor in units of L/d:

$accumulation = V_{liq}\dot{C}$ mol/d

$in = QC_{in}$ mol/d

$out = QC + V_{liq}\rho_{CO_2}$ mol/d

$made = \alpha_4\mu_1 X_1 + \alpha_8\mu_2 X_2 + \alpha_{12}\mu_3 X_3$ mol/d (contributions from reactions R_1, R_2, R_3)

$consumed = 0$ mol/d

The mass balance for inorganic carbon, Eqn 2.35, is therefore the result of balancing the terms above, dividing throughout by V_{liq} and defining the dilution rate D as $D = \frac{Q}{V_{liq}}$.

2.3.2.6. Mass Balance in Gas Phase

The partial pressure dynamics in CH_4 and CO_2 are given by:

$$\dot{P}_{CH_4} = -P_{CH_4}\frac{q_{gas}}{V_{gas}} + \rho_{CH_4}\frac{V_{liq}RT_{op}}{V_{gas}} \qquad Eqn.\,2.38$$

$$\dot{P}_{CO_2} = -P_{CO_2}\frac{q_{gas}}{V_{gas}} + \rho_{CO_2}\frac{V_{liq}RT_{op}}{V_{gas}} \qquad Eqn.\,2.39$$

with V_{gas} and V_{liq} are the volumes of gas and liquid phases in litres, respectively. R is the gas law constant, which is $0.0831\ barM^{-1}K^{-1}$ and T_{op} is the operating temperature in K. As discussed earlier, we implement a modified form of equations described above in CellDesigner and then fit this to our experimental data in chapter 4.1.

2.4. Glucose Yeast Fermentation

2.4.1. Fundamentals of Fermentation

There are other biological processes that, like anaerobic digestion, also yield gases and that therefore could also be affected by pressure in a similar way. One that we study in this work is fermentation of glucose by yeast to yield carbon dioxide. Fermentation is a process where organic compounds are catabolised by anaerobic bacteria under anaerobic conditions, and in the absence of electron acceptors. In fermentation processes, organic compounds play the roles of both

electron donor and acceptor (Müller, 2008). Furthermore, during fermentation, the substrate is just partially oxidised, thus, it can only yield a small amount of energy stored within. In principle, there are two forms of metabolic energy: energy-rich phosphate bond intermediates with adenosine triphosphate (ATP), which can be synthesised by substrate-level phosphorylation in most fermentative organisms; and electrochemical energy stored in ion gradients across cell membranes, which can be obtained from chemiosmotic free energy-conserving processes (Konings, *et al*., 1997). In most bacteria, protons are the main coupling ions, however, it can also be sodium ions for a number of bacteria in energy transducing processes (Lolkema, *et al*., 1994).

The majority of energy-conserving reactions in living organisms are oxidation-reduction reactions, also known as redox reactions. They are reactions in which one reactant is oxidised accompanied by the reduction of another. Oxygen is the substrate that is frequently reduced in chemoorganotrophic aerobes, whereas in respiring anaerobes, electron acceptor can be either organic or inorganic (Müller, 2008). Common examples for them are sulphate-reducing or methanogenic organisms (carbon dioxide). Most energy is produced by electron transport phosphorylation in respiring organisms both aerobically and anaerobically. In contrast to fermentation, most ATP is synthesised by substrate-level phosphorylation. Fermentation is a redox process in anaerobic conditions. Oxidation of the substrate is combined with the reduction of another substrate, or an intermediate derived from oxidation with different redox potential of the substrate. The outcome provides energy for ATP synthesis, as illustrated in

Figure 2.13. For most fermentations, the same substrate is used both as an oxidant and reductant. However, in some amino acid fermenting organisms, one amino acid is oxidised while another is reduced, this is known as the Stickland reaction. The reduction reaction is usually not combined with substrate-level phosphorylation although the oxidation reaction is (Müller, 2008).

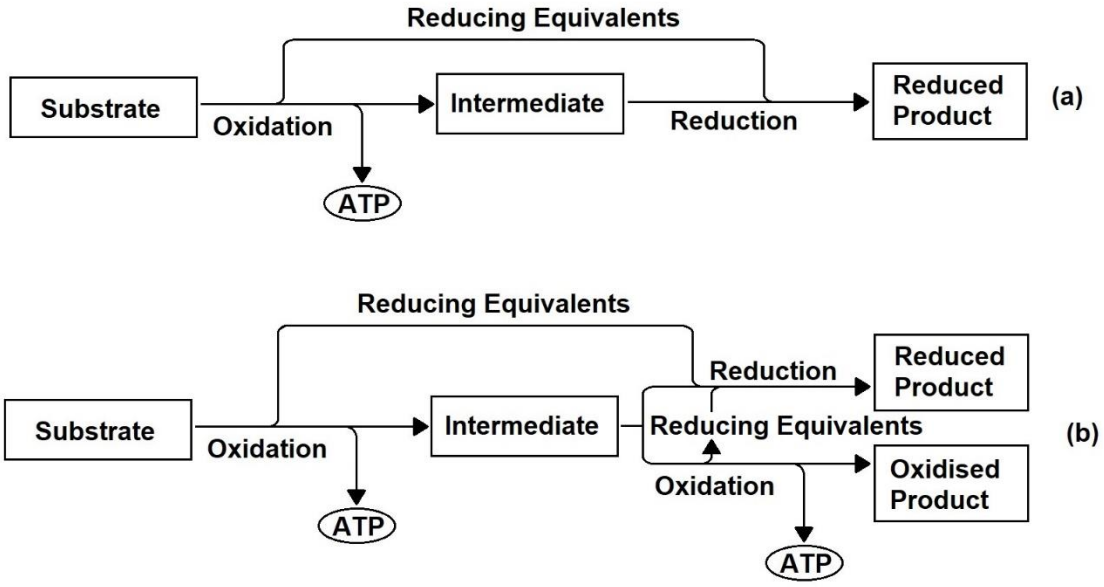

Figure 2.13 – Generalised schematic diagrams of fermentation pathways (adapted from Müller, 2008).

In Figure 2.13 (a), a substrate is oxidised and generates an intermediate, which is then reduced and excreted. In Figure 2.13 (b), the oxidised intermediate such as pyruvate is disproportionate, leading to a more complicated product pattern, which can be observed in numerous fermentations, as demonstrated in Figure 2.14.

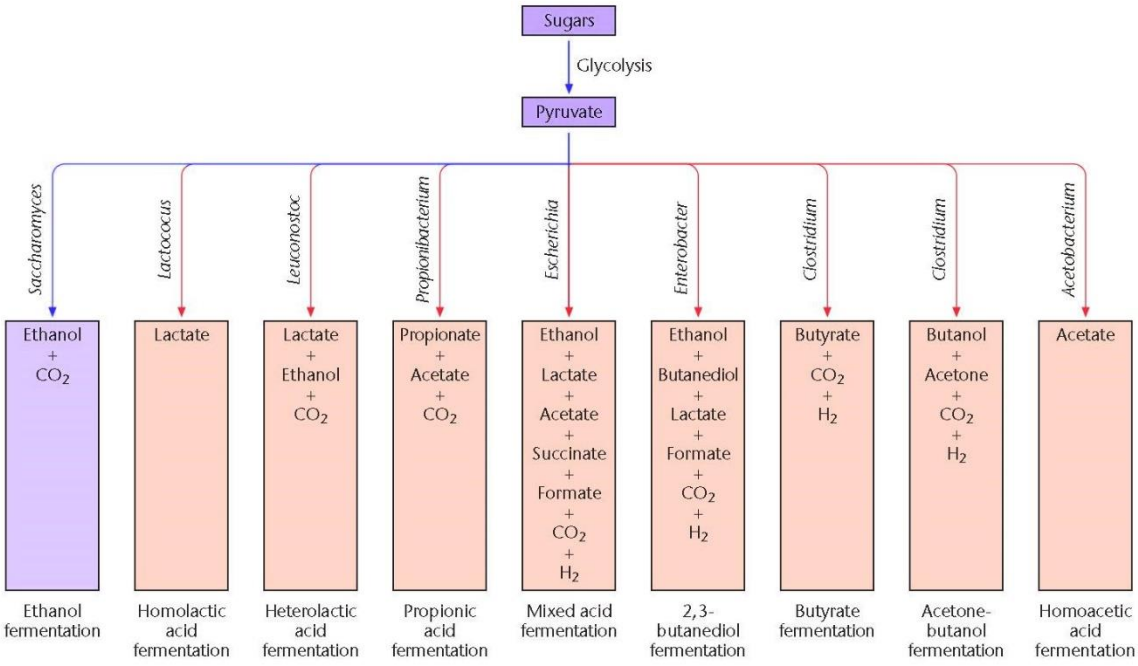

Figure 2.14 – The major pathways of sugars fermentation including organisms involved and final products formed, the pathway highlighted in purple is the pathway studied in this project (adapted from Müller, 2008).

The first major pathway of sugar and yeast fermentation would be ethanol fermentation. It was the pathway studied in this project. Anaerobic metabolism of yeast or *Zymomonas* species produces ethanol as the major end product. Yeasts ferment glucose through glycolysis to pyruvate, which is decarboxylated to acetaldehyde and carbon dioxide. This reaction is catalysed by the main enzyme of alcohol fermentation by yeast called pyruvate decarboxylase. Acetaldehyde is then degraded to ethanol with $NADH_2$, produced in the process of glyceraldehyde 3-phosphate dehydrogenase reaction as a reductant. Alcohol fermentation by

Zymomonas species is not by way of glycolysis but the Entner-Doudoroff pathway. In both scenarios, the reaction is as follows (Müller, 2008):

$$glucose \rightarrow 2CO_2 + 2\ ethanol$$

2.4.2. Factors Affecting the Process

Ethanol production is an intricate process involving fermentation of sugar or starch feedstocks by a variety of yeast strains. It can be affected by several factors: temperature, pH and sugar concentration have profound effects on this process.

2.4.2.1. Temperature

Temperature is considered one of the major factors affecting the sugar yeast fermentation process, since it is directly related to the growth rates and bacteria population (assuming other components in the process are monitored and controlled in a steady-state, *e.g.* pH, substrate concentration *etc.*), which subsequently influence ethanol and CO_2 production.

The effect of temperature on yeast population was studied by Torija, Rozès, Poblet, Guillamón & Mas (2003) is demonstrated in Table 2.6 and Figure 2.15.

Table 2.6 – Effect of fermentation temperatures on yeast population, length and rate of fermentation (taken from Torija, et al., 2003).

Temperature (°C)	Day of Maximal Population	Maximal Population reached (cfu/ml)	Length of Fermentation (days)	Maximal Fermentation Rate (g l^{-1} day^{-1})
15	6	1.18×10^{8}	15	9.41
20	3	1.46×10^{8}	15	20.87
25	3	1.73×10^{8}	15	52.87
30	3	1.95×10^{8}	20	63.23
35	2	0.97×10^{8}	20	69.69

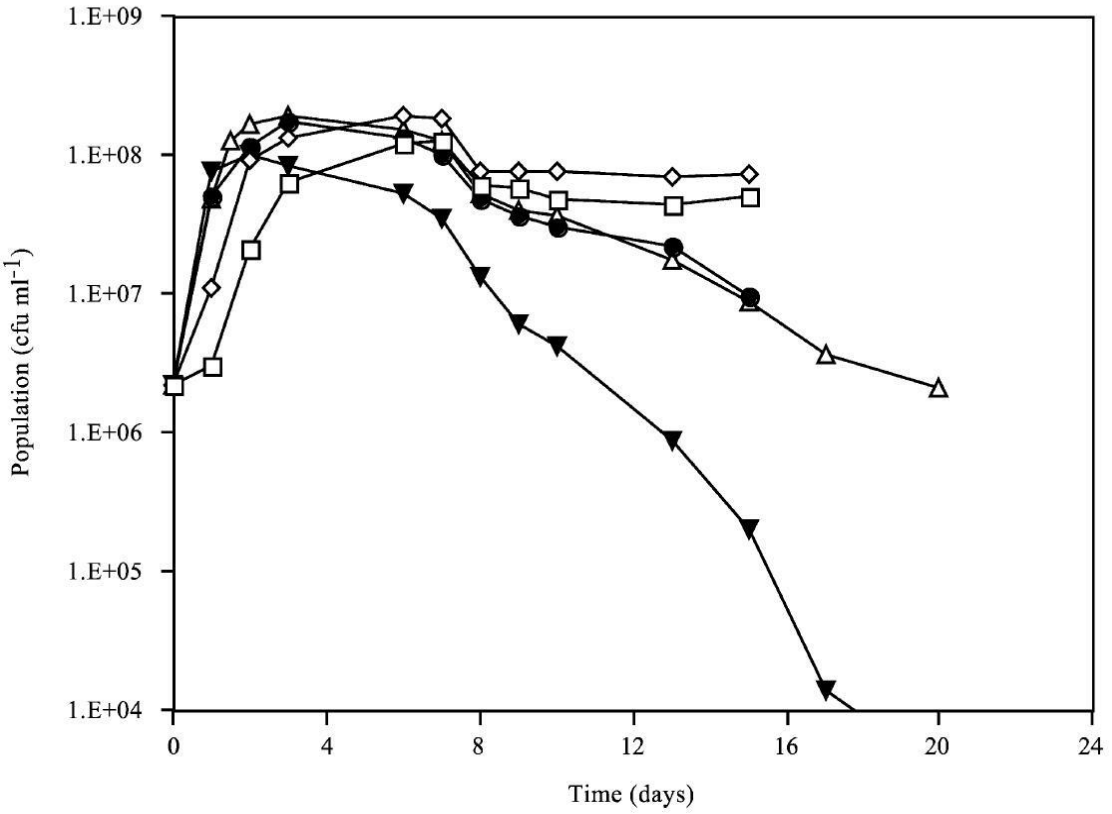

Figure 2.15 – Variation in population size during alcoholic fermentation at different temperatures. □ 15°C, ◊ 20°C, ● 25°C, Δ 30°C, ▼35°C (taken from Torija, et al., 2003).

The experimental results revealed that temperatures can be categorised into three different fermentation kinetics profiles. At 15 and 20°C, fermentations began more gradually, displayed by the lag phase and slower maximum fermentation rate, particularly at 15°C. However, once their maximum population was reached, there was a small decline then maintained at the high values for the rest of the process. At 25 and 30°C, fermentations reached similar maximal populations. In addition, the initial fermentation rates were faster than at lower temperatures. Lastly, at 35°C, fermentation had a rapid exponential phase and

achieved maximal population earlier without lag phase. Then the fermentation process progressed with a very short stationary phase followed by a decline phase.

As demonstrated above, temperature altered yeast growth hence the population of yeast. The standard growth curve contains short-lag, exponential, stationary and decline phases (Torija, *et al*., 2003). On one hand, at low temperatures, the decline phase was so minimal it could be neglected, the stationary phase could last till the end of fermentation process. On the other hand, at high temperature, large amount of yeast died rapidly, this may have provoked a slower fermentation and can lead to stuck fermentations with high sugar contents. The decrease in yeast population was concluded to be caused by a huge accumulation of intracellular ethanol at high temperatures. This would lead to the production of cell toxicity (Nagodawithana, *et al*., 1974) and would change the structure of the membrane and reduce its functionality (Lucero, *et al*., 2000).

2.4.2.2. pH

Multiple studies (Charoenchai, *et al*., 1998; Heard and Fleet, 1988; Arroyo-López, Orlić, Querol and Barrio, 2009) have shown that the effect of modest changes of pH on yeast growth during fermentation is insignificant. However, a study by Lin *et al.* (2012) showed pH values between 4.0 and 5.0 is regarded as the optimal operating condition for the anaerobic ethanol production process.

2.4.2.3. Substrate Concentration

The concentration of sugar is another factor which has an impact on the sugar yeast fermentation process. A study by Arroyo-López, *et al*. (2009) demonstrated when sugar concentration was at $110\ g/l$, the maximum specific growth rate of yeast was the highest and started to decline as the concentration increased for most of the yeast strains tested. However, for *Saccharomyces cerevisiae* T73, the maximum specific growth reached a minimum then rebounded when the sugar concentration was $211\ g/l$. Lin *et al*. (2012) found that increasing the substrate supply did not improve the specific ethanol production rate if pH was not controlled. Another study (Nagodawithana, Castellano & Steinkraus, 1974) showed that, compared to adding all the sugar at the beginning, adding sugar in increments of 2.5%, 5% or even 15% at the beginning then 10% after one hour can improve the yeast population at the end of the fermentation.

How temperature and substrate concentration affect glucose yeast fermentation was studied and discussed because this is a similar process to anaerobic digestion, and it was known to have a much shorter start-up time as well as a shorter duration. While fermentation takes place at a different pace at a different temperature, knowing the optimal conditions where the lag and exponential phase are both the shortest was informative for the design of the experiments discussed later in this thesis. With the optimal conditions, the experiment can be repeated in a short amount of time to find consistent results.

2.4.3. Transport of Gas Molecules Across Cell Membranes

Until comparatively recently it has been assumed that the transport of small molecules such as CO_2 or pharmaceuticals across cell membranes is a passive diffusion process that depends on a concentration difference between the inside and the outside of the cell (Dobson & Kell, 2008). It has further been assumed that the constant of proportionality between flux and concentration gradient, namely the membrane permeability, of a molecule increases with its hydrophobicity which is the basis of Overton's rules (Missner *et al*., 2008). The thinking behind these rules is that hydrophobic molecules will have a higher propensity to enter and migrate across the lipid bilayer. This idea has been refuted in the elegant analysis of Dobson and Kell (2008) who demonstrate that non-passive mechanisms including facilitated and active membrane transport of small molecules is surprisingly common. In addition, the combined experimental and model fitting work of Missner *et al*. (2008) contains the interesting insight that the unstirred aqueous layers on either side of the membrane may offer significantly more resistance to the transport of CO_2 than the cell membrane itself. Although these considerations are not the main thrust of this work, it is interesting to use our results to infer the intracellular concentration of CO_2 in yeast cells by assuming passive diffusion is the dominant mode of CO_2 efflux. This analysis is carried out in section 4.3.1 in the results.

2.5. Phylogenetic Analysis

Phylogenetics is the study of evolutionary relatedness among biological entities on the tree of life (Sleator, 2011; Yang & Rannala, 2012). It addresses various biological questions such as relationships among species or genes, origin and spread of virus and migration patterns and demographic changes of species (Yang & Rannala, 2012). Phylogenetics systematics emerged from the books published by the German entomologist Willi Hennig in 1950 (Wiley, 2008). In those books, his amalgam of three existing ideas presented a new paradigm to evolutionary biology. Those three ideas were: 1) the most basic relationships among organisms were common ancestry/genealogical relationships and not similarity relationships; 2) only certain homologous characters could acknowledge the basic hypothesis that two species are more closely related to each other than a third species; 3) the groups that include an ancestral species and all descendants of that species are natural groups of species (Wiley, 2008).

The first step in phylogenetic analysis is to define the problem to be solved. Given a single origin of life, all organisms are ultimately related (Wiley, 2008), therefore, only questions to be asked should be about some subgroups of the tree of life being studied. The second step is to analyse the similarities and differences among the species. The last step is to determine the ones came first from the differences (Wiley, 2008). This could be distinguished by looking into other organisms that are closely related yet outside the confined group.

There are several methods exist for deducing evolutionary relatedness, most of them can be classified as either distance based or character-based methods (Sleator, 2011). Figure 2.16 demonstrates the major analytical approaches to phylogenetic tree construction. Distance based methods, also known as algorithmic methods, utilise an algorithm comprising a model of evaluation to calculate a distance matrix. A phylogenetic tree is then computed from this distance matrix by means of progressive clustering. They include methods such as neighbour-joining (NJ) and unweighted pair group method using arithmetic averages (UPGMA) (Sleator, 2011; McCormack & Clewley, 2002). Character based methods, also known as tree searching methods, look for the most probable tree for a specific set of taxa based on the nucleotides at each position of sequence alignment and a model of evaluation. The most common character-based approaches include maximum parsimony (MP), maximum likelihood (ML) and Bayesian methods (Sleator, 2011; McCormack & Clewley, 2002).

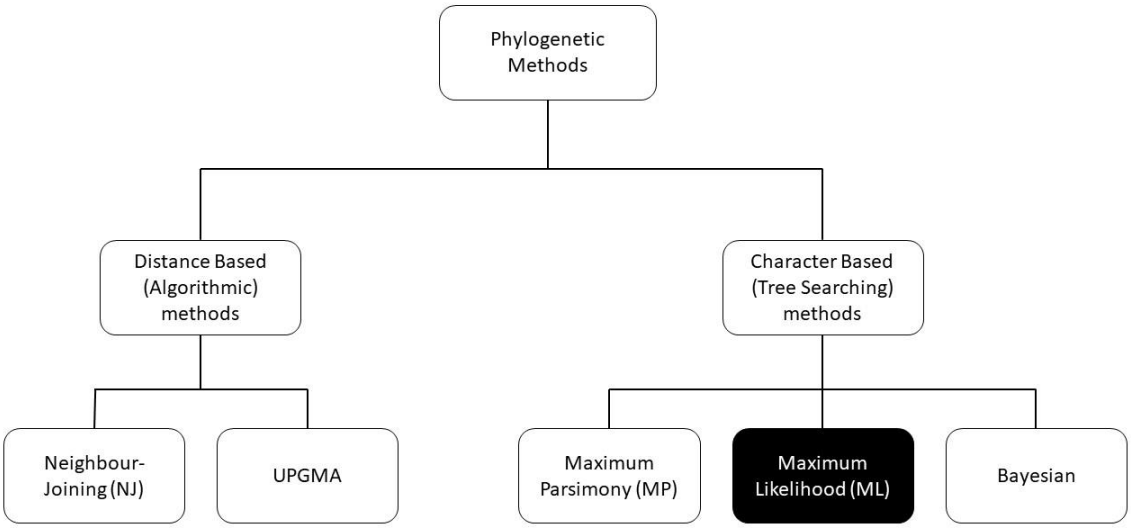

Figure 2.16 – Schematic overview of the relationships between phylogenetic methods (adapted from Sleator, 2011).

Maximum likelihood was the approach used to identify the unknown species of microalgae used in this project. The advantages of using maximum likelihood approach are as follows:

1. Uses all the sequence data.
2. Allows comparison of different trees, parameters and models.
3. Has strong statistical foundations.

In this chapter we have reviewed published results relevant to the research described later in this thesis. In the next chapter we summarise the experimental and computational methods used in this work.

3.*Methodology*

A variety of methods have been used in this work which include both experimental and computational techniques. These are described below.

3.1. Modelling Strategy

Based on an understanding of the growth kinetics of the microbes involved in anaerobic digestion or organic material to produce biogas, a model based on a system of ordinary differential equations (ODEs) can be developed.

3.1.1. CellDesigner Computational Modelling Environment

Based on the published paper by Mairet and his co-workers (2012), the reproduced MAD model can be constructed using CellDesigner. CellDesigner is a process diagram editor for drawing biochemical and gene-regulatory networks (Funahashi, *et al.*, 2008).

Although we are only interested in CellDesigner as a means of creating and integrating differential equations, it is instructive to summarise, in Figure 3.1, the list of symbols and modifications supported by this tool (Funahashi, *et al*., 2008). Note that very little of the diverse functionality of representing intracellular processes is used in this work.

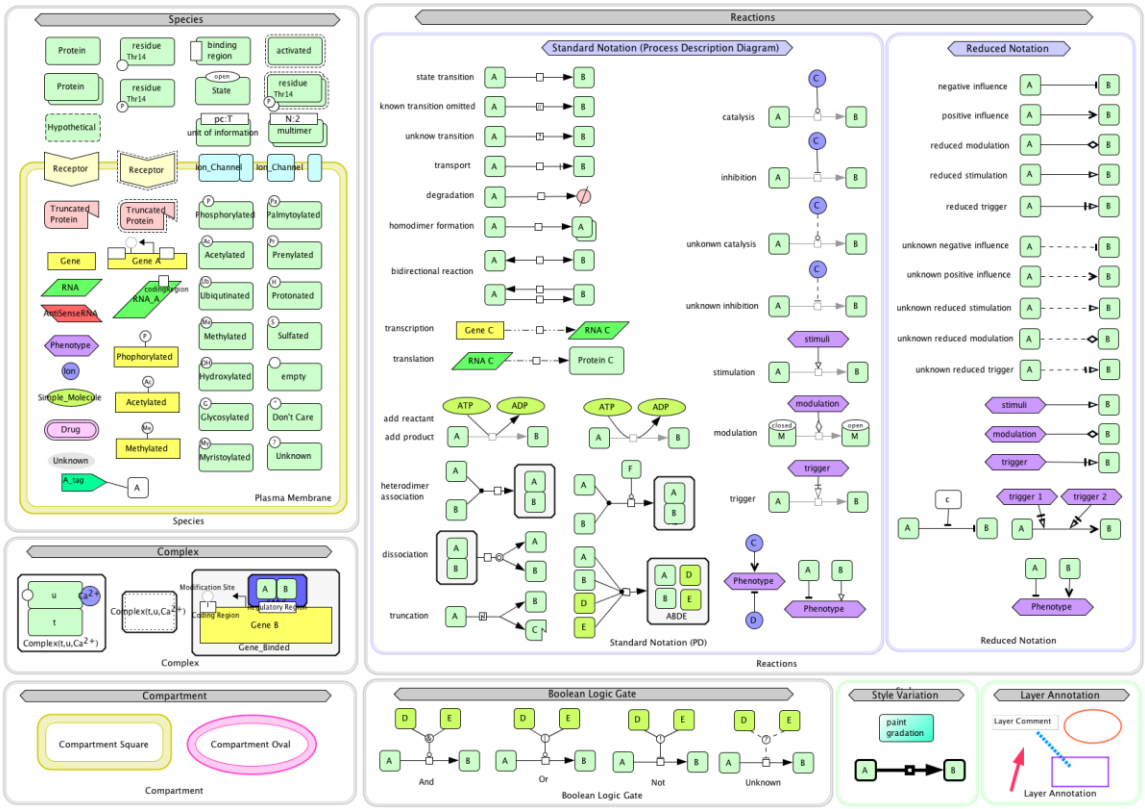

Figure 3.1– The symbols and modifications supported by CellDesigner (taken from Funahashi, et al., 2008).

SBML is a flexible, simple text format for exchanging a wide variation of data based on XML. CellDesigner utilises SBML as its initial model description language, thus, all the information will be stored in SBML once the model is created in CellDesigner. For ODEs based simulation, kinetic laws are required, and they are stored under <kineticLaw> tags, which are compatible with the Mathematical Markup Language (MathML) standard. Figure 3.2 is the illustration of how Systems Biology Graphical Notation (SBGN) and Systems Biology Markup Language (SBML) cooperate in CellDesigner (Funahashi, *et al*., 2008).

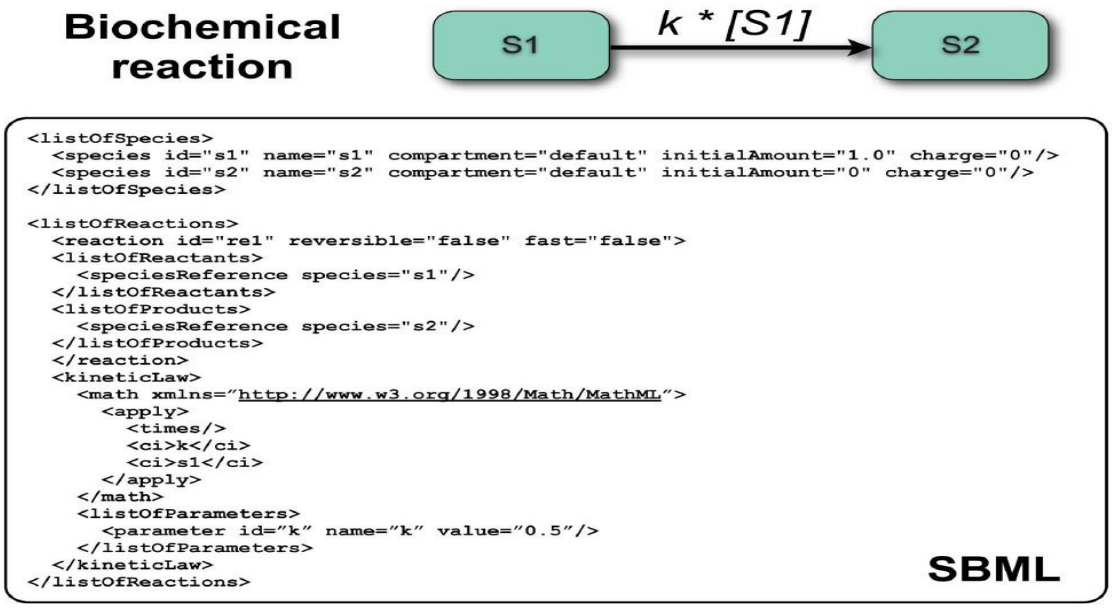

Figure 3.2 – Relationship between SBW broker and SBW modules (taken from Funahashi, et al., 2008).

Figure 3.3 is a demonstration of the relationship between SBW broker and SBW modules (Funahashi, *et al*., 2008).

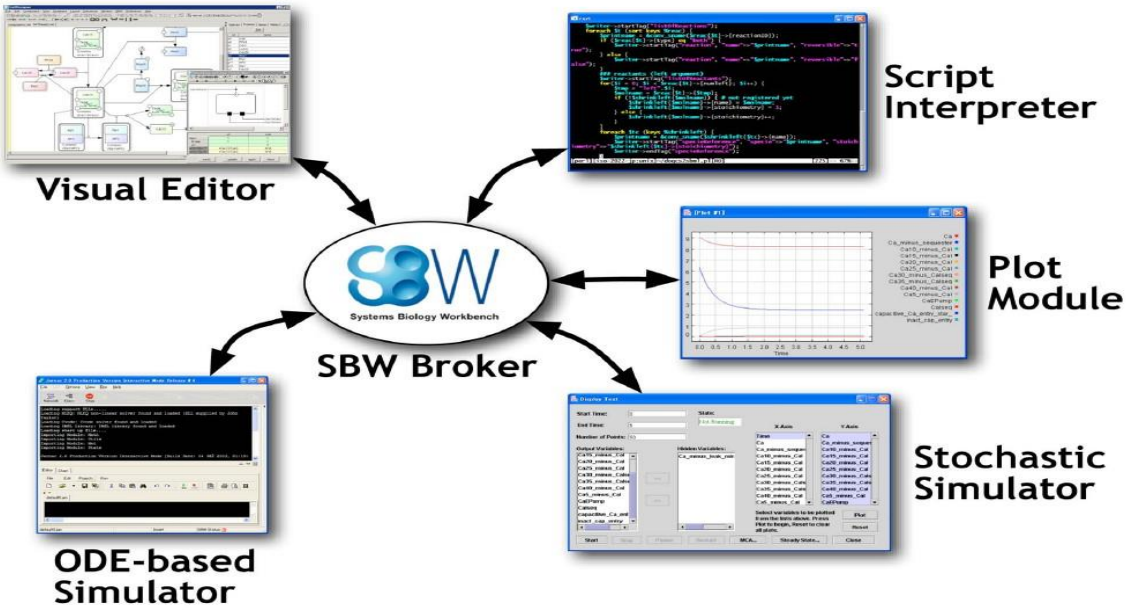

Figure 3.3 – Relationship between SBW broker and SBW modules (taken from Funahashi, et al., 2008).

3.1.2. Adaptation of and Modifications to the MAD Model

The adapted model based on the MAD model by Mairet *et al*. (2012) was built using CellDesigner and the results were compared to the original model. In order to represent the MAD model in Cell Designer and to extend it for the work described in this thesis, the following modifications were made:

1. Ionic equilibrium relationships have been explicitly modelled as fast, coupled forward and backward reactions to replace the algebraic equations used in the original MAD model.

2. Dissolved methane is included in the modified model whereas in the original model it was neglected due to the low solubility of methane as compared to carbon dioxide.
3. Increased headspace pressure is implemented in the modified model by reducing the value of the discharge pipe resistance coefficient k_{p_1}.

To adapt the MAD model (Mairet, *et al*., 2012), the three main reactions of the model were translated into the CellDesigner software. In this reproduced model, algal biomass substrate was divided into three parts, sugars and lipids (S_1), proteins (S_2) and inert (S_I). As the first step, a specific group of bacteria (denoted as X_1) decompose S_1 and ammonium (NH_4^+) to produce VFAs (S_3) and CO_2 while another group of bacteria (X_2) degrade S_2 to produce S_3 CO_2 and NH_4^+ simultaneously, as illustrated in R1 and R2 respectively in chapter 2.3.2.1. Then, the VFAs were further decomposed by methanogens to produce methane and carbon dioxide, as demonstrated in R3 in chapter 2.3.2.1. Once these reactions were established, the numerical equations for charge balance, biological reaction kinetics, liquid-gas transfer, mass balance in liquid phase and headspace as described in chapter 2.2.2 are translated to kinetic laws for those three main reactions in the CellDesigner. The adapted model, as demonstrated in Figure 0.1 in the Appendix, was simulated and verified.

Figure 0.1 is the reproduced model in CellDesigner based on the description in the paper. The original three-reaction MAD model was a set of ordinary differential equations and algebraic equations. In this reproduced model, the algebraic equations from the original model were replaced by forward and

backwards reactions between species, displayed as light green rectangles. A solid straight line with a square in the middle and a black arrow to the right represents a chemical reaction. The rectangles with light green background to the left of solid lines with a square mean they are reactants of that reaction, whereas the rectangles with light green background to the right of solid lines with a square are the products of that reaction. The dotted lines directly connected to the square means that species is a catalyst for that reaction. Furthermore, PCO_2 and PCH_4 are the partial pressures of biogases CO_2 and CH_4 respectively leaving the system in gas form.

The steady state simulated values in the reproduced model in this work had good agreement with the published values in the MAD model. The pH of the system was reported to be approximately 7 in the MAD model, whereas in the adapted model in CellDesigner it was 6.98. The methane content in the MAD model was approximately 62%, whereas the adapted model in CellDesigner gave a value of 62.5%. The biogas flow rate in the MAD model was around 0.1 litre per day and in the adapted model in CellDesigner it was 0.1 litre per day as well.

Since the MAD model was built under the experimental conditions from Mairet and his group, as mentioned in chapter 2.3.2, some parameters in the model would be different from the laboratory-scale experiment of anaerobic digestion of microalgae conducted for this research project. In order to further investigate the effect headspace pressure has on biogas production as well as the limitations presented by the laboratory equipment, it was crucial to apply the parameters from the experiments in this research project to the adapted model that were

different from the MAD model once the adapted model had been verified. The major differences in parameters from the experiments in this study compared to the original model were the physico-chemical parameters. The modified model with experimental parameters as well as the experimental conditions are demonstrated in Figure 0.2 in the Appendix. As discussed previously, the operating pressure for the original MAD model was atmospheric and there was considered to be no methane in liquid phase due to its negligible solubility in water at atmospheric pressure. However, for the purpose of this project, methane in liquid phase, denoted as 'CH_4' in Figure 0.2, was explicitly added for the modified CellDesigner version along with the corresponding Henry's constant. In this way, gas-liquid equilibrium is presented in the same manner for both biogases, although with very different Henry's constants to represent the different solubilities. As the headspace pressure keeps increasing, the amount of dissolved methane will increase as well and this cannot be disregarded. The differences between the adapted MAD model and modified model based on the experiment performed in this study are highlighted in red.

In the original MAD model, the pipe resistance coefficient k_p was a constant at $50000\ L \cdot d^{-1} \cdot bar^{-1}$ which ensured that the model was operating at atmospheric pressure. In the adapted model, however, this pipe resistance coefficient became an adjustable parameter, denoted as 'kp1' in Figure 0.2.

While the reactors were not venting and the caps were tightly sealed, k_{p_1} was $0\ L \cdot d^{-1} \cdot bar^{-1}$ which therefore kept all evolved biogas within the closed system. While they were venting with the caps slightly opened, on the other hand, k_{p_1}

was temporarily set to the original MAD model value of $50000\ L \cdot d^{-1} \cdot bar^{-1}$. These venting simulations were affected by utilising the parameter change functionality within CellDesigner whereby the value of k_{p_1} was be changed in 'Control Panel'. This was done by firstly clicking the 'Simulation' tab and selecting 'Control Panel', then clicking on the 'Change Amount' tab and ticking the 'Change amount' box below the tab. Then the value of 'Interval' was changed to 1 day which was the minimum granularity possible for time dependent parameter changes. The value of k_{p_1} could then be changed according to the desired venting frequency for the simulation, as measured in days. From there, the duration of the simulation could also be changed accordingly.

The results from this modified model were compared to the results from the experiments conducted using Erlenmeyer flasks as reactors. For the operating temperature, since there was no equipment to maintain the reactor temperature at 35°C, the experiments were performed at room temperature, 20°C instead. The reactors had a working volume of 500 ml. In order to achieve noticeable differences in headspace pressure with these reactors, the volumes of broth used were V_{liq}= 400 ml and 470 ml with volume of headspace V_{gas} = 140 ml and 70 ml respectively. The broth used came directly from the algal pond where the microalgae grew, and the pH was 7, which implied the MAD model parameter $h = 10^{-7}$. Once these new parameters were updated, the adapted model could be used as a tool to run simulations where it could exceed the limitations presented by the equipment in the laboratory.

3.1.3. Analysing the Model

Some parameters of the adapted model were modified to fit the experimental conditions and the results were compared. The model was used to predict how different headspace pressures would affect biogas production as well as the biogas composition in a continuous feed mode.

As the model was simulated in CellDesigner, the products of all the chemical reactions were monitored and measured throughout the simulation process. The state variable profiles were then accessible as either a graph or a table of values. For a better understanding of how different experimental conditions as parameters could affect the results, each set of results was extracted to Microsoft Excel and plotted on the same graph for easier comparison.

To determine the correlation between the headspace pressure and the amount of biogas produced by the model, simulations were run with 2 different headspace volumes V_{gas} of 140 and 70 ml with their corresponding culture volumes V_{liq} of 400 and 470 ml with venting frequencies of venting once every 2, 3, 5 and 10 days using the default maximum specific growth rate from the paper and physico-chemical parameters from the laboratory experiments. Since the model directly calculates partial pressure for both CH_4 and CO_2, by using the Ideal Gas Law:

$$PV = nRT \; and \; n = \frac{m}{M}$$

the amount of biogas produced in terms of weight can be calculated using the following equations:

$$m_{CH_4} = \frac{P_{CH_4} V_{gas} M_{CH_4}}{RT} \qquad Eqn. 3.1$$

$$m_{CO_2} = \frac{P_{CO_2} V_{gas} M_{CO_2}}{RT} \quad Eqn.\ 3.2$$

where m_{CH_4} is the mass of CH_4 in headspace, P_{CH_4} is the partial pressure of CH_4, V_{gas} is the headspace volume, M_{CH_4} is the molar mass of CH_4, m_{CO_2} is the mass of CO_2 in headspace, P_{CO_2} is the partial pressure of CO_2, M_{CO_2} is the molar mass of CO_2, R and T are the physico-chemical parameters from the laboratory-scale experiments. Note that the partial pressures of the gases used above are gauge pressure since the venting reduces the headspace pressure to atmospheric. With the partial pressure of CH_4 and CO_2 for each day calculated by the model, the vented mass of each biogas could be calculated. As a result of this, the total biogas produced in terms of mass and the average biogas produced in terms of ml/day for each simulation can be calculated accordingly using the ideal gas law. In addition, since the composition of the group of bacteria used in building this MAD model are likely to be different from the bacteria used in anaerobic digestion with microalgae experiments for this project, the maximum specific growth rates for VFA production from hydrolysis-acetogenesis of sugars-lipids denoted as $\bar{\mu}_1$, VFA and ammonium production from hydrolysis-acetogenesis of proteins denoted as $\bar{\mu}_2$ and methane production via methanogenesis of VFAs denoted as $\bar{\mu}_3$ are considered to be adjustable parameters. It is informative to fit these maximum specific growth rates for the laboratory-scale experiments because it helps to characterise the biological digestion process that is explored in this work, potentially making it easier to improve its performance. The maximum specific growth rates for the bacteria used in the laboratory-scale experiments could be obtained by running simulations with different values from

the original ones, so that the results of the simulation could match or get as close to the experimental results as possible.

To determine how headspace pressure could affect the composition of biogas produced, the various venting frequencies with both headspace volumes were simulated. For comparison, the venting frequencies were set to be once every 5 and 10 days. The results of the same venting frequency but with different headspace volume were put side by side to evaluate the effects the headspace had on the composition of biogas.

3.2. Experimental Materials and Methods

In this section, the bioreactors and materials used for different laboratory-scale experiments are discussed.

3.2.1. Anaerobic Digestion of Pondweed

The bioreactors used in the first few sets of the experiment were original laboratory bottles with DIN thread, GL 45 cap with 500 ml working volume (DURAN Group GmbH, Germany). The issue with these reactors was they were not leak proof. Various methods had been applied to prevent leaks but none of them were foolproof, therefore, new reactors were employed for the experiments. These were 500 ml Erlenmeyer flask with DIN thread and GL 32 cap (DURAN Group GmbH, Germany). There was a layer of rubber liner in the cap which

provided a better seal and prevented biogas leaks during fermentation. Figure 3.4 is the operational principle of the bioreactor.

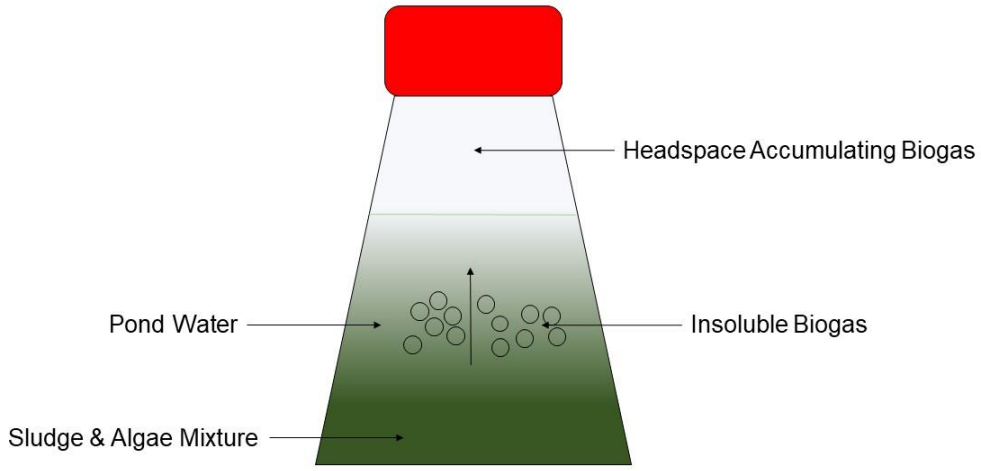

Figure 3.4 – Bioreactor in working mode.

The sludge containing hydrolytic bacteria, acidogens, acetogens and methanogens were obtained from the same pond where the pondweed were grown and harvested (Thornton Science Park, University of Chester, Ellesmere Port, UK).

A key consideration in this work, as discussed previously, is that the pressure in the headspace of these bottles could not be measured directly but was inferred by measuring the weight loss before and after venting to atmospheric pressure. Implicit in this calculation is an assumption of the composition of the biogas which also could not be measured. When the reactors were not being vented or

measured for their weight difference during the fermentation process, they were put in a metal basket and then into the shaking water bath OLS200 at room temperature (Grant Instruments Ltd., UK).

3.2.2. Reactor for Glucose Yeast Fermentation

One major issue with anaerobic digestion is that the process takes several days to get started and a few weeks to finish. Therefore, a new experiment of glucose yeast fermentation was proposed due to its fast response time and quick finish. The glucose yeast fermentation was carried out in reactor 1, labelled 'VS01' of a custom-built twin reactor which could hold pressure up to 6 barg with safety valves set at 5.5 barg. This is similar to the bioreactor used for pressurised anaerobic digestion of seaweed, the design of which is discussed in section 3.2.3. These bioreactors, unlike the bottles, had direct measurement of headspace pressure. One end of the plastic tube was connected to a manual valve labelled 'HV02' and the other end was placed in an inverted graduated cylinder in a bucket to capture the carbon dioxide produced. The setup of the reactor was illustrated in Figure 3.5. The glucose used in these experiments was D-(+)-Glucose ($C_6H_{12}O_6$) (Sigma-Aldrich Ltd., USA) with assay of $\geq 99.5\%$ (GC) and the yeast used was baker's yeast (*Saccharomyces cerevisiae*) bought from Tesco.

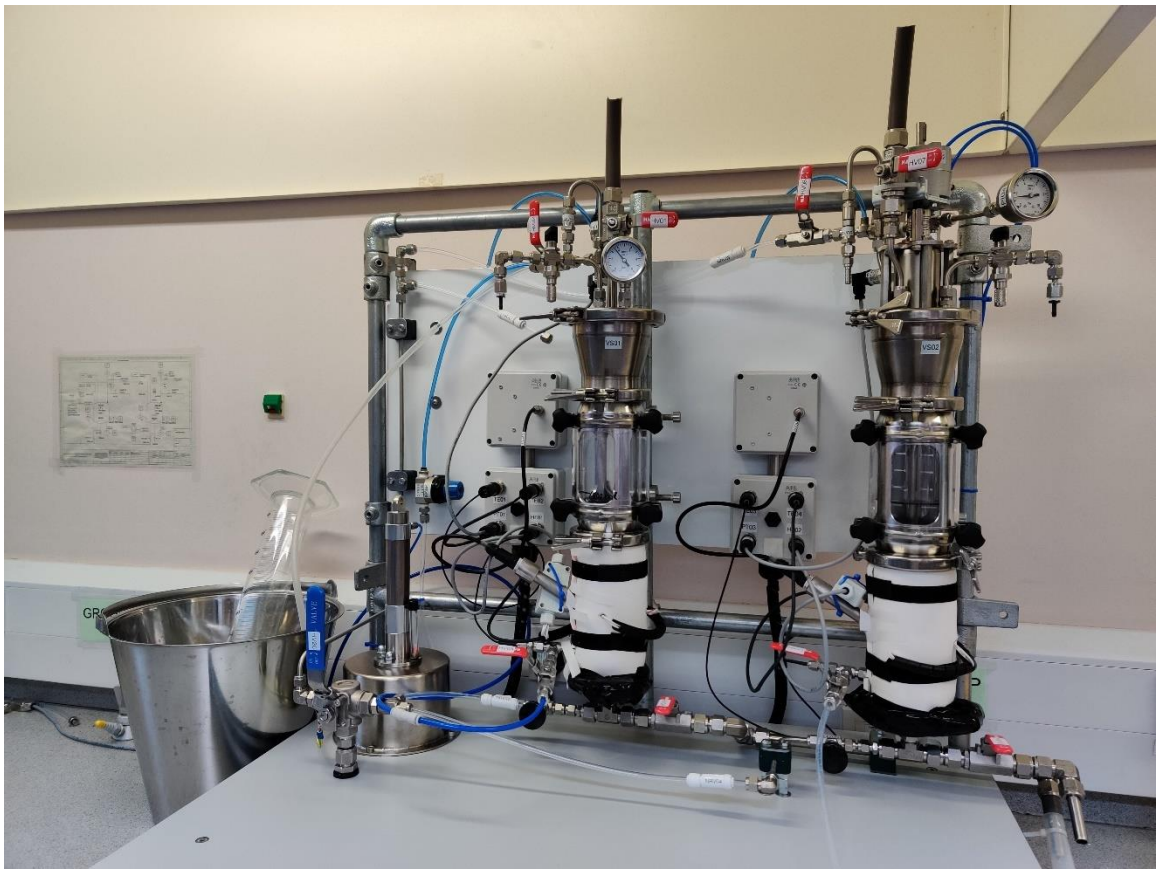

Figure 3.5 – The custom-built twin reactor used for the glucose yeast fermentation experiments. Reactor 1 is the reactor on the left labelled 'VS01'.

3.2.3. Bioreactor for Pressurised Anaerobic Digestion Process of Seaweed

For this research, the goal was to specify a custom bioreactor that can withhold up to 5 barg pressure with a self-sparging system. This reactor must allow feedstocks to be fed, injection of chemicals to maintain the pH at a steady level, sparging biogas accumulated in headspace to the bottom of the reactor for mixing, taking small samples of biogas and sludge for analysis. This bioreactor

must allow online monitoring and recording of key parameters such as temperature, pH value of the culture and the headspace pressure. The design and fabrication of this reactor was in cooperation with Autichem LTD. UK. This bioreactor is a similar design to the one used for glucose yeast fermentation.

The seaweed used for this experiment as feedstock was beach cast seaweed collected from the beach in Anglesey, Wales in March 2018. The reactor used was a custom fabricated reactor made with Borosilicate glass and 316 stainless steel. The total volume of the reactor was 750 ml and it could withhold pressure up to 6.5 barg. A Platinum Resistance Pt100 Class B Sensors with Teflon® Insulated lead in a Stainless Steel Tube (RS Components Ltd., UK) temperature sensor and a sparging port was built at the bottom of the reactor to monitor the temperature of the process and periodically sparge the culture as a substitution of agitation. The pH electrodes used were ecoLine 201005 series pH electrode (JUMO GmbH & CO. KG, Germany), plastic shaft version with push-on protection basket and the glass shaft version. The pH probe was screwed to the centre of the lid of the reactor and it could work in conditions where pressure did not exceed 6 barg. A temperature sensor measuring ambient temperature was attached to the back pole of the stand which was used to hold the reactor in place with a clamp. Both the temperature sensors and the pH electrode were connected to DrDAQ Data logger (Pico Technology Ltd., UK), and the data logger was connected to computer via a USB cable. The condition of the process was monitored and recorded to the computer through the software PicoLog 6 (Pico Technology Ltd., UK).

The pressure sensor used was GS4200-USB Digital Pressure Transducer (ESI Technology Ltd., UK). It was directly connected to the computer via USB cable and the condition in the reactor was monitored and recorded through ESI-USB software (ESI Technology Ltd., UK). The pressure sensor measured the gauge pressure in the headspace – i.e., that above atmospheric. When the lid of the reactor was closed and sealed at the beginning of the fermentation and the headspace pressure was atmospheric, the reading displayed on the software was 0 barg because it was designed to measure the offset from atmospheric pressure. For the safety of the experiment, a safety valve set to 5.5 barg was connected to the same connecting pipe as the pressure transducer. The valve would open and release the excess pressure safely into the fume cupboard if the pressure exceeded 5.5 barg. Furthermore, there was a port on the lid designed for chemical injections to adjust the pH of the process so that the process could maintain at its optimal range as well as feeding biomass. There was also a port at the bottom for taking sludge samples.

The process was designed to achieve self-sparging with the biogas produced and stored in the headspace, but since the process was in equilibrium throughout, PM/31041 Compact air bellows (IMI Norgren, UK) with manual compression was used as an assistance to temporarily store and pump the biogas from headspace to the sparging port at the bottom of the reactor. A three-way valve with a knob switch were connected to bellows where the switch was used to regulate the direction of the biogas flow. When the switch is at the ‘Charge’ position, it opens the inlet pipe and allows the biogas from the

headspace to flow into the bellows while shutting the outlet pipe completely. When the switch is at the ‘Sparge’ position, it opens the outlet pipe and allows the biogas in the bellows to flow into the bottom of the reactor through the sparge port when external force is applied to it while shutting the inlet pipe. The third pipe is connected to a pressure regulator that is set to 6 barg for the safety and protection of the bellows and reactor. The switch should be set to the ‘Charge’ position by default. Figure 3.6 is a photograph of the setup for the reactor and the bellows with manual compression.

Figure 3.6 – The setup of the reactor and the bellows with manual compression.

Since the optimal operating conditions for the hydrolytic bacteria, acidogens, acetogens and methanogens were at 37°C and there was no built-in heat source, an external heat source was required. For the last two runs, a 150 by 200 mm, 12 V dc 30 W silicon heat mat (RS Pro, UK) and a 2455R NC 10 A Bi-Metallic

Thermostat (Honeywell, UK) which opens at 50°C with insulation were used to keep the contents in the reactor from falling to room temperature.

3.2.4. Pressurised Anaerobic Digestion of Pondweed with Twin Bioreactor

The reactor used for this experiment was the same custom-built twin reactor used for glucose yeast fermentation, as shown in Figure 3.5. The total volume for ‘Vessel 1’ on the left was 2080 ml whereas the total volume for ‘Vessel 2’ on the right was 2035 ml because of the space taken up by the blade for mixing. Pondweed was used as feedstock and the sludge containing hydrolytic bacteria, acidogens, acetogens and methanogens were collected from the same pond as the anaerobic digestion of pondweed in the bottle experiments.

3.3. Experimental Procedure

The experiments of anaerobic digestion of pondweed were batch experiments. The objective of these experiments was to determine the relationship between headspace pressure and biogas production. The glucose yeast fermentation experiment was designed to test the hypothesis obtained from the experiments of anaerobic digestion with microalgae since the fermentation process was much shorter and triggered much quicker than the anaerobic digestion process and could be repeated multiple times within a short period. The pressurised

anaerobic digestions of seaweed were performed using the custom designed reactor with multiple sensors and online monitoring to study the effects of headspace pressure on biogas production rate. Identifying the species for the pondweed used in the experiments of anaerobic digestion was a collaboration with Dr Jon Pittman from The University of Manchester. The detailed experimental procedures are described in the following subsections.

3.3.1. Anaerobic Digestion of Pondweed

This experiment was designed to test the hypothesis of this project as well as the simulated results from the model. Some test runs were conducted to learn how long the process would last with different weights of organic loading and then determine which to use. After revealing the duration of all tested loading weights, 6 g/L of dry plants was then designated as the loading weight for all experiments from that point forward.

The weight of dry pondweed was measured with an AX223/E balance (OHAUS Europe GmbH, Switzerland). Both the original laboratory bottles and Erlenmeyer flasks (DURAN Group GmbH, Germany) had a working volume of 500 ml, the amount of pond water used was 400 ml for GL 45 original laboratory bottles and 400, 470 ml for the Erlenmeyer Flask. Therefore, the dry pondweed loading weight was scaled down to 2.4 g. For the original laboratory bottles, the venting frequencies were once per day, once every three days, once a week and once every two weeks with the same head space volume. For the Erlenmeyer flasks,

the venting frequencies were once per day for reactors using 400 ml pond water and once every two days for reactors using 470 ml pond water. The reason for using different amounts of broth was to create different headspace volumes paired with different venting frequencies, was to create noticeable differences in headspace pressure and biogas production. The experiments with all different venting frequencies were run in triplets in case of accidents or mistakes.

60 ml of bacteria containing sludge were measured and used in each reactor. Once all these ingredients were all added to the reactors, the caps were then screwed till airtight, minimising the biogas loss from leakages while they were not vented. Next, all reactors were gently swirled, ensuring the dry microalgae were well mixed and had sufficient contact with the bacteria. Lastly, all the reactors were placed in a metal basket which was then put into a Shaking water bath OLS200 (Grant Instruments Ltd., UK) to provide the mixing required for the process. The speed of the shaker was set to 60 RPM and shaking was turned on throughout the entire experiment and the temperature remained at room temperature.

3.3.2. Glucose Yeast Fermentation

As the anaerobic digestion process is rather time consuming, a quick way to discover how pressure affects the solubility of carbon dioxide as well as gas production rate is to examine glucose yeast fermentation due to its fast response time and short duration compared to anaerobic digestion.

For the experiment, 50 grams of glucose and 30 grams of yeast were used, and they were measured with the AX223/E balance (OHAUS Europe GmbH, Switzerland). They were poured into beaker 1 with 2 litre capacity and thoroughly mixed. Next, water at 41°C (±1°C) was prepared in a measuring beaker with 2 litre capacity. Then a portion of the water was poured into beaker 1 and stirred until the solution was evenly mixed and poured into reactor 1. After that, another portion of the water was poured into beaker 1 to rinse the residue and poured into reactor 1. Lastly, the rest of the water was poured into reactor 1 till the solution reached the 1 litre mark on the reactor. Since the reactor was kept at room temperature of 20°C, the temperature of the mixture dropped to 35-37°C after it was poured into the vessel just before the lid was sealed, which was the ideal temperature for glucose yeast fermentation (Jones and Hough, 1970). The reactor was then sealed and connected to the inverted measuring cylinders filled with water through plastic pipe to collect the carbon dioxide at various headspace pressures measured by the pressure sensor displayed on the control panel and on top of the reactor.

Another experiment was conducted to determine, by extrapolation, at what pressure the glucose and yeast fermentation would completely stop producing carbon dioxide. For this experiment, the relief valve remained closed throughout the fermentation process and the headspace pressure was recorded every five minutes.

3.3.3. Pressurised Anaerobic Digestion Process of Seaweed

The objective of this experiment was to run an anaerobic digestion process above atmospheric pressure in the custom fabricated reactor with some built-in sensors. With the assistance of some software, online monitoring of the process was achieved. Once the digestion process had finished, the composition of the biogas was analysed and compared to conventional biogas produced at atmospheric pressure to determine whether it could be feasible as a replacement for the traditional biogas upgrade processes.

For the preliminary experiments, the process was run at atmospheric pressure, with inoculum and biomass concentration remaining the same as they were when ran with original laboratory bottles and Erlenmeyer flasks, to examine how well the new reactor would work. Both the seaweed and inoculum used contained 5% volatile solids (VS) for each run. 50 ml of inoculum with a concentration of 50 grams VS per litre, 70 ml of blended seaweed with a concentration of 40 grams VS per litre, 380 ml of distilled water and no buffer solution were used to make up the 500 ml during the first run. For the second test run, the ratio of seaweed to inoculum was 1:1 with 70 ml and a concentration of 50 grams VS per litre each, 225 ml buffer solution with 90% weak acid sodium hydrogen carbonate ($NaHCO_3$) and 10% conjugate base sodium carbonate ($NaCO_3$) both at a concentration 0.1 mol/l and 135 ml distilled water was used. To create the anaerobic environment,

inert gas argon (Ar) was used to flush the oxygen out of the headspace for 5 minutes through the sparging port at the bottom of the reactor.

From the third run forward, it was decided to increase the amount of both seaweed and inoculum. The new seaweed to inoculum ratio was 3:2, with 30 grams of seaweed and 20 grams of inoculum in order to intensify the process. In this run, the seaweed used contained 58.8 grams VS per kilogram (wet) and the inoculum used contained 53.3 grams VS per litre. To achieve that ratio in with 500 ml content, the seaweed needed was $\frac{15\ g}{58.8\ g/kg} = 255\ g$, and the inoculum required was $\frac{10\ g}{53.3\ g/l} = 187.6\ ml$. Since the contents increased, the concentration of buffer solution had to increase while the volume was reduced in order to maintain the pH at an optimised level. The buffer used was 45 ml with a concentration at 0.5 mol/l. The ratio of sodium hydrogen carbonate to sodium carbonate stayed the same. Argon was used to rinse out the oxygen in headspace for 5 minutes as well as to charge up the headspace to 1.0285 barg at the beginning of processing. For the fourth run, the seaweed concentration was 75.6 grams VS per kilogram (wet) and the inoculum was 40.12 grams VS per litre, therefore, the amount of seaweed required was $\frac{15\ g}{75.6\ g/kg} = 198.4\ g$ and the amount of inoculum needed was $\frac{10\ g}{40.12\ g/l} = 249.3\ ml$. The buffer solution used was the same as the third run and argon gas was used to flush the oxygen out of the headspace for 5 minutes. For the fifth run, the amount and concentration of seaweed used was the same as the fourth run and the concentration of inoculum

was 43.16 grams VS per litre. Hence, the amount required was $\frac{10\ g}{43.16\ g/l} = 231.7\ ml$.

As previously mentioned, sparging was achieved with the assistance of a bellows with manual compression. First of all, biogas from headspace flowed to the bellows through ‘NRV-01’ (see Figure 3.11) when ‘HV-02’ was switched open and pressure in headspace dropped. The valve was then switched off when the pressure in the headspace of the reactor and the bellows reached equilibrium. Next, the knob switch was switched to ‘Sparge’ position and the valve ‘HV-03’ was opened. And then, the handle was used to press the platform resting on top of the bellows down and pushed the biogas out of it into the bottom of the reactor through the sparging port to create the mixing it required. While the platform was held down with the handle, the valve ‘HV-03’ was switched off before releasing the handle and letting the bellow bounce back. Lastly, the knob switch was switched back to ‘Charge’ position.

3.3.4. Pressurised Anaerobic Digestion of Pondweed with Twin Bioreactor

The objective of this experiment was to test the hypothesis of this project by comparing the biogas composition of anaerobic digestion running at atmospheric pressure and elevated pressure.

For the first run, the total volume of culture was determined to be 1300 ml, then the corresponding headspace volume was 780 ml. Following the food ratio from previous experiment of 6 g/l, the feed needed for this experiment would be 7.8 grams of dry plants. It was measured with the AX223/E balance (OHAUS Europe GmbH, Switzerland) and was roughly grinded with a pestle and a mortar before being put into vessel 1. Next, a full laboratory bottle of sludge containing hydrolytic bacteria, acidogens, acetogens and methanogens was poured into the same vessel. Two portions of 200 ml of deionised water were subsequently used to rinse the laboratory bottle in order to get the remaining sludge to the reactor. After that, more deionised water was poured into the reactor until it reached the marked line on the plastic sleeve of the reactor so that the total volume of the culture was 1300 ml before the lid was put on. Lastly, compressed air was pumped from the bottom of the reactor for 10 seconds to provide mixing before the reactor was fully sealed.

For the second run, 380 ml more sludge containing hydrolytic bacteria, acidogens, acetogens, methanogens and 15 grams of feed were added to the reactor to reduce the headspace volume so that the headspace pressure could get higher for a given amount of biogas production. Vessel 2 was also used to run an experiment with similar conditions to the second run in Vessel 1. The remaining dry plants weighed 9.7 grams were roughly grinded with a pestle and a mortar, then put into vessel 2. A litre of sludge containing hydrolytic bacteria, acidogens, acetogens and methanogens was poured into vessel 2 and the remaining sludge was rinsed with deionised water and poured into vessel 2.

Next, more deionised water was poured into vessel 2 to make the total volume of culture in vessel 2 to 1635 ml, which would leave the vessel with 400 ml of headspace volume when the top of the reactor with the mixing blade was put back in. Lastly, compressed air was pumped through the bottom of vessel 2 for 30 seconds to mix the culture before all the valves were shut to seal the reactor properly.

3.4. Analysis Methods

3.4.1. Anaerobic Digestion of Pondweed

The composition of biogas is normally 60-70% methane, 30-40% carbon dioxide on a molar basis with some trace gas in the mix (Petersson & Wellinger, 2009). Due to the lack of equipment to measure the exact composition of biogas produced, the composition of biogas was assumed to be one third carbon dioxide and two thirds methane (molar basis) with other trace gas being completely neglected to simplify the calculation.

The amount of biogas produced was measured by the difference in weight of each reactor before and after venting. The average molar mass of biogas produced would be

$$M_{ave} = \frac{1}{3} M_{CO_2} + \frac{2}{3} M_{CH_4} \ (g/mol)$$

$$M_{ave} = \frac{1}{3} \times 44 + \frac{2}{3} \times 16 \ (g/mol)$$

$$M_{ave} = 25.33 \ (g/mol)$$

The increase in headspace pressure just before venting could be calculated using Ideal Gas Law

$$PV = nRT \quad Eqn.3.3$$

where *P* is change in headspace pressure measured in bar, *V* is the headspace volume measured in litres, *n* is loss in biogas after venting measured in mol, *R* is the gas law constant, which is $0.00831\ \mathrm{L \cdot bar/(mol \cdot K)}$ and *T* is the operating temperature, which is 293.15K (at room temperature 20°C).

$$n = \frac{\Delta m}{M_{ave}} \quad Eqn.3.4$$

where Δm is the mass of gas vented, measured in grams using LA4200S balance (Sartorius Stedim Plastics GmbH, Germany). By substituting Eqn. 3.4 into Eqn. 3.3 and rearranging it, the change in headspace pressure ΔP could be calculated with the following equation, where V_{gas} is the headspace volume of the reactor measured in litres.

$$\Delta P = \frac{\frac{\Delta m}{M_{ave}} RT}{V_{gas}} \quad Eqn.3.5$$

The average elevation in headspace pressure $\Delta \bar{P}$ over the course of a series of venting events can be calculated using Eqn. 3.6, where ΔP_j is the increase in headspace pressure before each venting event j, Δt_j is number of days elapsed between each venting and t is the number of days elapsed since the start of the experiment.

$$\Delta \bar{P} = \frac{\frac{1}{2}\sum_0^j \Delta P_j \Delta t_j}{t} \quad Eqn.3.6$$

The average amount of biogas produced per day $\bar{V}$ (in ml/day) could also be calculated through the rearranged ideal gas law equation demonstrated as follow

$$\bar{V} = \frac{\frac{m_T}{M_{ave}} RT}{P_{atm} t} \times 10^3 \quad Eqn. 3.7$$

where m_T is total biogas produced in weight measured in grams, P_{atm} is the headspace pressure just after venting, which is equal to atmospheric pressure. This method of measurement would work based on the following reasons. Raoult's law states that in an ideal mixture of liquid, the partial pressure of each component is equal to the vapour pressure of the pure component multiplied by its mole fraction in the mixture. In each reactor, water was the major component. The partial pressure of water was supposed to be high. However, according to Wexler's calculation (1976), the water vapour pressure at 20°C is 2338.54 Pa, which was less than 1% of the total pressure achieved, hence, neglected. The next most abundant volatile component in the liquid phase was likely to be acetic acid but, being present in very low quantities, was therefore ignored.

3.4.2. CO_2 Production Rate for Glucose Yeast Fermentation

Since this was the alternative, faster process to anaerobic digestion with microalgae to determine how headspace pressure affects biogas production, there was a valve on top of the pressure gauge to control headspace pressure. Firstly, it was set to remain open throughout to determine how much carbon dioxide the fermentation process would produce without the influence of

headspace pressure. Next, the valve was set to remain closed until pressure reached 0.4, 0.8, 1.0 and 1.2 barg and then it would be slightly cracked open to collect carbon dioxide produced and retained in headspace equivalent to 0.2 barg pressure and its volume was measured. The carbon dioxide was collected using inverted measuring cylinders filled with water as demonstrated in Figure 3.5. Measurements from these experiments were taken during the first 70 minutes of the fermentation since this was its most active period. The timing started from the moment when the top section of the reactor with the pressure sensor and valves was put back onto the vessel. The time taken to collect 1 litre of carbon dioxide when the valve remained open throughout, the volume of carbon dioxide collected during each venting when there was a target pressure to achieve, the time taken to reach the target pressure, and the total amount of carbon dioxide collected through the first 70 minutes of each fermentation were all recorded.

3.4.3. Pressurised Anaerobic Digestion Process of Seaweed

The ideal gas law was used to determine the amount of biogas produced. The headspace volume remained the same at 0.25 L for all the experiments. The temperature of the culture started warm, with the inoculum started at 37°C (310.15 K) and seaweed started at 20°C (293.15 K), then eventually dropping to 20°C (293.15 K) as the experiment went on. The universal gas constant was

0.0831 $L \cdot bar/(mol \cdot K)$. Because of the characteristic of gas, it would always occupy the entire headspace regardless of the amount of biogas produced, the specific volume would always be 0.25 L. By applying and rearranging the ideal gas law equation, the amount of biogas produced in moles could be calculated with

$$n = \frac{PV_{specific}}{RT} \quad Eqn. 3.8$$

where the pressure was recorded via the pressure sensor. To calculate the actual volume of biogas produced under atmospheric pressure, rearrange the equation and substitute the pressure *P* with atmospheric pressure, which is 1.01325 bar, giving:

$$V_{actual} = \frac{nRT}{P_{atm}} \quad Eqn. 3.9$$

After the experiment, the remains were collected for further analysis. The analyses included measuring the weight of total solids and volatile solids (TSVS analysis), soluble protein analysis using the Lowry method and soluble carbohydrate analysis using the Anthrone method and VFA analysis. All these analyses were performed following the protocols (Blue Sky Bio [BSB], 2018). These analyses were performed in triplicates and the results averaged. For protein and carbohydrate analysis, the samples were put in a centrifuge at 5000 RPM for 20 minutes to separate liquid from solids, the liquid part was kept for the analysis while the solids were thrown away.

For TSVS analysis, 25 ml from the remains of the digestor were taken out and weighed in dishes to determine the weight of wet samples. Next, the samples were put in an oven at 105°C overnight to vaporise the water, then the samples were taken out to cool down and weighed again to determine the weight of total solids. After that, the samples were put in a furnace at 550°C for two hours to burn out all the volatile solids. Lastly, the samples were taken out to cool down in air and weighed again to determine the weight of ashes (inorganics). The weight of volatile solids was then calculated by subtracting the weight of inorganic from total solids.

For protein analysis using the Lowry method, two reagents were used. The first reagent was a mixture of 143 mM sodium hydroxide ($NaOH$) with 270 mM sodium carbonate (Na_2CO_3), 57mM copper (II) sulphate ($CuSO_4$) and 124mM sodium tartrate ($Na_2C_4H_4O_6$). The ratio of this mixture was 100:1:1 accordingly. The second reagent was diluted Folin reagent with Folin to distilled water ratio of 5:6. For the first step, 0.5 ml sample or bovine serum albumin with known concentration and 0.7 ml reagent 1 were added to the test tubes and mix well. Next, 0.1 ml diluted Folin reagent was added to the test tube and mix well. Then the solutions were left to rest in room temperature for 45 minutes. Lastly, the absorbance was measured at 750 nm using LAMBDA 35 UV/Vis Spectrophotometer (PerkinElmer Inc., USA). The results were compared to the standard curve of absorbance created by a series of diluted bovine serum albumin from its original concentration of 2 g/l. These diluted bovine serum

albumin solutions were prepared in volumetric flasks of 100 ml with target concentration of 20, 60, 100 and 200 mg/l.

In the carbohydrate analysis using the Anthrone method, the reagent used was a solution of 0.125% Anthrone weight to volume ratio (w/v) and 94.5% sulphuric acid (H_2SO_4) volume to volume ratio (v/v). The standard curve of absorbance was established using glucose solutions with concentrations of 0, 5, 10, 50 and 100 mg/l. For the first step, 0.8 ml sample or glucose solution with known concentration and 1.6 ml reagent solution were added to the test tubes and mix well. Next, the test tubes were sealed with rubber stoppers and placed in a water bath at 100°C for 14 minutes. After that, they were placed in another water bath at 4°C for 5 minutes. Lastly, the absorbance of the samples was measured using LAMBDA 35 UV/Vis Spectrophotometer (PerkinElmer Inc., USA) at 625 nm and compare the results to the standard curve of absorbance.

The biogas composition for the last two fermentations was analysed with The Rapidox 5100 Portable Gas Analyser (Cambridge Sensotec, UK). This analyser is capable of analysing biogas and syngas components including: $CO_2, CO, H_2O, O_2, C_2H_4, SO_2, CH_4, H_2$ and H_2S. A piece of plastic tube with an adapter was used to connect the right end of the filter unit to the analyser as displayed in Figure 3.7. The left end of the filter unit was connected to the exit port for biogas from the bioreactor through another piece of plastic tube with an adapter. When the valve was switched on and the gas was flowing into the analyser, the monitor displayed the composition of the gas. The result can be

printed on a slip of paper once the analysis is finished by pressing ‘Print’ on the touch screen monitor.

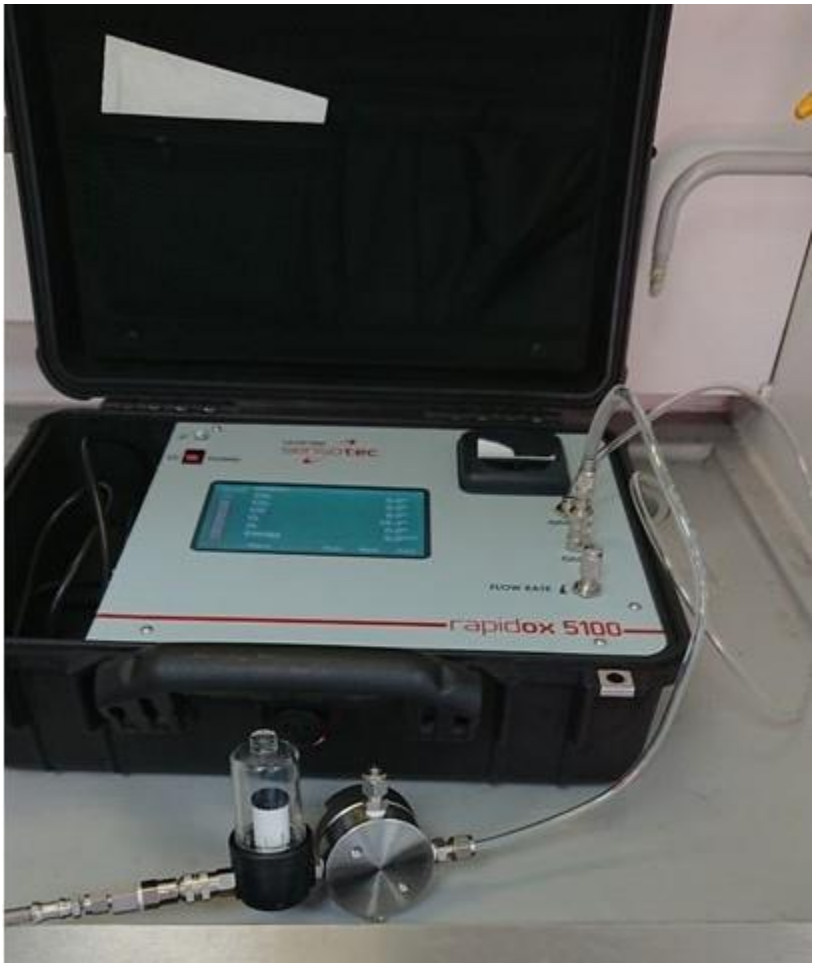

Figure 3.7 – A photograph of Rapidox 5100 Portable Gas Analyser with the filter connected.

3.4.4. Pressurised Anaerobic Digestion of Pondweed with Twin Bioreactor

The key parameters of the experiment, such as headspace pressure, were recorded by the on-board memory of the control platform of the system, set to log

once every ten minutes. The recorded data could then be downloaded to a computer for further analysis. Once the headspace pressure reached the targeted level, the biogas was directly drawn from the needle valve on the top of the reactors and the composition of the biogas was analysed by the Rapidox 5100 Portable Gas Analyser (Cambridge Sensotec, UK), as shown in Figure 3.7. Note that the volume of gas that was required to be withdrawn for sampling was a significant fraction of the headspace volume, which therefore resulted in a large reduction in the headspace pressure.

It is instructive to perform a mass balance for each gas species for two reasons:

1. To estimate the relative production of biogases (methane and carbon dioxide) between each venting (sampling) event. These production amounts could be expected to be reasonably constant and in the same ratio in the steady phase of anaerobic digestion since they are determined by the metabolic pathways of the bacterial consortium in the reactor.
2. To estimate the actual value of the Henry's constant which determines the distribution of the gaseous species between the liquid and gas compartments of the reactor. This is likely to be significantly less than the value for pure water due to the competing presence of other dissolved species (other gases, salts, sugars, acids etc.) in the digestate.

Figure 3.8 gives the 3 key reactor states that are used to develop the mass balance which are cycled through repeatedly for each venting/sampling event. In the first state, just before the sampling, the reactor is pressurised with the liquid and gas compartments in equilibrium as determined by Henry's law. During

sampling we make the important assumption that no desorption occurs from the liquid phase since the duration of the sampling is relatively short (1-2 minutes) and the liquid phase appears to be quiescent during this time. This means that, on completion of sampling and resealing the headspace at the new lower pressure, the mole fractions in the headspace and concentrations in the liquid phase remain constant at their pre-venting values.

State 2, therefore, just after venting, represents a non-equilibrium situation whereby there is an excess concentration of each gaseous species in the liquid which therefore gradually desorb over 1-2 hours to restore equilibrium and go into state 3 in which the headspace pressure is slightly higher than that in state 2 (pressure recovery). We can make the further reasonable assumption that the total mass of each species in the reactor in state 3 is unchanged from state 2 since the rate of generation of biogases due to fermentation is slow compared to the rate of restoration of gas-liquid equilibrium. We can therefore employ the mass balance and the Henry's law relationship to calculate the new pressure and concentrations in state 3.

Critically, by comparing the calculated value of the recovered headspace pressure in state 3 to the actual measured value, we can treat the Henry's law constant as an adjustable parameter that can be inferred in order to make the calculated value agree with the measured value.

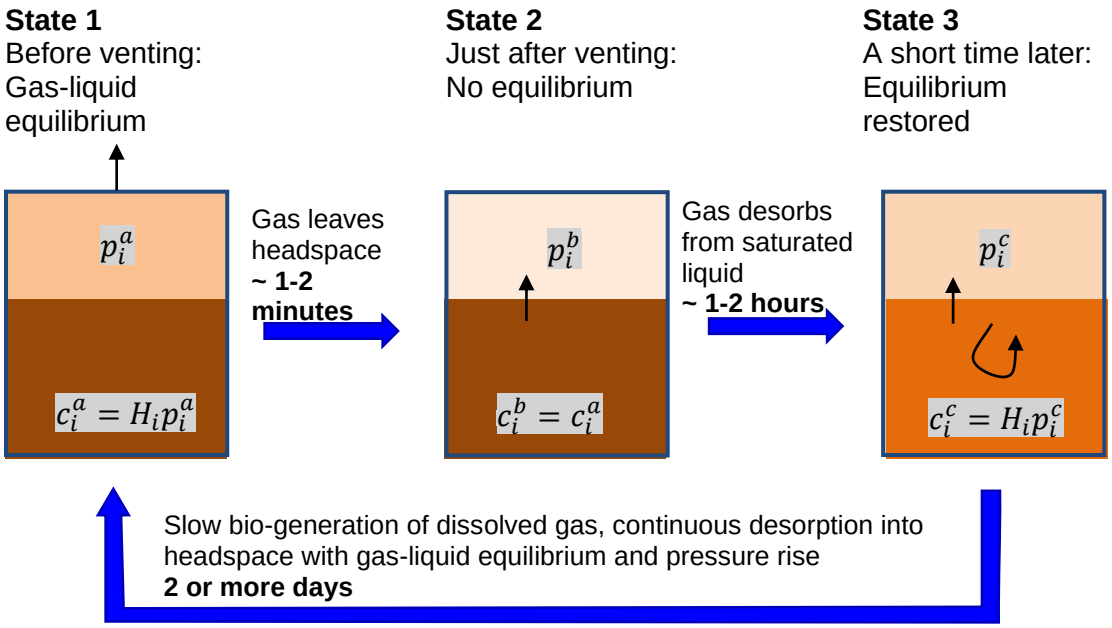

Figure 3.8 – Three different states of each bioreactor which apply for each sampling/venting event.

For the first stage, biogas composition is detected by the gas analyser, which involves venting the reactor headspace for 1-2 minutes by manually opening needle valve NV-06. The headspace pressure forces the headspace gas into the sampling line for the analyser, where it flushes the existing gas (air or the previously sampled gas) from the sampling line and 1-2 minutes are required until the reading becomes steady. The partial pressure of each gas in headspace is given as follows:

$$p_i^a = P^a x_i \quad Eqn\ 3.10$$

where p_i^a is the partial pressure of each gas i in the headspace, P^a is the total pressure in the headspace and x_i is the fraction of each gas in the headspace as

reported by the gas analyser. Assuming ideal gases, the mass of each gas $m_{i,g}^{a}$ in the headspace in state 1 is calculated by:

$$m_{i,g}^{a} = \frac{M_i \, p_i^a V_g}{RT} \quad Eqn\ 3.11$$

where M_i is the molar mass of each gas, V_g is the headspace volume, T is the operating temperature $(295.15\ K)$ and R is the gas constant $(8.314\ J \cdot K^{-1} \cdot mol^{-1})$. The concentration of each gas dissolved in the liquid just prior to venting c_i^a can be calculated by assuming gas-liquid equilibrium:

$$c_i^a = H_i \, p_i^a \quad Eqn\ 3.12$$

where H_i is the Henry's law constant. The mass of each gas dissolved in the liquid $m_{i,l}^{a}$ is then be calculated by:

$$m_{i,l}^{a} = M_i c_i^a V_l = M_i H_i \, p_i^a V_l \quad Eqn\ 3.13$$

where V_l is the total volume of the culture. Therefore, the total mass m_i^a of each gas species contained within the reactor headspace and liquid in state 1 is as follows:

$$m_i^a = m_{i,g}^{a} + m_{i,l}^{a} = \frac{M_i \, p_i^a V_g}{RT} + M_i H_i \, p_i^a V_l = M_i \, p_i^a \left(\frac{V_g}{RT} + H_i \, V_l\right) \quad Eqn\ 3.14$$

Mention should also be given to the mass of each gas that leaves the headspace during the venting since this represents the production of biogas and the mass that leaves the closed system:

$$s_i = \frac{M_i \, V_g}{RT}\left(p_i^a - p_i^b\right) = \frac{M_i \, V_g x_i}{RT}\left(P^a - P^b\right) \quad Eqn\ 3.15$$

For state 3, the liquid-gas equilibrium is restored and, assuming no biogas was produced during this time, the total mass of each gaseous species in the reactor in state 3 m_i^c is the same as in state 2. Introducing the corresponding variables for the distribution of the total mass between the mass in the liquid $m_{i,l}^a$ and the mass in the gas $m_{i,g}^a$ we can therefore write the following:

$$m_i^c = m_{i,g}^c + m_{i,l}^c = m_i^a - s_i \quad Eqn\ 3.16$$

Since Henry's law applies, the total mass of each gas species in reactor in state 3 as calculated from the sum of the masses in the gaseous and dissolved states is given by an equation that is entirely analogous to Eqn 3.14. The only difference is that we need to change the superscripts to 'c' to denote state 3 which yields the following:

$$m_i^c = M_i\, p_i^c \left(\frac{V_g}{RT} + H_i\, V_l\right) \qquad Eqn\ 3.17$$

Since, for state 3, the objective is to calculate the partial pressure from the total mass (rather the other way round as previously for state 1), and therefore the total restored headspace pressure we can re-arrange Eqn 3.17 to make the partial pressure of each gas the subject and then sum them to give P^c - the total pressure predicted headspace pressure in state 3:

$$P^c = \sum_i p_i^c = \sum_i \left\{ \frac{m_i^c}{M_i \left(\frac{V_g}{RT} + H_i\, V_l\right)} \right\} \qquad Eqn\ 3.18$$

Systematic application of Eqns 3.10, 3.14, 3.15, 3.16 and 3.18 therefore provide a means to estimate the recovered headspace pressure P^c in state 3 based on the measured values of:

1. the mole fractions of each gas in the headspace x_i which are assumed to be constant during sampling and therefore the same in state 1 (prior to sampling) and in state 2 (immediately following sampling).
2. the total pressure in the headspace P^a and P^b in states 1 and 2 respectively.

As discussed later in the results in section 4.5.1, the recovered pressure in state 3 for each sampling event tends to be much less than the predicted values calculated using Henry's constant for gases dissolved in pure water. Comparison of the inferred and predicted values therefore provides a means to infer the real value of the effective Henry's constant for biogas solubility in digestate.

4.*Results and Discussion*

Several different types of experimental result are described in the section. Firstly, both models are discussed in section 4.1. This includes verifying the reproduced MAD model, modifying the reproduced model to fit the experimental work in chapter 4.2, adjusting the maximum specific growth rate parameters of the modified model to get an estimation of the bacteria growth rates in the experimental work as well as the effects of headspace pressure on biogas production and biogas content. Next, the laboratory-scale experimental work is discussed in section 4.2. This includes how venting frequencies and headspace volume can affect the headspace pressure and biogas production. After that, the results for an alternative experiment of a biological process which yields biogas with faster and shorter response time is discussed in section 4.3. In section 4.4, the results for the pressurised anaerobic digestion using a custom fabricated reactor with online monitoring is discussed. Lastly, section 4.5 discusses the results of pressurised anaerobic digestion of pondweed with twin bioreactor. Application of a mass balance to analyse the measured headspace composition and pressure data allows for some interesting findings.

All the simulations and all the experiments with 500 ml laboratory-scale bottles and custom-fabricated reactors were performed with initial headspace pressure at atmospheric pressure (unless specified at the beginning of the corresponding results section).

4.1. Computational Modelling

4.1.1. Model Verification

Figure 4.1 demonstrates how the results of model simulations in CellDesigner are presented as a plot of the concentration or amount of the reactants and products from the reactions involved against time.

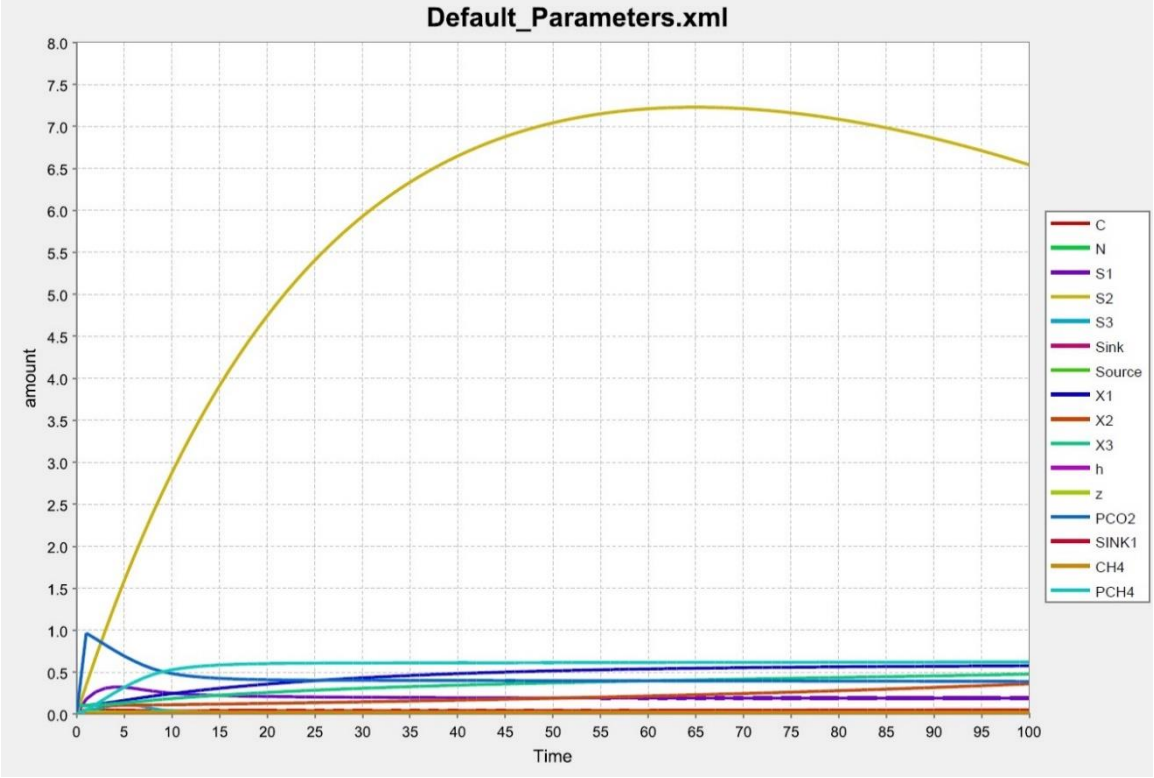

Figure 4.1 – Variation of MAD model state variables over time as presented in CellDesigner.

The agreement between the published steady state variable in the original MAD model and the model reproduced in CellDesigner was very close. In the MAD model, the pH of the system was 7 during the steady-state period, whereas the adapted model in CellDesigner was 6.7. The methane content in the MAD model

was approximately 62%, whereas, in the adapted model in CellDesigner, it was 62.5%. The biogas flow rate in the MAD model was approximately 0.1 litre per day and in the adapted model in CellDesigner it was also 0.1 litre per day. Table 4.1 compares the key results of the MAD model and the adapted model.

Table 4.1 – Comparisons of some key results between the MAD model and the adapted model.

	MAD Model	Adapted Model
pH	7	6.7
Methane Content	62%	62.5%
Biogas Flowrate	0.1 litre	0.1 litre

k_p is the pipe resistance coefficient which regulates the amount of produced biogas leaving the system. The default value in the MAD model is 50000, which means the reactor does not significantly contain the biogas produced in the reactor to create pressure in the headspace. To determine whether the *'k_p'* from the reproduced MAD model and *'k_{p1}'* from the modified model would be the parameter to create headspace pressure, some tests were run and the results were summarised in Table 4.1. The simulations for the modified MAD model with adjustable pipe resistance were kept constant throughout each run. *'P_{total}'* represents the overall headspace pressure, which is made up of only CO_2 and CH_4, *'P_{CH_4}'* represents the partial pressure of CH_4 in the headspace, and *'$\%\ CH_4$'* represents the methane content in headspace as a percentage. When k_p and k_{p1} are both greater than 5, there is barely any pipe resistance for the effluent gas,

therefore, the effects on total pressure and CH_4 content are negligible. As they are both decreased further, their effects on total headspace pressure and CH_4 content become more significant.

Table 4.2 – The summary of how the values of 'k_p' and 'k_{p1}' can affect the headspace pressure and the content of biogas produced.

Reproduced MAD Model				Modified MAD Model			
k_p	P_{total}	P_{CH_4}	% CH_4	k_{p1}	P_{total}	P_{CH_4}	% CH_4
50000	1.013	0.633	62.5	50000	1.013	0.633	62.4
5000	1.013	0.633	62.5	5000	1.013	0.633	62.4
500	1.014	0.634	62.5	500	1.014	0.633	62.4
50	1.019	0.637	62.5	50	1.019	0.636	62.5
5	1.073	0.672	62.6	5	1.070	0.669	62.6
0.5	1.451	0.920	63.4	0.5	1.433	0.906	63.2
0.05	3.019	2.006	66.4	0.05	2.943	1.939	65.9
0.005	7.878	5.828	74.0	0.005	7.516	5.462	72.7

4.1.2. Comparing the Model to Experimental Results

The default maximum specific growth rates from the MAD model and the physico-chemical parameters from the laboratory-scale experiments were applied to the modified model. In order to test whether the model would produce results that concur with laboratory-scale experiments, eight simulation conditions which resembled the experiments were required. Simulations were run with volume of culture V_{liq} = 400 ml and 470 ml and headspace volume V_{gas} = 140 ml and 70 ml respectively. The venting frequencies are every 2, 3, 5 and 10 days. Table 4.3 demonstrates these eight conditions with their corresponding order of simulation.

Table 4.3 – The eight conditions of simulations with their respective order of simulation.

	Venting Once Every 2 Days	Venting Once Every 3 Days	Venting Once Every 5 Days	Venting Once Every 10 Days
$V_{gas} = 140\ ml$	1	2	3	4
$V_{gas} = 70\ ml$	5	6	7	8

Once the simulation for one of these eight conditions was finished, the biogas produced just before each venting, which were the maximum values for partial pressure of CH_4 and CO_2, would be highlighted and copied to Excel, under columns labelled 'P_{CH_4}' and 'P_{CO_2}' respectively. Then, by utilising Eqn 3.1 and 3.2 derived from Ideal Gas Law equation, demonstrated in chapter 3.1.3, the biogas produced in terms of mass could be calculated. Eqn 3.6 and 3.7 illustrated in chapter 3.4.1 could be used for calculating the average headspace pressure and biogas production rate in ml/day for each simulation. Once they were all calculated, a table of these figures could be generated, like the table demonstrated in Figure 4.2.

Model with Experimental Parameters								
Bottle No.	1	2	3	4	5	6	7	8
Δm (g)	3.89	2.85	2.14	1.53	1.95	1.46	1.13	0.85
Average Pressure (barg)	0.58	0.64	0.80	1.16	0.61	0.68	0.89	1.34
l per day (ml)	93.59	68.41	51.42	36.88	46.78	35.06	27.26	20.34

Figure 4.2 – Results of the model simulation using maximum specific growth rates from the MAD model, the physico-chemical parameters from the laboratory-scale experiments and simulation conditions that resembled the laboratory-scale experiments.

The result of model simulations was put onto the same graph with the laboratory-scale experiments to determine whether they concur or not. As demonstrated in Figure 4.3, the modified model and the laboratory-scale experiments concurred as the accumulated headspace pressure increased, it reduced the rate of biogas production rate. However, the modified model produced more biogas and accumulated higher headspace pressure than the laboratory experiments.

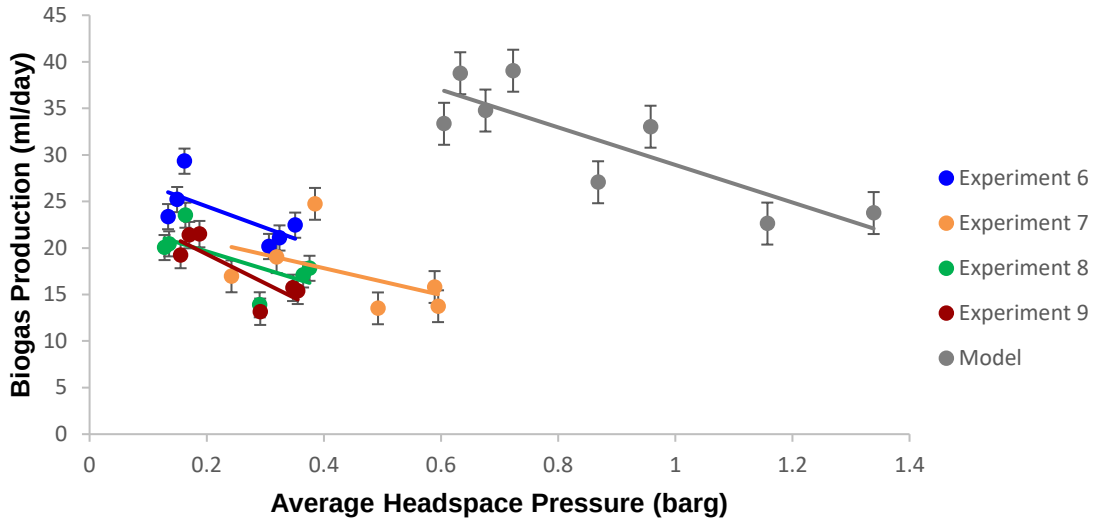

Figure 4.3 – How the rate of biogas production is affected by the average headspace pressure. The result of modified model simulations demonstrated in Figure 4.2 agrees with the results from laboratory-scale experiments. Each dot represents one bioreactor or one simulation of the model with certain headspace volume and venting frequency. The straight lines are the added trendline of each data set.

For the modified model to produce similar results as the experiments, the maximum specific growth rates $\bar{\mu}_1$, $\bar{\mu}_2$ and $\bar{\mu}_3$ would have to be modified.

4.1.3. Tailoring the Model to the Experiments

The major outputs monitored were rather similar and the trend of decreasing biogas production rate with increasing headspace pressure matched between the modified model and the laboratory-scale experiments. The next step was to adjust the maximum specific growth rates of the bacteria $\bar{\mu}_1$, $\bar{\mu}_2$ and $\bar{\mu}_3$ in the modified model for all eight simulating conditions listed in Table 4.3 to try and match the biogas production rate from the experiments in order to obtain the growth rates for the bacteria used.

Figure 4.4 is a demonstration of how different maximum specific growth rates affect the biogas production rate and accumulated headspace pressure of the modified model. The straight lines were the corresponding trendline to its set of data with the same colour. When $\bar{\mu}_1$, $\bar{\mu}_2$ and $\bar{\mu}_3$ were all increased by 10% simultaneously, the biogas production rate and the accumulated headspace pressure increased slightly. When $\bar{\mu}_1$, $\bar{\mu}_2$ and $\bar{\mu}_3$ were all reduced by 50%, 60%, 70% and 80% sequentially, the biogas production rate and the accumulated headspace pressure decreased accordingly as well as the gradient of the trendlines kept getting steeper, as illustrated in Figure 4.4. However, when $\bar{\mu}_1$, $\bar{\mu}_2$ and $\bar{\mu}_3$ were reduced by 90%, as displayed by the green dots and the green straight line, the trend reversed so more biogas would be produced at higher headspace pressure.

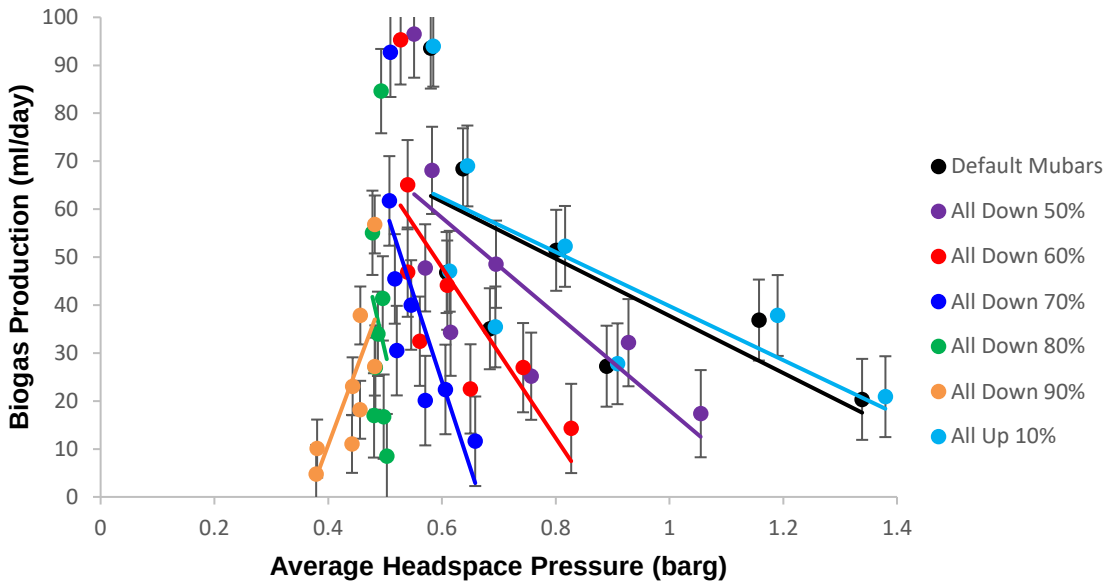

Figure 4.4 – The effects of maximum specific growth rates of bacteria have on biogas production rate and average headspace pressure for each simulation. Black represents the default values from MAD model, purple represents all values reduced by 50% simultaneously, red (all reduced by 60%), yellow (all reduced by 70%), blue (all reduced by 80%), green (all reduced by 90%) and orange (all increased by 10%). Each dot represents one simulation of the model with certain headspace volume and venting frequency. The straight lines are the added trendline of each data set.

Surprisingly, the simulation results from reducing maximum specific growth rates were unexpected in that each simulation had one data point that was extremely high and isolated from the rest. The effects these adjustments had on maximum specific growth rates had on the partial pressure of methane and carbon dioxide during the anaerobic digestion process needed to be investigated.

The partial pressure of methane and carbon dioxide with various maximum specific growth rates from the simulations are demonstrated in Figures 4.5 to 4.8. When headspace volume was 140 ml and 70 ml with default maximum specific

growth rates from MAD model, the partial pressure of methane overtook carbon dioxide in six days to become the main composition, as demonstrated in the Figures 4.5 and 4.6 respectively. Bioreactor with headspace volume of 70 ml had a steeper drop for partial pressure after each venting compared to 140 ml. As the simulation continued, the partial pressure of methane and carbon dioxide reached steady state.

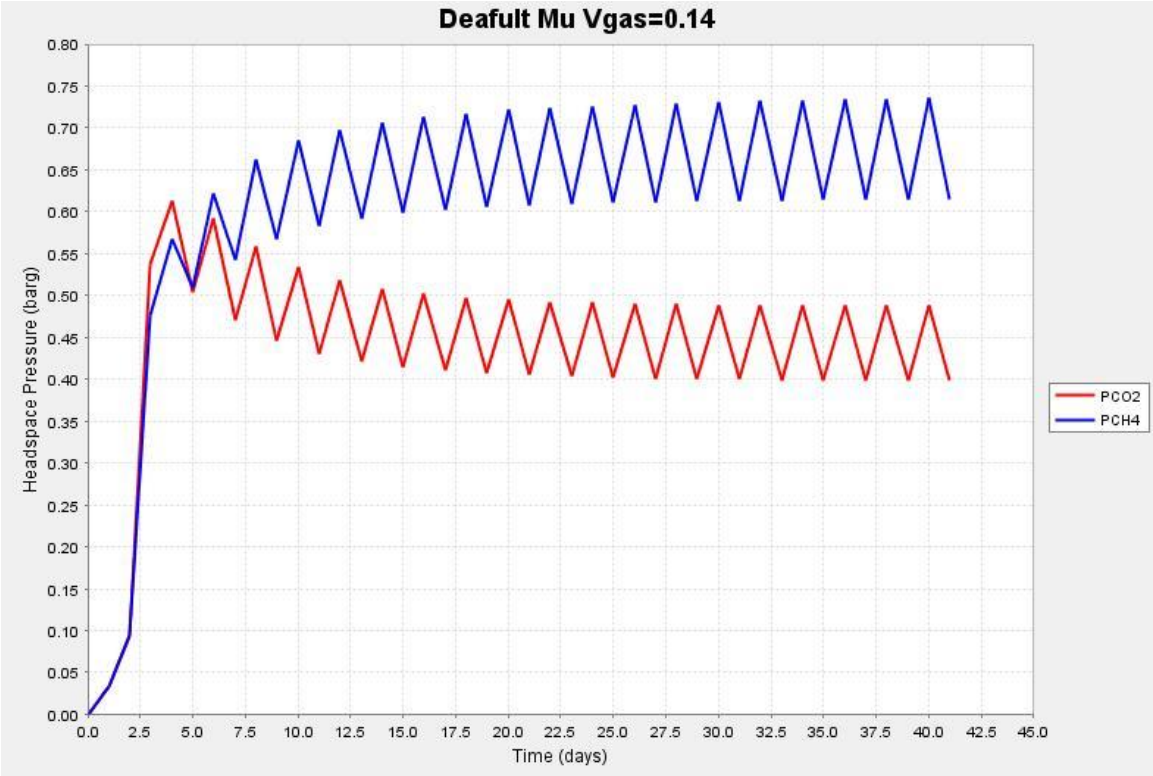

Figure 4.5 – The partial pressure of methane (blue, PCH4) and carbon dioxide (red, PCO2) with default specific growth rate from MAD model when headspace volume was 140 ml and venting frequency was once every 2 days.

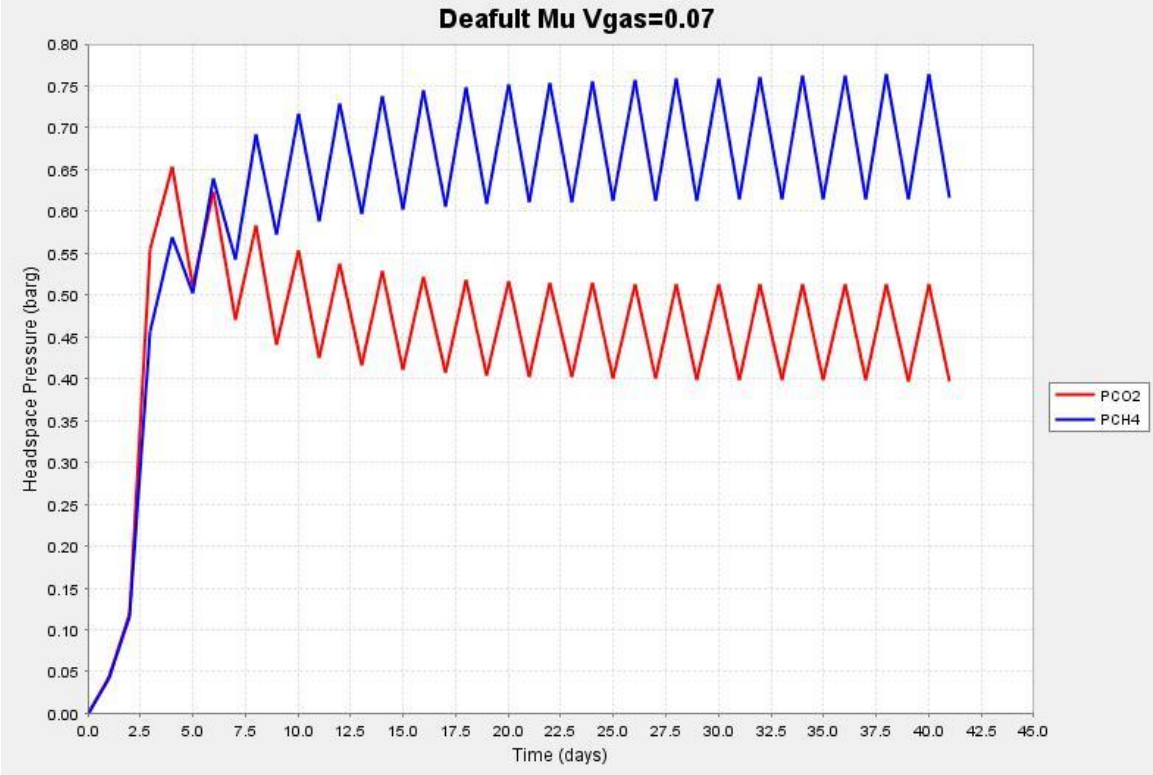

Figure 4.6 – The partial pressure of methane (blue, PCH4) and carbon dioxide (red, PCO2) with default specific growth rate from MAD model when headspace volume was 70 ml and venting frequency was once every 2 days.

The partial pressure of methane and carbon dioxide for the rest of the simulating scenarios mentioned in Figure 4.4 with venting frequency once every 2 days are illustrated in Figures 4.7 and 4.8. When maximum specific growth rates were all increased by 10%, the partial pressure of methane and carbon dioxide followed the same trend as the defaults but accumulated higher headspace pressure, as displayed in Figure 4.7 (a) and (b). However, when maximum specific growth rates were all reduced by 50% or more, the trend became irregular for each set.

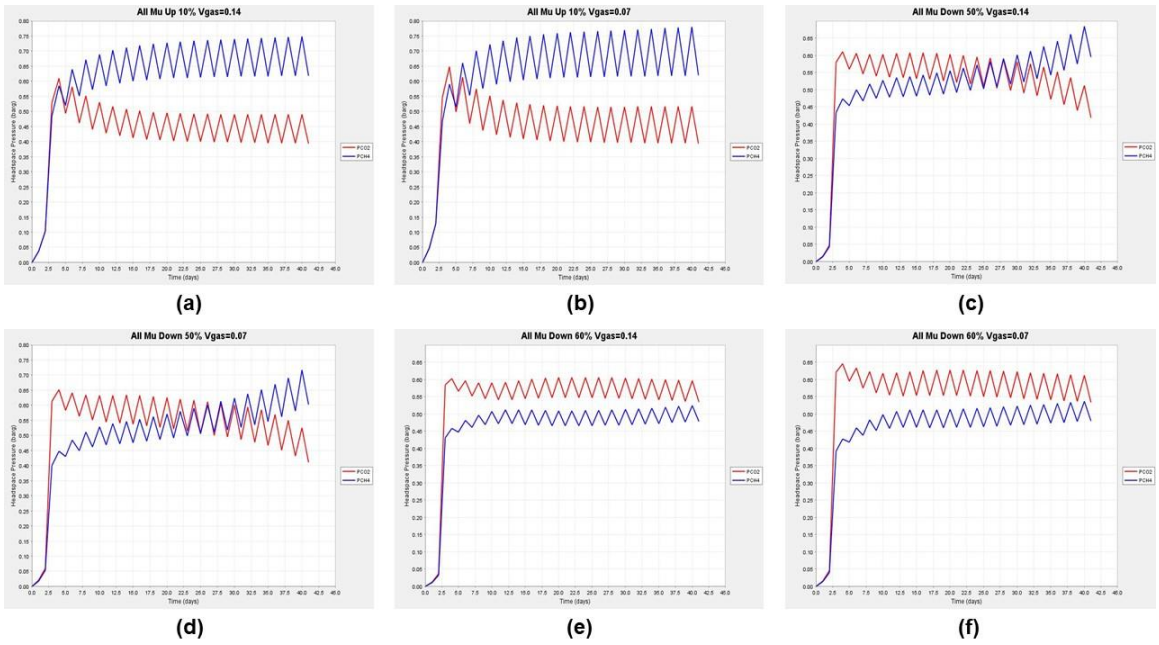

Figure 4.7 – The partial pressure of methane (blue, PCH4) and carbon dioxide (red, PCO2) when all maximum specific growth rates were increased by 10%, reduced by 50% and 60%. (a) (c)and (e) were simulations for bioreactors with headspace volume of 140 ml where (b) (d) and (f) had 70 ml headspace volume.

When the specific growth rates were reduced by 50%, the partial pressure of carbon dioxide was decreasing while the partial pressure of methane was increasing and overtook it around halfway through the simulation, as displayed in Figure 4.7 (c) and (d). When the specific growth rates were decreased by 60%, partial pressure for carbon dioxide remained higher than methane when headspace volume was 140 ml, but when headspace volume was 70 ml, the partial pressure of methane gradually increased and got closer to carbon dioxide, as demonstrated in Figure 4.7 (e) and (f) respectively.

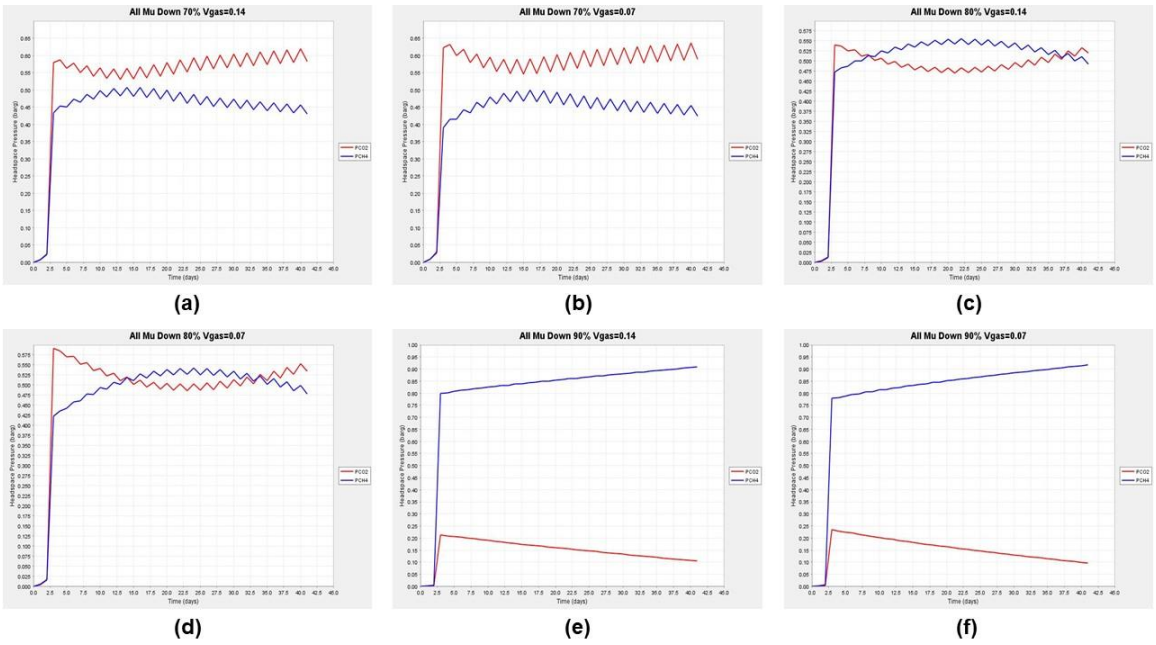

Figure 4.8 – The partial pressure of methane (blue, PCH4) and carbon dioxide (red, PCO2) when all maximum specific growth rates were reduced by 70%, 80% and 90%. (a) (c)and (e) were simulations for bioreactors with headspace volume of 140 ml where (b) (d) and (f) had 70 ml headspace volume.

When maximum specific growth rates were decreased by 70%, as demonstrated in Figure 4.8 (a) and (b), the partial pressure of carbon dioxide was decreasing while the partial pressure for methane increased until a third of the way through the simulation, where the partial pressure of methane started to decline and the partial pressure of carbon dioxide started to rise. When the maximum specific growth rates were all reduced by 80%, the partial pressure of methane was lower at the beginning, rose to surpass the partial pressure of carbon dioxide and reached the peak, then decreased to become lower than the partial pressure of carbon dioxide, as demonstrated in Figure 4.8 (c) and (d). Finally, Figure 4.8 (e) and (f) show that when all maximum specific growth rates were reduced by 90%,

the partial pressure for methane and carbon dioxide showed a very different trend. The partial pressure of methane was much greater than carbon dioxide and kept increasing while the partial pressure for carbon dioxide reached its peak then started the decline.

Figures 4.9 to 4.11 are demonstrations of how the headspace pressure affected the composition of the biogas. During all the simulations, the peak value of partial pressure for methane kept rising slightly just before venting while the peak value of partial pressure for carbon dioxide kept decreasing slowly just before venting. With the default parameters used as shown in Figure 4.9 (a), the total pressure reached 2.0 barg where the partial pressure of methane reached 1.19 barg and the partial pressure of carbon dioxide reached 0.81 barg. This gave the methane content of 59.5% for reactor venting once every 5 days. For the reactor venting once every 10 days, the total pressure was 3.08 barg where the partial pressure of methane was 1.86 barg and the partial pressure of carbon dioxide was 1.22 barg as displayed in Figure 4.9 (b), this gave a modestly increased methane content of 60.4% when compared to the aforementioned value for the 5-day venting.

When simulating the anaerobic digestion process using the parameters from laboratory-scale experiments, the results showed a similar trend as compared to the results using default parameters, i.e. that of methane content increasing in a very insensitive manner with increasing headspace pressure (or decreasing venting frequency). Figure 4.10 demonstrates the simulation result for venting once every 5 days with headspace volume of 0.14 and 0.07 litre respectively.

The total pressure was 1.77 barg when the partial pressure of methane reached 1.06 barg and the partial pressure of carbon dioxide got to 0.71 barg, which gave a methane content of 59.9% in Figure 4.10 (a). When the headspace volume was reduced to 0.07 litre, as illustrated in Figure 4.10 (b), the total pressure just before venting was 1.94 barg. The partial pressure of methane was 1.16 barg and the partial pressure for carbon dioxide reached 0.78 barg, which made the methane content 59.8%.

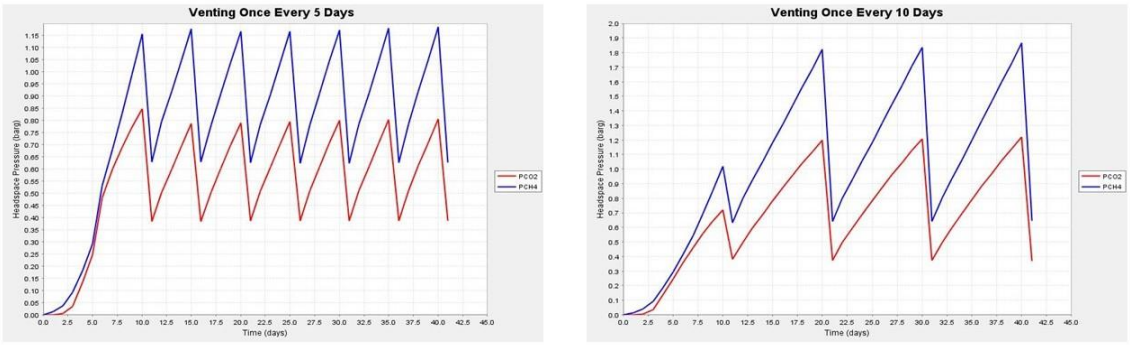

Figure 4.9 – The effects of headspace pressure on biogas composition with default parameters where $V_{liq} = 1\ litre$ and $V_{gas} = 0.1\ litre$. The blue line is the partial pressure for methane and the red line is the partial pressure for carbon dioxide.

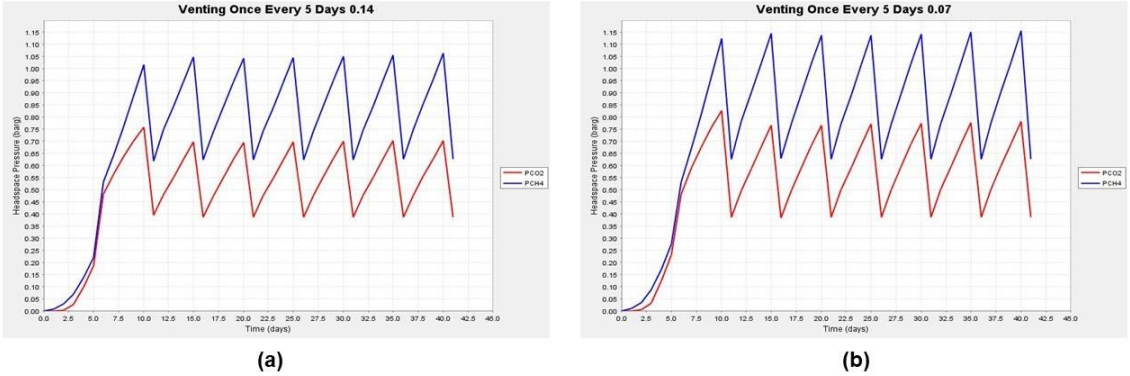

Figure 4.10 – The effects of headspace pressure on biogas composition using parameters from the laboratory-scale experiments for venting once every 5 days. The blue line is the partial pressure for methane and the red line is the partial pressure for carbon dioxide.

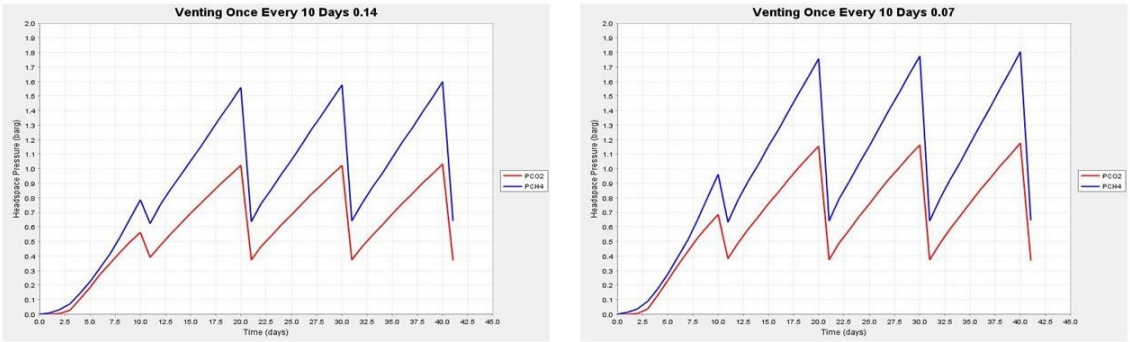

Figure 4.11 – The effects of headspace pressure on biogas composition using parameters from the laboratory-scale experiments for venting once every 10 days. The blue line is the partial pressure for methane and the red line is the partial pressure for carbon dioxide.

Figure 4.11 illustrated the simulation result for venting once every 10 days with respective headspace volume of 0.14 and 0.07 litre. The total pressure was 2.63 barg when the partial pressure of methane reached 1.59 barg and the partial pressure of carbon dioxide got to 1.04 barg, as displayed in Figure 4.11 (a), which gave a methane content of 60.5%. When the headspace volume was reduced to 0.07 litre, as demonstrated in Figure 4.11 (b), the total pressure just before venting was 2.98 barg. The partial pressure of methane was 1.80 barg and the partial pressure for carbon dioxide reached 1.18 barg, which made the methane content of 60.4%.

4.1.4. Discussion

Adapting, reproducing and validating the MAD model using CellDesigner, identifying the specific growth rate of bacteria for the laboratory-scale experiments using the adapted model on CellDesigner, and investigating the effect of headspace pressure on the methane content of biogas production by an anaerobic digestion process with this model were the objectives of this experiment.

The adapted model built in CellDesigner was proven to work and the key results were almost identical compared to the MAD model. The pipe resistance coefficient k_p was the parameter that could have been adjusted to a new constant lower value to achieve the steady state headspace pressure in the reactor. However, since the model equations are inherently dynamic, and CellDesigner gives the modeller the ability to dynamically change a parameter, we were able to more faithfully reproduce, in the model, the periodic venting used in the experiments. In this a new, dynamically adjustable parameter k_{p1} was used to overwrite the pipe resistance coefficient when necessary, as demonstrated in Figure 3.5, so the modified model could emulate laboratory-scale experiments. The modified model which considered dissolved methane and rapid more productive in terms of biogas when compared to the laboratory-scale experiments. The maximum specific growth rate parameters were therefore adjusted to better match the laboratory-scale pressure increases. When

modifying the maximum specific growth rates for the three groups of bacteria in the model, the behaviour changed unexpectedly, hence the fluctuation in biogas content from the production process. For instance, if all specific growth rates were reduced by more than 50% at the same time, the pattern for biogas content became unpredictable, as demonstrated in chapter 4.1.3. When the specific growth rates were all reduced by 90% at the same time, differences of headspace pressure before and after venting became minimal such that it could be neglected and an interesting pattern for the biogas content emerged.

For the investigation of the effect that headspace pressure has on biogas production rate and biogas content using the modified model, the results showed that as pressure increased the biogas production rate decreased. However, the methane content had a small increase as the overall headspace pressure increased.

4.2. Anaerobic Digestion of Pondweed

4.2.1. Results

The effects of headspace pressure have on biogas production from anaerobic digestion of pondweed were examined by the weight change of the bioreactors before and after venting the biogas produced and accumulated in the headspace from the process. The assumption adopted was a that of a constant composition of biogas of a third carbon dioxide and two thirds methane, with all other trace gases being neglected.

Despite various methods being applied to improve sealing of the bioreactors for Experiments 1 to 5, the biogas leakage issue with original laboratory bottles was not resolved, so no conclusion could be drawn from the inconsistent results, therefore, these results are not presented. As for experiments 6 to 9, once the reactors were replaced by the new Erlenmeyer flask with DIN thread and GL 32 cap reactors with a better seal, the headspace pressure accumulated by different venting frequencies and headspace volume became more significant.

These experiments were set up with initial headspace pressure at atmospheric pressure. The vertical axes represented the change in headspace pressure above atmospheric pressure. ‘O 1’ and ‘O 2’ meant the reactors were vented once every day and every 2 days accordingly. As displayed in Figure 4.12, the reactors that were vented less frequently normally accumulated higher headspace pressure before being vented.

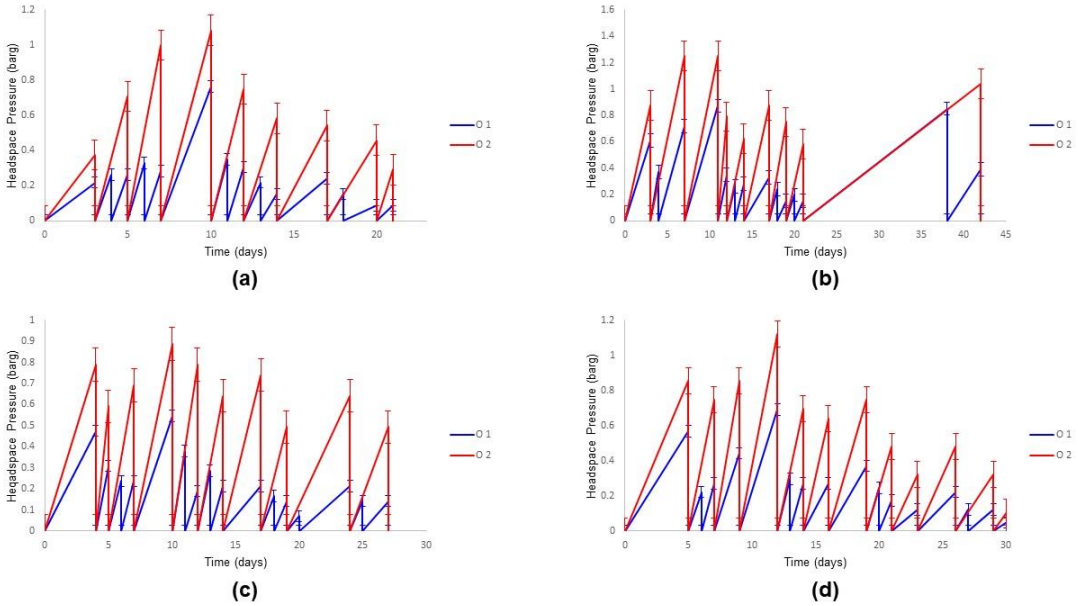

Figure 4.12 – The average of change in headspace pressure for bioreactors with same headspace volume and venting frequency as biogas production proceeded with their corresponding error bars. (a) represented Experiment 6, (b) represented Experiment 7, (c) represented Experiment 8 and (d) represented Experiment 9.

As demonstrated in Figure 4.13, the effect headspace pressure has on biogas production rate was identical to the simulation results. At increased headspace pressure, the biogas production rate decreased. With these new reactors the higher headspace pressure was easier to achieve because the headspace volume was halved and twice the time was allowed to accumulate the pressure. The reasons for experiment 7 having slightly higher average headspace pressure while producing approximately the same amount of biogas could be because it might have set up with a higher bacterial population. In addition, after the first three weeks of venting as usual, the reactors were left to accumulate the

headspace pressure without venting for two weeks while the weights of all reactors were monitored for hermeticity and then venting as normal for the last week. According to Eqn 3.4, $\Delta P_i \; and \; \Delta t_i$ would be greater, therefore, causing higher average headspace pressure.

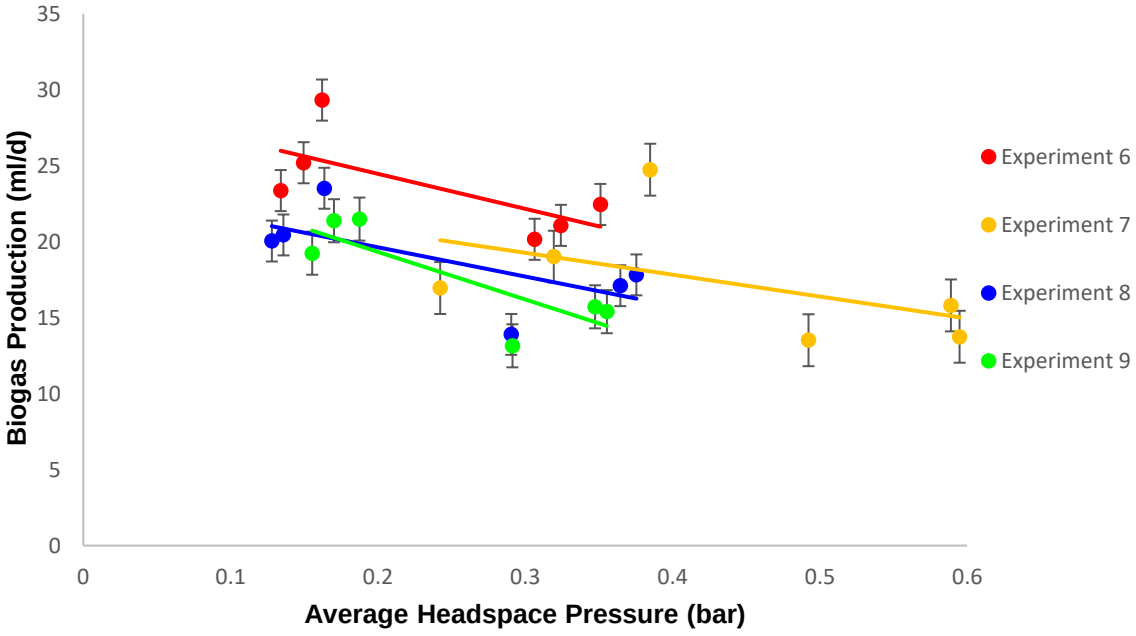

Figure 4.13 – Comparing the biogas production rate against different headspace pressure with new reactors for Experiment 6 to 9. Each dot represents one bioreactor with certain headspace volume and venting frequency. The straight lines are the added trendline of each data set.

4.2.2. Discussion

The effects of headspace pressure on anaerobic digestion were studied (Latif, Mehta, & Batstone, 2018; Merkl, *et al*., 2017; Chen, *et al*., 2014). By increasing the headspace pressure of the bioreactor, the methane content increased from 79.8 ± 1.01% at 10 bar to 90.45 ± 0.73% at 50 bar (Merkl, *et al*., 2017).

Meanwhile, the pH value decreased from 6.65 ± 0.05 at 10 bar to 6.55 ± 0.02 at 50 bar (Merkl, *et al*., 2017). The work presented in this thesis differs from these previously published findings in three key ways that we believe make our results more useful for practical application. Firstly, we examined considerably more modest pressure increases. Secondly, we allowed the system to self-pressurise with only the evolved biogas. Thirdly, we used periodic venting to simulate the semi-continuous harvesting of the biogas product. The objective of this experiment was to determine whether varying the headspace pressure by altering headspace volume and using a variety of venting frequencies would have any effect on the amount of biogas produced from the anaerobic digestion process. The hermeticity issue with the reactor bottles with DIN thread, GL 45 cap with 500 ml working volume (DURAN Group GmbH, Germany) made the first five runs of experiments give rather inconsistent results. No clear conclusion could be drawn from them; therefore, they were not included. Once the reactors were replaced with Erlenmeyer flask with DIN thread and GL 32 cap (DURAN Group GmbH, Germany), the hermeticity issue was resolved and experiments started to yield consistent results in the last four runs.

For experiments 6 to 9, both headspace volume and venting frequency were variables. The reactors vented once a day also had two times the headspace volume compared to reactors that were vented once every two days, so it was expected to achieve a larger difference in headspace pressure and average biogas production between these two sets of reactors. The difference in headspace pressure accumulated or the biogas produced in terms of weight did

not get as large as expected but still had a noticeable difference between the two sets. The reactors vented once every two days with half the headspace volume could accumulate about double the headspace pressure while the average daily biogas produced in ml/day only dropped around 20 to 25 per cent.

4.3. Glucose Yeast Experiment

4.3.1. Results

The effect headspace pressure had on biogas production for glucose and yeast fermentation was the same as for the anaerobic digestion of microalgae, as displayed in Figure 4.14. For this experiment, the calculation for average headspace pressure was simplified by taking the mean of the target pressure and the pressure after collection. For instance, for fermentations at atmospheric pressure, meaning the valve was fully opened throughout, the average headspace pressure was 0 barg. For fermentations with target pressure of 0.8 barg before collecting 0.2 barg of gas in the headspace, the average headspace pressure was $\frac{0.8+0.6}{2} = 0.7\ barg$. Table 4.4 and 4.5 summarises the experimental conditions and results of the fermentations.

Table 4.4 – Summary of the fermentations at atmospheric pressure and target pressure of 0.4 barg.

Average Headspace Pressure (barg)	0			0.3		
Experiment No.	1	2	3	4	5	6
Total CO_2 Produced (ml)	6980	6720	6600	5300	5310	5380
CO_2 Production Rate (ml/min)	99.71	96	94.29	75.71	75.86	76.86

Table 4.5 – Summary of the fermentations with target pressure of 0.8 and 1.2 barg.

Average Headspace Pressure (barg)	0.7			1.1		
Experiment No.	7	8	9	10	11	12
Total CO_2 Produced (ml)	4830	4600	4200	3620	3880	3790
CO_2 Production Rate (ml/min)	69	65.7	60	51.71	55.43	54.14

As demonstrated in Figure 4.14, as the average headspace pressure increased, the production rate of carbon dioxide kept decreasing. If a linear trendline is fitted to the data, its extrapolation until it cuts the horizontal axis would predict that, when the absolute headspace pressure reaches 3.49 barg, the carbon dioxide production would stop completely.

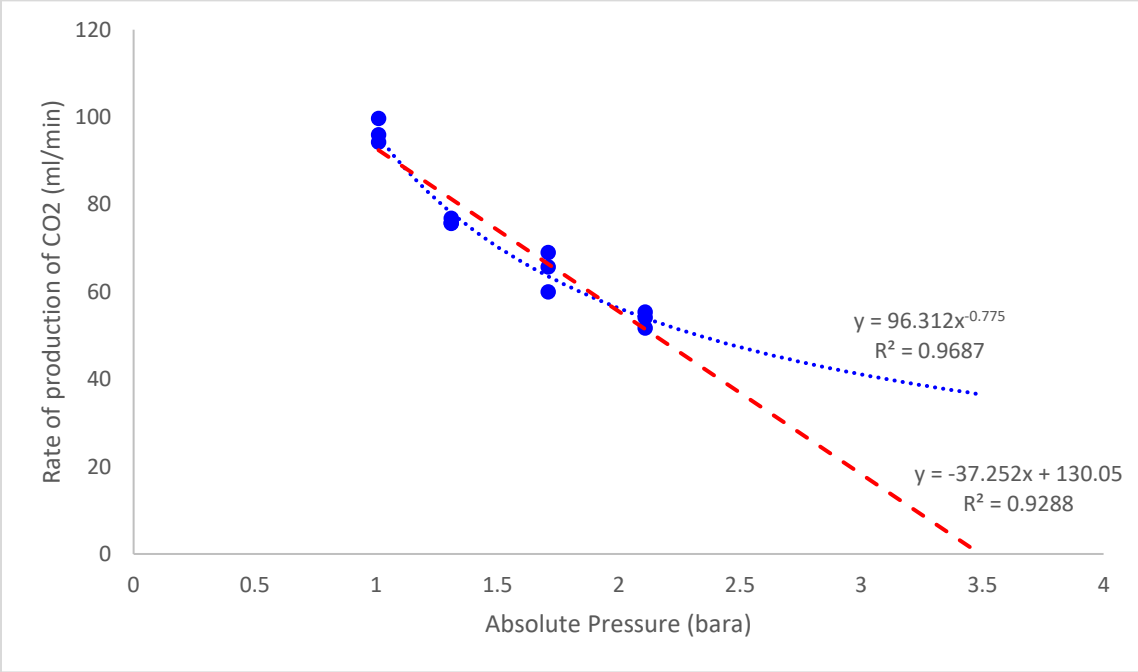

Figure 4.14 – The effect of headspace pressure on biogas production for sugar and yeast fermentation with two types of fit: linear and power law. Note that pressures are expressed as absolute pressures in order to allow the power law fit.

Since it appears, however, that the gradient of a fitted line should perhaps become less negative as pressure increases, it can be seen that a power law gives a better fit. The exponent of the best fit power law is -0.775 which is in rough agreement with the values of -0.90 and -1.28 of Galanakis *et al*. (2012), although these researchers were studying higher pressures (3-7 bara) and using yeast immobilised on microporous alumina pellets.

Returning to the linear extrapolation, it is interesting to use the value of 3.49 bara as the headspace pressure at which CO_2 efflux stops (i.e. where this line of fit crosses the x-axis) on order to infer the intracellular concentration of CO_2 for the yeast cells. Small molecules such as CO_2 can be assumed to move across cell membranes vis passive diffusion. If we neglect mass transfer resistance due to internal/external unstirred boundary layers in contact with the membrane, the flux of CO_2 across the cell membrane can be thought of as being proportional to the concentration difference across the membrane as follows:

$$J_{a,CO_2} \propto \Delta c_{a,CO_2} \propto c_{a,CO_2} - H_{CO_2}^{cp}\, p$$

In the above expression p is the overall pressure assuming that the headspace for fermenting yeast is pure CO_2. At the particular pressure p^* which CO_2 efflux stops, we can assume that the intracellular aqueous CO_2 concentration is equal to the extracellular value which, by Henry's law, is given by:

$$c_{a,CO_2} = H_{CO_2}^{cp}\, p^*$$

Clearly, the value of p^* depends on the type of line we fit to the data. For the power law fit p^* is infinite since the curve never actually crosses the x-axis. For the case of the linear fit, however, the intracellular concentration is:

$$c_{a,CO_2} = H_{CO_2}^{cp}\, p^* = 0.034 \times 2.46 = 0.0836\, M \approx 80\, mM$$

4.3.2. Discussion

It should be noted that the linear versus the power law fit have alternative physiological interpretations which can be expressed in terms of mass transfer driving force and metabolic control. The linear fit presumes a linearly reducing driving force for passive diffusion across the cell membrane. In other words, the intracellular dissolved gas concentration remains constant: transport across the membrane is fast compared to, for example, other enzyme catalysed steps and it therefore does not exert control over the overall process of CO_2 evolution.

The power law fit, however, implies a driving force for passive diffusion that reduces as the 'back pressure' against which the cell is 'pumping' CO_2 increases to higher values. This would occur if the intracellular concentration increases, thereby causing the relationship between flux and headspace pressure to veer off a straight line and intersect the horizontal axis at a higher pressure. In this case, passive diffusion is not as fast when compared to other processes involved in the chain of steps involved in the production of CO_2 and can therefore be inferred as exerting some metabolic control.

Despite these interesting speculations, however, it can be seen that the paucity of the data (lack of higher pressure measurements) makes it difficult to choose one type of fit over the other.

In the absence of direct measurements for yeast in the literature, the extrapolated value of 80 mM we obtain above can be compared to the values in the range 10-30 mM as reported by Longmore, Niethe and McDaniel (1969) for perfused rats liver cells. Although the agreement within an order of magnitude is significant, it can be seen that our value is considerably higher. We provide a discussion of two factors which could cause this discrepancy. Firstly, it is likely that the presence of dissolved sugars and other species in the extracellular medium will serve to reduce the solubility of CO_2 from that of pure water which would have the effect of reducing the estimated intracellular values above (this is, in fact observed for the anaerobic digestion post-sampling pressure recovery discussed in section 4.5.1). Secondly, the actual CO_2 values inside rapidly fermenting yeast cells could well be higher than those inside more complex mammalian cells. Either or both of these considerations could serve bring the values into closer agreement.

To summarise the contribution of this experiment to the overall thesis, a fermentation bioprocess was studied because it is similar to anaerobic digestion in that it yields biogas, but it has the advantage that the time required to set it up and the duration of the process is much quicker. This process was shown to be affected by pressure in a similar way as for anaerobic digestion and it points the way to a separate strand of future work that could use headspace pressure to

investigate principles of metabolic control of trans-membrane fluxes of gas molecules.

4.4. Pressurised Anaerobic Digestion of Seaweed

As a result of the collaboration with Autichem LTD. UK, a fully instrumented custom bioreactor was built.

4.4.1. Custom Fabricated Reactor

Figure 4.15 is the piping and instrumentation diagram (P&ID) of the reactor used in the experiment. Feed 1 is the feed of chemicals through HV-01, a hand control valve. NRV is a non-return valve and the arrow indicates the direction of the flow. The valve connected to the bellows with no notes attached is a three-way valve. AE stands for analysis primary element, in this process it is for the pH and AIR stands for analysis indicator and recorder. PT is a pressure transmitter and PIR is the pressure indicator and recorder. BPRV stands for back pressure regulator valve and BPRV-01 is the safety valve which is set to 5.5 barg. NV is a hand operated gate valve where NV-05 is a simple gate valve with basic on and off function whereas NV-06 is a needle valve with a scale printed on which can be used for precise control of the flow rate. This pipe is used for taking biogas samples for analysis and sparging. The purpose of the three-way valve is to

direct the biogas in the headspace released from HV-02 and NRV-01 back to the bottom through HV-03 to sparge the sludge with the assistance from the bellows. HV-04 is the port used for sampling the sludge or feeding biomass. TE stands for temperature element (heater) combined with a temperature sensor the temperature of the reactor contents to be measured and controlled. TIR is the temperature indicator and recorder. The indicators and recorders (IR) are the respective software installed on the computer which displays and records the readings from the sensors. Figure 4.16 is the annotated photograph of the bioreactor and the bellows with manual compression with regards to the P&ID of the system.

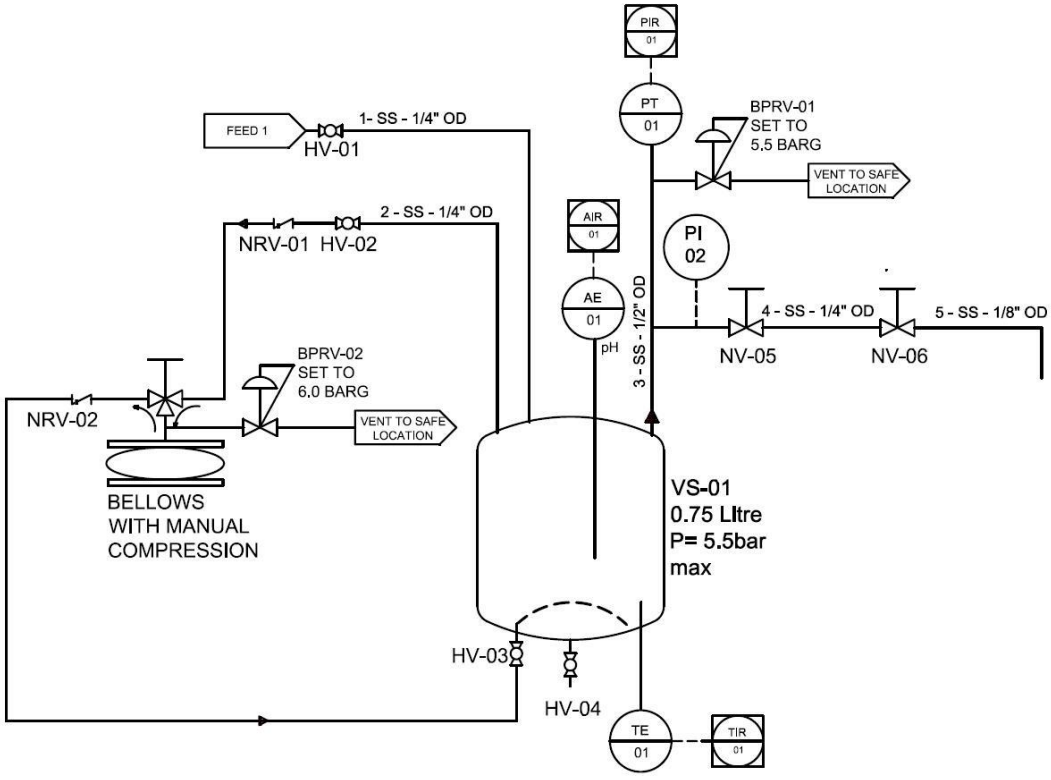

Figure 4.15 – P&ID of the reactor used for the experiment.

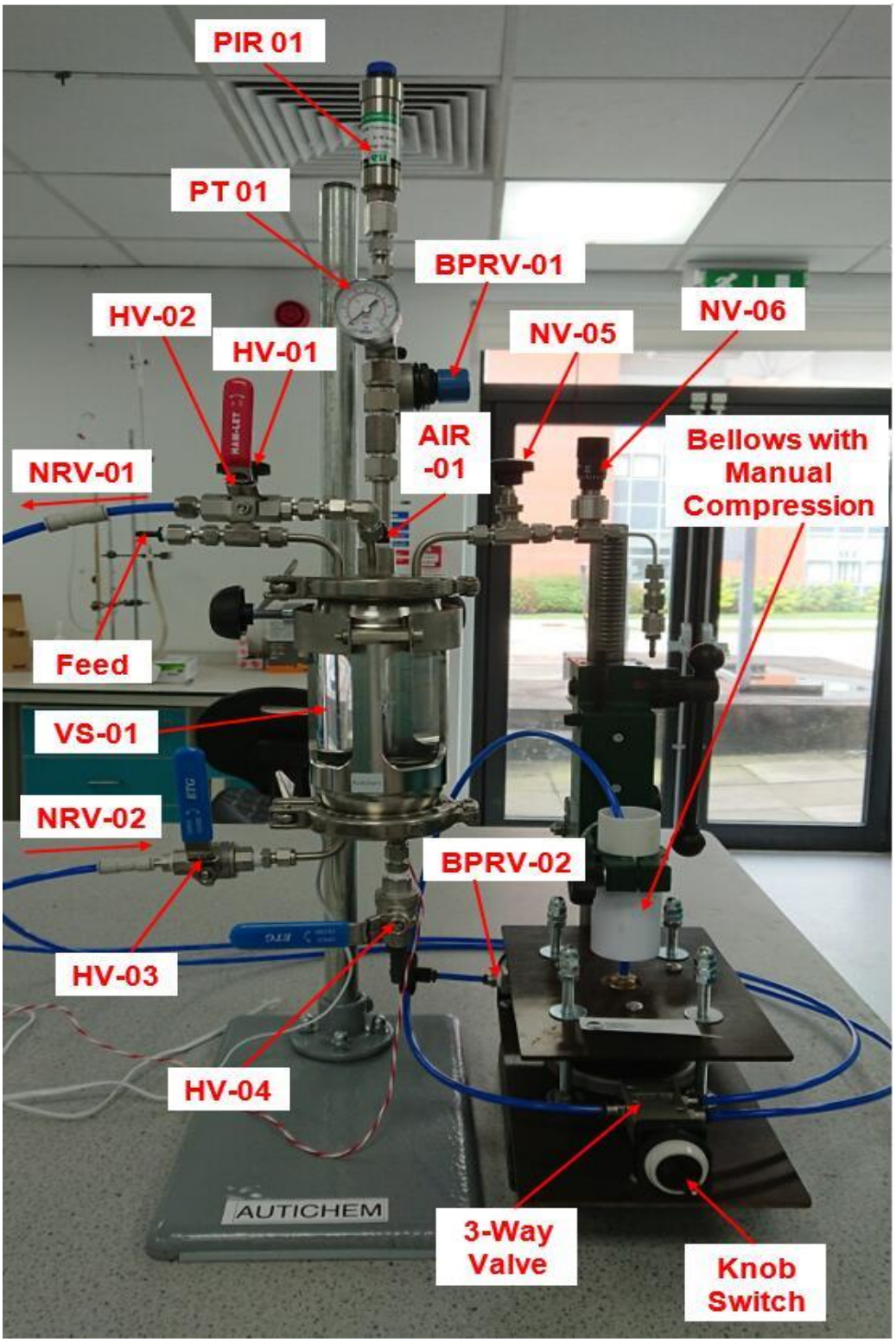

Figure 4.16 – Annotated photo of the bioreactor and the bellows with manual compression with regard to the P&ID of the system.

4.4.2. Preliminary Runs

For the first test run, because no buffer solution was used, the pH dropped to around 3 during the first night. With such an acidic environment no methanogens could survive, so no methane could be produced. Therefore, the batch had to be discarded the next day and a new batch had to be started.

For the second run, the pH started at 7.78 and the recorded initial headspace pressure was -0.1395 barg indicating a small offset error on the pressure measurement.

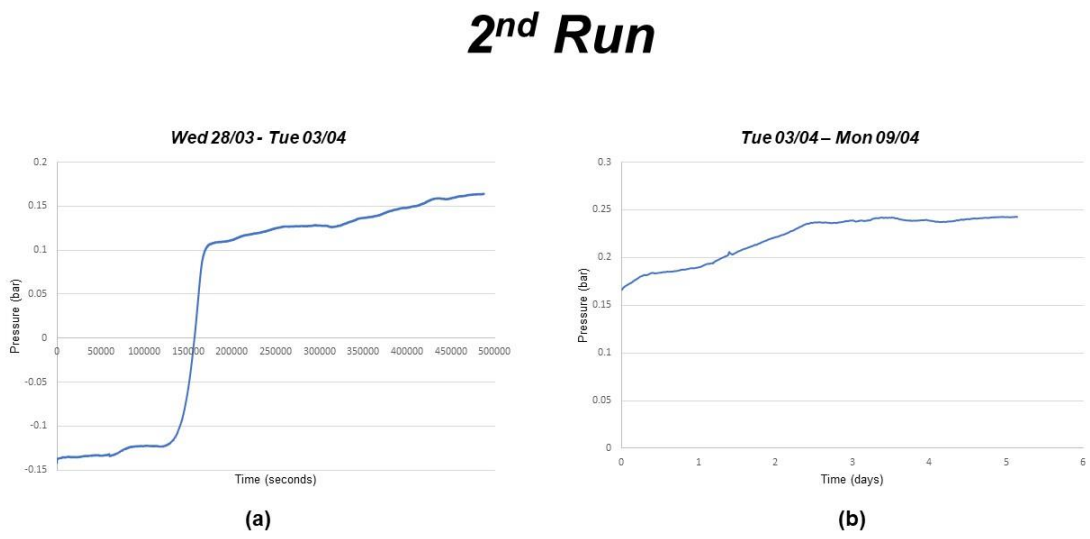

Figure 4.17 – The growth of pressure for the 2nd run.

For the first half of the 2nd run, as displayed in Figure 4.17 (a), the sampling frequency was set to 1 reading per second instead of 1 reading every 5 minutes, hence, there were almost 500 thousand readings for pressure. The overall growth of headspace pressure was slow and steady except during the second day, there was a substantial amount of biogas produced and this significantly raised the headspace pressure. Throughout this fermentation, the total headspace pressure accumulated was 0.3795 bar and pH at 6.47. Applying Equation 3.8, the amount of biogas produced during this period could be calculated.

$$n = \frac{PV_{specific}}{RT} = \frac{0.3795 \times 0.25}{0.08314 \times 293.15} = 3.89 \times 10^{-3}\ mol$$

and by substituting *n* into Equation 3.9, the volume of biogas produced would be

$$V_{actual} = \frac{nRT}{P_{atm}} = \frac{3.89 \times 10^{-3} \times 0.08314 \times 293.15}{1.03125} = 0.092\ l$$

4.4.3. The Third Run

The starting pH for the third run was 7.05 and headspace pressure was 1.0285 barg. This was also the first run where the bellows with manual compression was connected to the reactor for sparging as a method of mixing. The reduction in headspace pressure towards the end in Figure 4.18 (a) was caused by sparging with the bellows. Similarly, the loss in headspace pressure between Figure 4.18 (a) and (b), (b) and (c), (c) and (d) and lastly, between (d) and (e) were all caused by sparging with the bellows. The reason for these pressure drops in the

headspace was because of the nature of the bellows as well as the design of the manual compression system.

By default, the height of the bellows must be 50 mm at rest and volume of air in the bellows would be 0.2 litre at atmospheric pressure. When ‘HV-02’ was switched open and the bellows were charged with biogas from the reactor, the pressure in the bellows would reach a temporary equilibrium with pressure in the headspace. Then, when the manual compression pump was pressed down, the pressure in the bellows would travel back to the reactor and temporarily reach equilibrium state with the partial pressure of soluble gas in the liquid phase. Once the pump was released, the bellows would bounce back up depending on the amount of gas left in it. Since it would require up to 5500 N of thrust to fully press all the additional gas in the bellows back to the reactor, once the pressure achieve a level that surpassed the thrust that could be provided, there would always be some biogas left in the bellows.

The decrease in headspace pressure on Thursday the 26th April demonstrated in Figure 4.18 (e) was caused by sampling the biogas accumulated in headspace for its composition. The drop at the end of Figure 4.18 (f) was at the end of the fermentation when it was barely producing biogas for the last few days and the valve was opened to release the biogas when the run was terminated. The overall biogas production in this run was smooth and there was no sudden burst of biogas production.

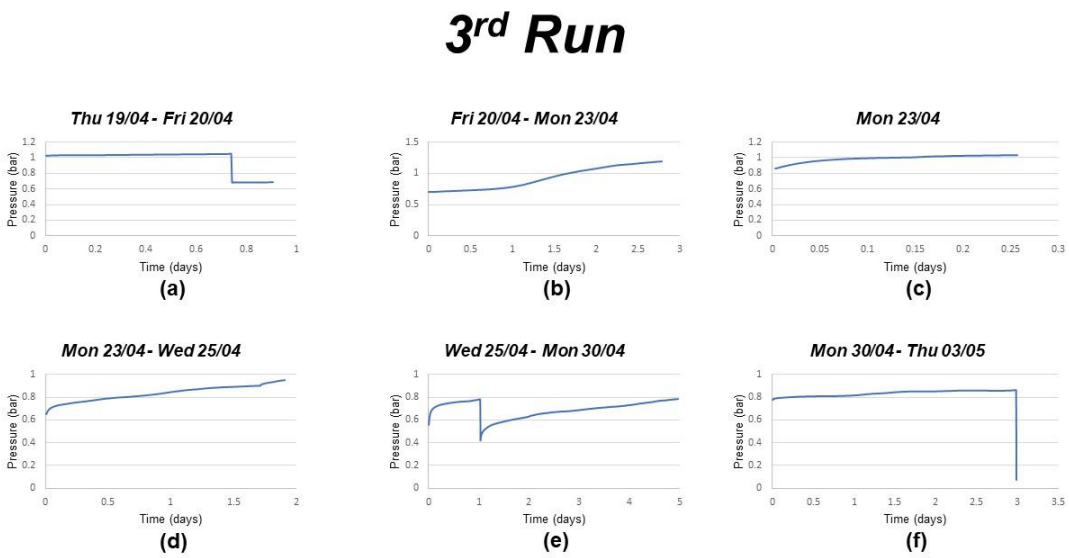

Figure 4.18 – The growth and change in headspace pressure over the course of the third fermentation.

Figure 4.19 is the demonstration of the change in headspace pressure during those sparging processes. There were small but noticeable increases in headspace pressure in Figure 4.19 (c) and (d) when biogas was released to the bellows. As soon as the biogas in the bellows was pushed back into the reactor from the bottom, there was a tiny and sudden drop in headspace pressure in all four sparges. This circumstance could be explained through Henry's law. When biogas was released to the bellows, the dissolved carbon dioxide in liquid phase and in headspace would no longer be at equilibrium state with more dissolved carbon dioxide in liquid phase than gas phase. A portion of the dissolved carbon dioxide would be immediately released to headspace to regain the steady-state. However, as soon as the biogas in the bellows was pumped back to the reactor,

there would be too much carbon dioxide in the headspace and a small portion of it would be push back into liquid phase.

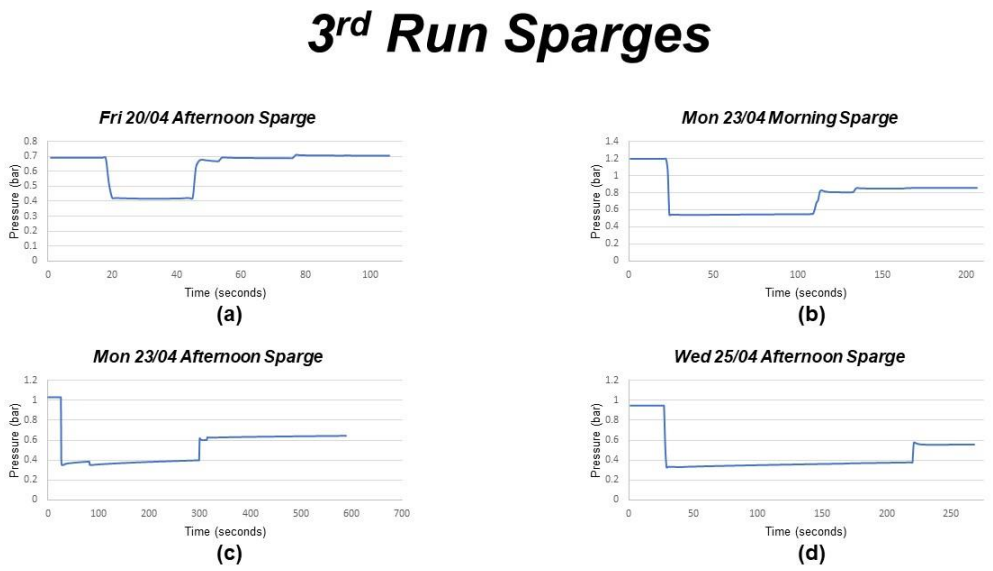

Figure 4.19 – The change of headspace pressure during the sparging processes for the third run.

Over the entire 14-day run, the amount of biogas produced in terms of pressure was 1.6666 bar and the pH at the end of the run was 5.7. By applying Equation 3.8, the amount of biogas produced was

$$n = \frac{PV_{specific}}{RT} = \frac{1.6666 \times 0.25}{0.08314 \times 293.15} = 0.0171\ mol$$

and by substituting *n* into Equation 3.9, the volume of biogas produced was

$$V_{actual} = \frac{nRT}{P_{atm}} = \frac{0.0171 \times 0.08314 \times 293.15}{1.03125} = 0.411\ l$$

After a few attempts of sparging the system using the bellows with manual compression, the decision was made not to use it until towards the end of the fermentation since the biogas that travelled to the bellows could not be all pushed back to the reactor by manual power, causing unintentional loss in headspace pressure once the pressure got over certain level. Occasionally shaking the reactor would be used as mixing instead. The reactor was shaken three times a day, the first one was in the morning, the second one was at midday and the last one was in the afternoon. Each shake lasted thirty seconds.

4.4.4. The Fourth Run

For the fourth run, the pH started at 6.6 and the headspace pressure was left at atmospheric pressure. The overall production rate of the biogas production was highest of all the runs. During the second day, the culture in the reactor was aerated and raised to the top of the reactor,which caused a blockage at the pressure sensor, hence the pressure merely increased during the second night compared to the previous night, as demonstrated in Figure 4.20 (a). On the third day, the culture was still aerated to the top of the reactor, the reactor was shaken until the culture fully settled and there were no bubbles in it. This caused the pressure to drastically increase in a short period of time. A heater mat with a thermostat which opens at 50°C and insulation was put on the reactor later that day. The effects of the heater mat could be seen from the pattern of the curve. When the heater mat was on, the temperature inside the reactor increased, the biogas expanded causing a small rise in pressure. When the heater mat was

turned off when the surface temperature reached 50°C, the biogas cooled causing a small drop in pressure.

The spike that appeared on the 10th day was caused by thermostat falling off of the surface of the reactor. As a result of this, the heater mat was not turned off when the surface temperature exceeded 50°C. With the insulation still wrapped around, the temperature kept rising and heating up the biogas further to increase the headspace pressure for a few hours. Since the biogas production had practically come to a stop by day 7, the insulation and heater mat were taken off as well to allow the reactor to cool down. The reactor was sparged with the bellows after a few hours of cooling down, hence causing the noticible pressure drop on the tenth day. After the sparging, the process was left to continue over the weekend to investigate what would happen to the biogas production. Furthermore, the recorded data from when it started to spike would not be counted towards biogas production analysis, it was recorded for post fermentation investigation after the thermostat falling off.

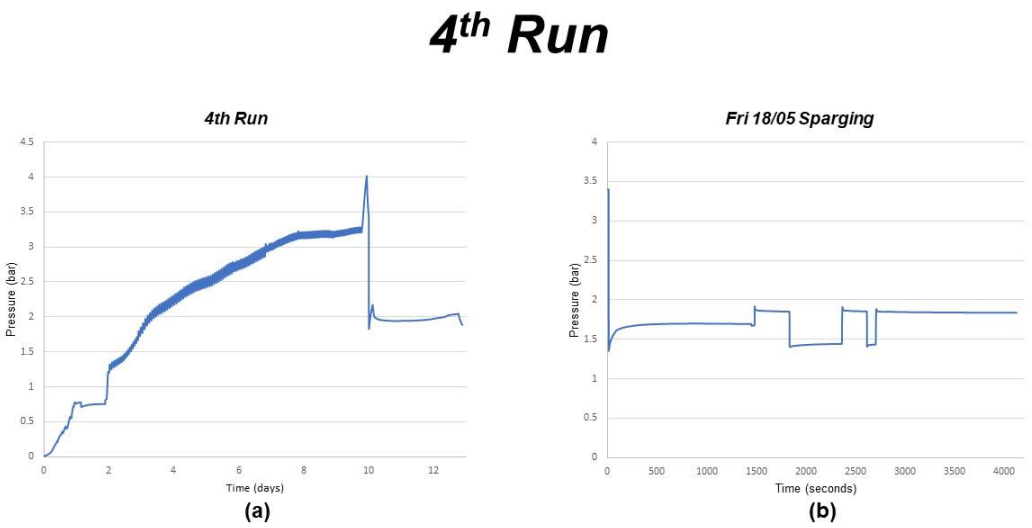

Figure 4.20 – The biogas production and the change in headspace pressure for the sparge towards the end of the fourth fermentation.

Figure 4.20 (b) illustrated the change in headspace pressure during the sparging process. It was similar to the sparges from the third run. When the headspace pressure and the pressure in the bellows reached a temporary equilibrium and 'HV-02' was switched off, the balance of partial pressure in gas phase and the liquid phase in the reactor was disturbed, causing the dissolved gas in liquid to be released into headspace to increase the pressure. When the biogas was pumped back to the reactor, the partial pressure in the headspace would momentarily be higher, thus pumping a small portion of it back to liquid phase and reducing headspace pressure.

On the tenth day of fermentation, a few hours after removing insulation and heater mat allowing the reactor to cool down, the headspace pressure decreased to 3.4241 bar right before the sparge. The pH was at 6.37 at the end of the 13 - day run. By applying Equation 3.8, the amount of biogas produced would be

$$n = \frac{PV_{specific}}{RT} = \frac{3.4241 \times 0.25}{0.08314 \times 298.15} = 0.0345\ mol$$

and by substituting n into Equation 3.9, the volume of biogas produced would be

$$V_{actual} = \frac{nRT}{P_{atm}} = \frac{0.0345 \times 0.08314 \times 298.15}{1.03125} = 0.830\ l$$

4.4.5. The Fifth Run

For this run, the pH started at 6.38 with atmospheric pressure. The overall biogas production for this run was similar to the fourth run. The reason for the flat line in the first day as demonstrated in Figure 4.21 was caused by the hermeticity from the stopper which replaced the broken pH probe. This hermeticity issue was resolved immediately the next day when it was discovered. The effect could be seen instantaneously as the headspace pressure raised steeply for a short period of time. As the fermentation progressed, the overall biogas production was at a reasonable rate till the night of the fourth day an early morning of the fifth day when the production seemed to come to a stop. The reason for this could be culture in the reactor got aerated and blocking the pressure just like the fourth run before the heater mat and insulation were put on. More vigorous shakes were provided in attempt to settle down the foam and aerated culture. The result

of this could be seen as the pressure had a steep increase instantly after the mixing on the same day. The production rate for the rest of the fermentation was rather smooth.

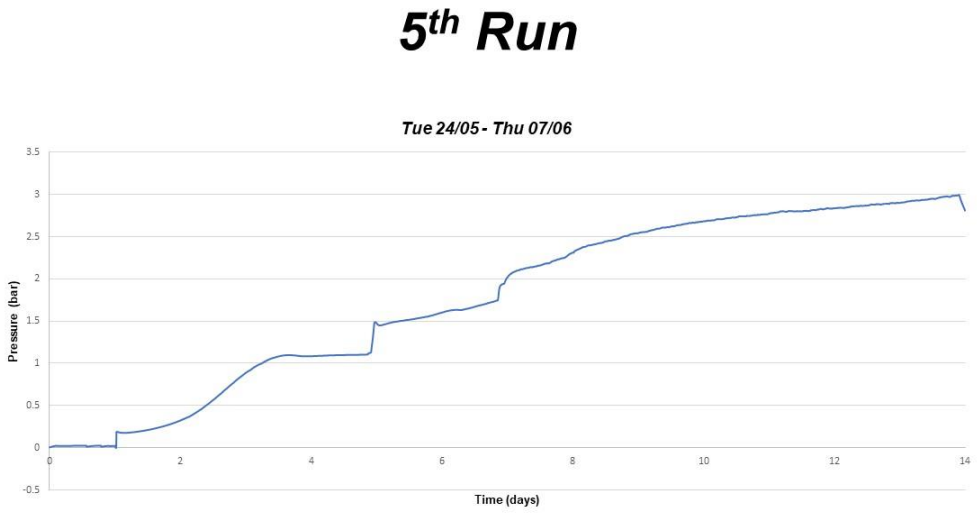

Figure 4.21 – The biogas production in terms of headspace pressure for the fifth fermentation.

By the end of a 14-day run, the biogas produced for this run in turns of headspace pressure was 2.8129 bar and the final pH was 6.37. By applying Equation 3.8, the amount of biogas produced would be

$$n = \frac{PV_{specific}}{RT} = \frac{2.8129 \times 0.25}{0.08314 \times 298.15} = 0.0284\ mol$$

and by substituting n into Equation 3.9, the volume of biogas produced would be

$$V_{actual} = \frac{nRT}{P_{atm}} = \frac{0.0284 \times 0.08314 \times 298.15}{1.03125} = 0.682\ l$$

4.4.6. Post Fermentation Analysis

Table 4.6 summarises the results for post fermentation analysis on TSVS, soluble protein, soluble carbohydrate and VFA. For the third run, the seaweed fed was 58.8 grams VS per kilogram (wet), and after the run, the remaining amount was 38.43 grams VS per kilogram (wet), the percentage decomposed was $\frac{58.8-38.43}{58.8} \times 100\% = 34.6\%$. For the fourth run, the seaweed fed was 75.6 grams VS per kilogram (wet), the residue was 41.14 grams VS per kilogram (wet), the decomposed percentage was $\frac{75.6-41.14}{75.6} \times 100\% = 45.6\%$. For the fifth run, the seaweed fed was 75.6 grams VS per kilogram (wet), the residue was 30.86 grams VS per kilogram (wet), the percentage of digested was $\frac{75.6-30.86}{75.6} \times 100\% = 59.2\%$. Combining this with the soluble protein, carbohydrate and VFA left in the system, the fifth run was considered the best run in terms of biomass degradation.

Table 4.6 – Summary of the post fermentation analysis results.

	3rd run	4th run	5th run
Total Solids (TS)	59.59 g/l 57.05 g/kg (wet)	63.27 g/l 62.71 g/kg (wet)	47.65 g/l 46.61 g/kg (wet)
Volatile Solids (VS)	40.16 g/l 38.43 g/kg (wet)	41.52 g/l 41.14 g/kg (wet)	31.55 g/l 30.86 g/kg (wet)
Soluble Protein	3.359 g/l	2.722 g/l	2.442 g/l
Soluble Carbohydrates	1.076 g/l	2.591 g/l	2.556 g/l
VFA	11.77 g/l	14.78 g/l	11.97 g/l

For the biogas composition analysis, the results demonstrated a different prospect on how the fermentation performed.

Table 4.7 – Composition of biogas analysis.

	4th run		5th run
	Reactor	Bellows	Reactor
CH_4	4.1%	4.8%	1.2%
CO_2	44.8%	56.1%	8.6%
O_2	5.9%	4.5%	13.8%
Ar	45.2%	34.6%	76.4%

Table 4.7 displays the composition of biogas at the end of each run. The reason the third run was not analysed was because the analyser was not calibrated and ready to use at the time. As mentioned before, for the fourth, the sparge took place on the tenth day. The portion that could not be pushed back to the reactor was kept in the bellows, the reactor was left to ferment further over the weekend for three more days. This was the reason for differences in biogas composition from the same run. The oxygen in the biogas could be left over from headspace that was not flushed out by argon, bonded oxygen from phosphate ion (PO_4^{3-}), sulphate ion (SO_4^{3-}) or nitrate ion (NO_3^-). The cause for the fifth run to have much higher oxygen levels could be the temporary gas exchange when replacing the leaking stopper and oxygen from atmosphere got into the reactor.

The overall high VFA concentration from the residue of the fermentation and low percentage of methane from biogas production could be caused by following reasons. Firstly, a week before the sludge was obtained from the 500-litre anaerobic baffled reactor for the third run, the reactor was started with a mixture of sugar and protein powder instead of homogenised seaweed. Even though anaerobic baffled reactors are good at retaining solids in the reactor, the sugar and protein powder solution can go through the reactor in a much shorter time and disturb the bacterial population. Secondly, methanogenesis is the last step of anaerobic digestion which uses methanogens to convert VFA to methane. Oxygen is one of the inhibitors of methanogens and since it is present in the system, it prevents methanogens from producing methane.

4.4.7. Discussion

There is only one study (Latif *et al*., 2018) that investigate the effect of pressure on the microbial community of an anaerobic digestion process. Considering pressure as a continuous factor (p>0.05), there was no significant effect of pressure on bacterial dominance (Latif *et al*., 2018). The bacterial community was significantly impacted, $p = 0.0003$. the rise of a specific dominant OTU (approximately 10%) associated with *Bacteroidales rikenellaceae Blvii28* (*Aceto-bacteroides hydrogenigenes*) is the main reason causing this shift at 4 and 6 bara. *Rhodocyclaceae* also emerged at 2, 4 and 6 bara while there was a consistent decline in a various range of bacterial OTUs. The archaeal community was also significantly impacted by pressure, $p = 0.0005$ because of the crucial shifts in the archaeal community (Latif *et al*., 2018). In test reactor, OTUs associated with *Methanobacteriales* (hydrogen utilisers) and *Methanosaetaceae* (acetate utilisers) dominated the control samples at 1 bara. However, a single dominant OTU (within the archaea) associated with DSEG (Deep Sea Euryarchaeotic Group-a marine microbe) within the phylum *Euryarchaeota* rose as dominant at 2 bara, with multiple *Methanocella* species rose at 4 and 6 bara (Latif *et al*., 2018).

The purpose of this experiment was to use the custom fabricated reactor to run the anaerobic digestion process at even higher headspace pressure than the experiments using the laboratory bottles or flasks made of glass to investigate the effects of pressure on biogas production and biogas content with the assistance of on-board continuous online monitoring sensors.

The results of the experiments showed headspace pressure had overall smooth growth over the two-week fermentation period. The fluctuations from the fourth experiment were caused by the expansion and contraction of biogas in headspace with heat provided by the heater mat and insulations wrapped outside the reactor. The fifth run was also wrapped with the same heater mat, but the glued side lost its stickiness, so the contact with the surface of reactor was not that good.

The manual sparging system with the bellows was designed with the intention to provide periodic mixing for the reactor by taking some of the biogas in the headspace and pumping it back to the bottom of the reactor through the bellows. As demonstrated in the third run, when the headspace pressure in reactor was at 0.7 bar or lower, all the biogas could be pumped back to the reactor. If the headspace pressure was higher than 0.7 bar, due to the limitation from the man-power and the equilibrium state between the reactor and the bellows when it was pressed down, not all the biogas could be pumped back to the reactor, as illustrated by the other sparges in the third run and the fourth run.

The biogas composition for the fourth run and the fifth run showed low methane content because of the low population of methanogens in the sludge from the source. The main reactor where sludge came from had a low population of methanogens and needed to mix with fresh sludge with a high methanogen population. Seaweed was fed continuously just to keep the rest of the bacteria alive.

Since these experiments were about commissioning the new pressurised reactor system and understanding its capabilities and constraints, the value of the results is rather limited. Further experiments were therefore done using a resigned twin reactor system as described in the next section.

4.5. Pressurised Anaerobic Digestion of Pondweed with the Twin Bioreactor

4.5.1. Results

The effects that headspace pressure have on biogas production rate and composition were examined using the twin pressurised bioreactor system. The biogas composition was analysed with the Rapidox 5100 Portable Gas Analyser (Cambridge Sensotec, UK), as discussed in the methods chapter and shown in Figure 3.7. In the results presented below, the only gases that were detected in measurable (non-zero) amounts were CO_2, O_2 and CH_4 with the balance of the gas needed to make the total up to 100% being assumed to be nitrogen.

Figure 4.22 demonstrates the change of headspace pressure of vessel 1 during the first run. Once the digestion process got past the initial starting-up stage, it had two weeks of almost identical biogas production rate before the feedstock slowly ran out and the production rate slowly decreased. Each sampling event vented completely to atmosphere. The negative values indicate an offset error in

the pressure sensor.

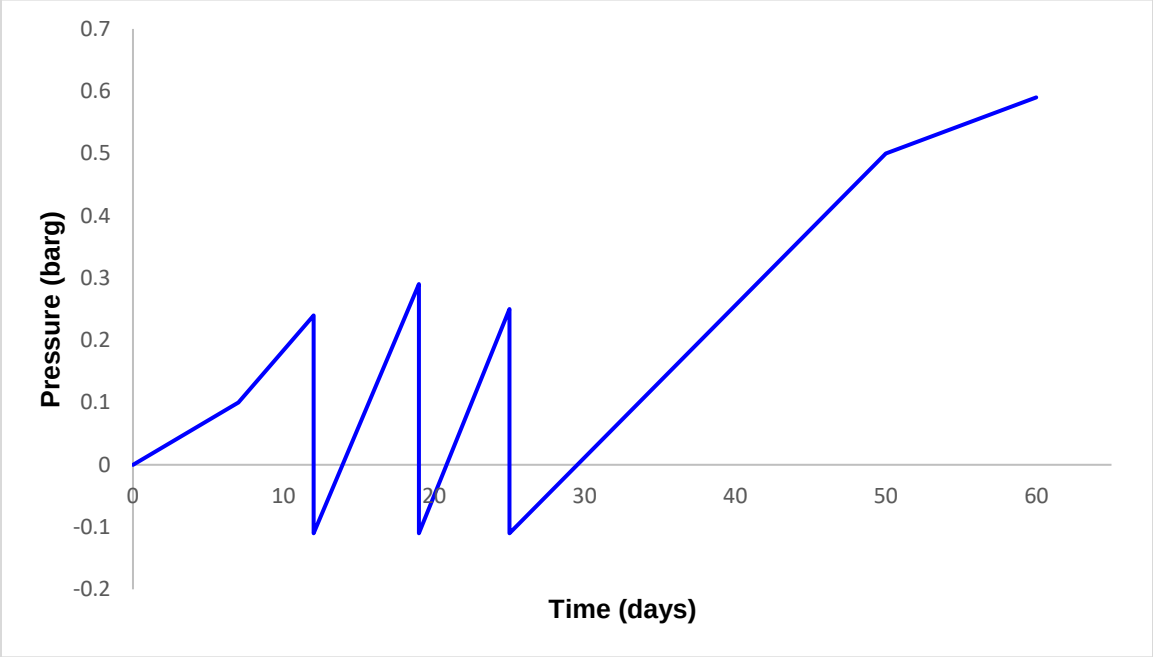

Figure 4.22 – The pressure profile of vessel 1 during the first run. The drops in headspace pressure were the days that biogas was sampled to determine its composition.

Table 4.8 shows the composition of gas and the headspace pressure before and after each sampling. Note that this run was somewhat exploratory in that pressures were only allowed to build up to modest levels.

Table 4.8 – The composition of biogas and headspace pressure in vessel 1 during the first run. $N_2{}^a$ is the composition of nitrogen plus all other gases that cannot be detected by the analyser (i.e. calculated to make the total 100%). Pressures p^a and p^b are, respectively, the absolute pressures (bara) just before and just after sampling as discussed in section 3.4.4. N/A denotes the lost data that could not be recovered due to unknown issues.

Date	Day	CH_4	CO_2	O_2	$N_2{}^a$	p^a	p^b
13/08/2020	0	0	0	21%	79%	1.01	1.01
25/08/2020	12	14.2%	18%	2.2%	65.6%	1.25	0.89
01/09/2020	19	33.5%	23%	1%	42.5%	1.30	0.89
07/09/2020	25	41.7%	24.6%	1.3%	32.4%	1.26	0.89
12/10/2020	60	57.5%	23.5%	0	18.8%	1.60	1.01

For the second run, both vessels were used, however, vessel 2 was set up eight days after vessel 1. Figure 4.23 shows the pressure profile of both vessel 1 and 2 during the second run. The sudden drop in pressure was caused by sampling of the biogas. It can also be seen that there are several gaps in the recorded data (*e.g.* only a couple of values recorded between days 8 to 16) due to an unknown issue with the pressure recording. As illustrated in the Figure 4.23, even though the process in vessel 2 was set up eight days later than vessel 1, it still had a very similar biogas production rate compared to vessel 1.

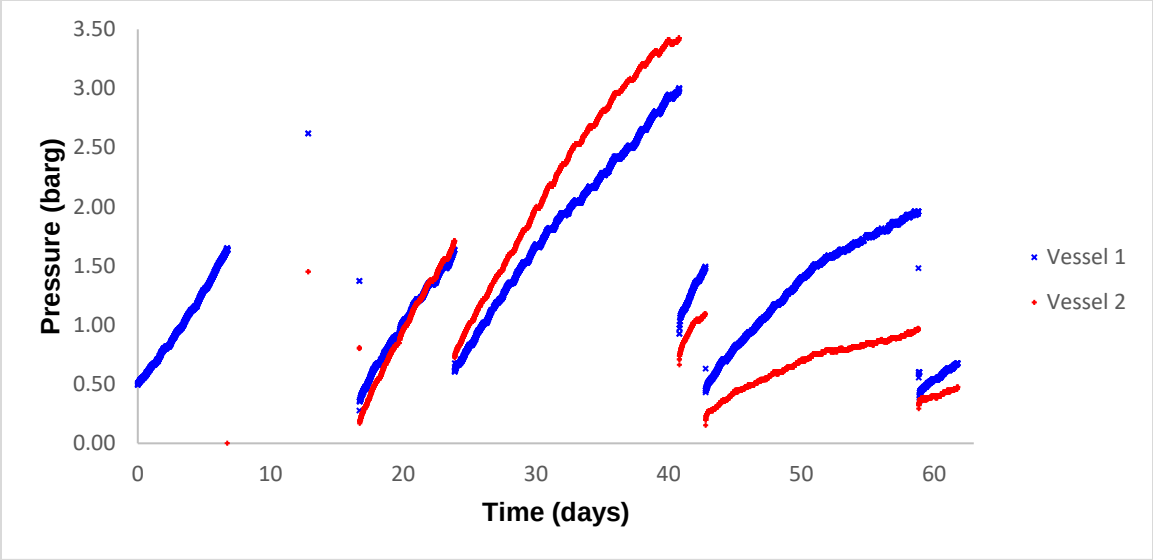

Figure 4.23 – The pressure profile of both vessels during the second run. The drops in headspace pressure were the days that biogas was sampled to determine its composition. Note the gaps in the data due to pressure recording failures.

Table 4.9 shows the biogas composition from both vessels for each sampling during the second run. The main difference between the first run and second run was that for the first run, headspace pressure was kept close to atmospheric pressure for most of the run. For the second run, the aim was to accumulate biogas in the headspace to increase the pressure as high as possible. By comparing the composition of biogas from Table 4.8 and Table 4.9, it can be seen that the biogas had a higher methane content when headspace pressure was higher. The presence of oxygen from the sampling of vessel 2 on the sixth

November was due to a simple error from the sampling technique in which air must have been allowed to ingress into the reactor.

It can also be observed from Table 4.9 that the calculated headspace pressure after re-equilibration p^d is much less than the real measured pressure when the Henry's constants for pure water are used $(\alpha = 1.0)$. If, however, all Henry's constants are reduced to 10% of this value $(\alpha = 0.1)$ then the measured and calculated values are in better agreement. This implies that the solubility of biogases, or at least that of carbon dioxide (as the more soluble biogas versus methane), is a lot less in digestate than that of pure water. A study by Gros *et al*. (1999) showed that soluble gases such as O_2 and CO_2 have different solubilities in different aqueous solutions.

Table 4.9 – The composition of biogas and the headspace pressure for both vessels during the second run. $N_2{}^a$ is the composition of nitrogen plus all the other gases that cannot be detected by the analyser (i.e. calculated to make the total 100%). Pressures p^a, p^b, p^c are, respectively, the absolute pressures (bara) just before sampling, just after sampling and following pressure recovery (re-equilibration) as discussed in section 3.4.4. Pressure p^d $(\alpha = 1.0)$ and p^d $(\alpha = 0.1)$ are, respectively, the calculated values of p^c given by the mass balance equations using a Henry's

constant adjustment factor of $\alpha = 1.0$ and $\alpha = 0.1$. N/A denotes the lost data caused by the unknown data logging issue.

	Date	Day	CH_4	CO_2	O_2	${N_2}^a$	p^a	p^b	p^c	p^d $(\alpha = 1.0)$	p^d $(\alpha = 0.1)$
Vessel 1	12/10/2020	0	0	0	21%	79%	1.01	1.01	1.01	1.01	1.01
	27/10/2020	15	44.3%	31.9%	0	23.8%	3.71	1.81	N/A	2.41	1.98
	30/10/2020	18	52.6%	40%	0	7.4%	2.38	1.29	1.38	1.70	1.41
	06/11/2020	25	58.7%	40.9%	0	0.4%	2.64	1.61	1.63	2.01	1.73
	23/11/2020	42	70.0%	30.0%	0	0	4.01	1.94	2.04	2.60	2.12
	25/11/2020	44	65.0%	35.0%	0	0	2.51	1.44	1.46	1.82	1.55
	11/122020	60	65.0%	33.2%	0	1.8%	2.97	1.57	1.61	2.04	1.70
Vessel 2	20/10/2020	0	0	0	21%	79%	1.01	1.01	1.01	1.01	1.01
	27/10/2020	7	32.3%	24.6%	5.0%	38.1%	2.61	1.01	N/A	1.42	1.12
	30/10/2020	10	47.5%	40.2%	0	12.3%	1.82	1.18	1.19	1.42	1.25
	06/11/2020	17	39.7%	22.6%	7.5%	30.2%	2.72	1.73	1.74	1.98	1.80
	23/11/2020	34	75.0%	24.5%	0	0.5%	4.43	1.67	1.72	2.44	1.87
	25/11/2020	36	63.6%	32.9%	0	3.5%	2.11	1.16	1.21	1.47	1.25
	11/12/2020	52	63.7%	36.3%	0	0	1.98	1.30	1.33	1.54	1.37

The mass balance analysis also gives the amount of biogas produced during the process as calculated using equations in mentioned section 3.4.4.

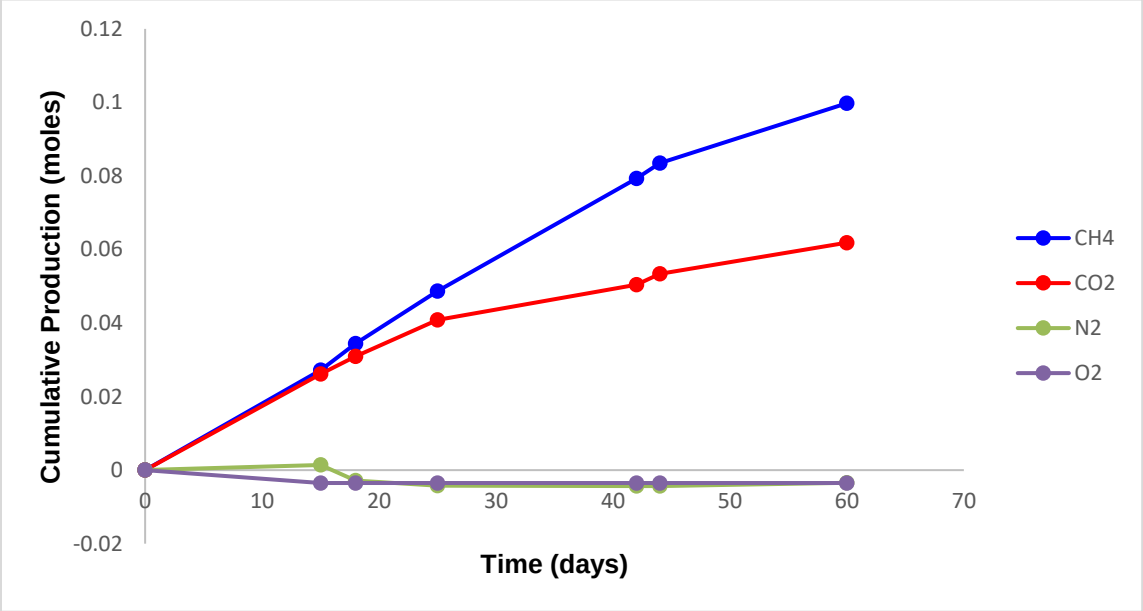

Figure 4.24 – Cumulative change of different gases in vessel 1 during the second run $(\alpha = 0.1)$.

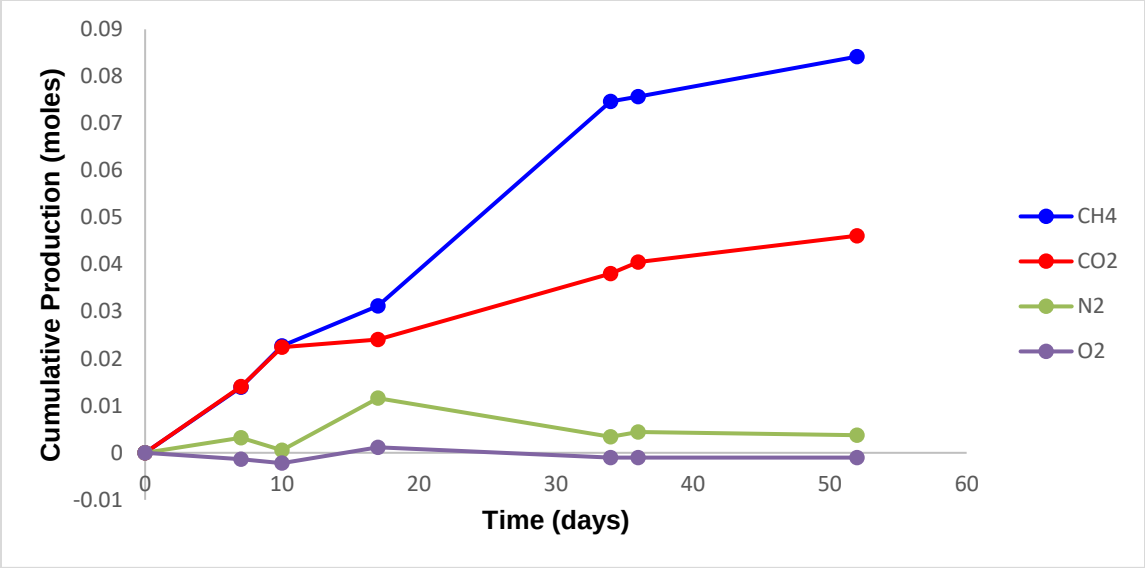

Figure 4.25 – Cumulative change of different gases in vessel 2 during the second run $(\alpha = 0.1)$**.**

Figure 4.24 and 4.25 demonstrate the results of the mass balance analysis. The cumulative change of each gas during the second run was calculated from the composition of biogas obtained from each sampling. The results for each vessel are in quite close agreement. The fact that relatively more CO_2 is produced in the early phase is probably due to the presence of aerobic metabolism until the oxygen is used up. Since N_2 and O_2 are not produced from the anaerobic digestion process, the cumulative change is negative due to the decrease in concentration after each sampling. The small spike of N_2 and O_2 in vessel 2 from the third sampling was caused by the wrong sampling technique.

Once the sampling is finished, it takes some time (1-2 hours) for the system to re-establish the liquid-gas equilibrium. Figure 4.26 illustrates this phenomenon for one of the sampling events.

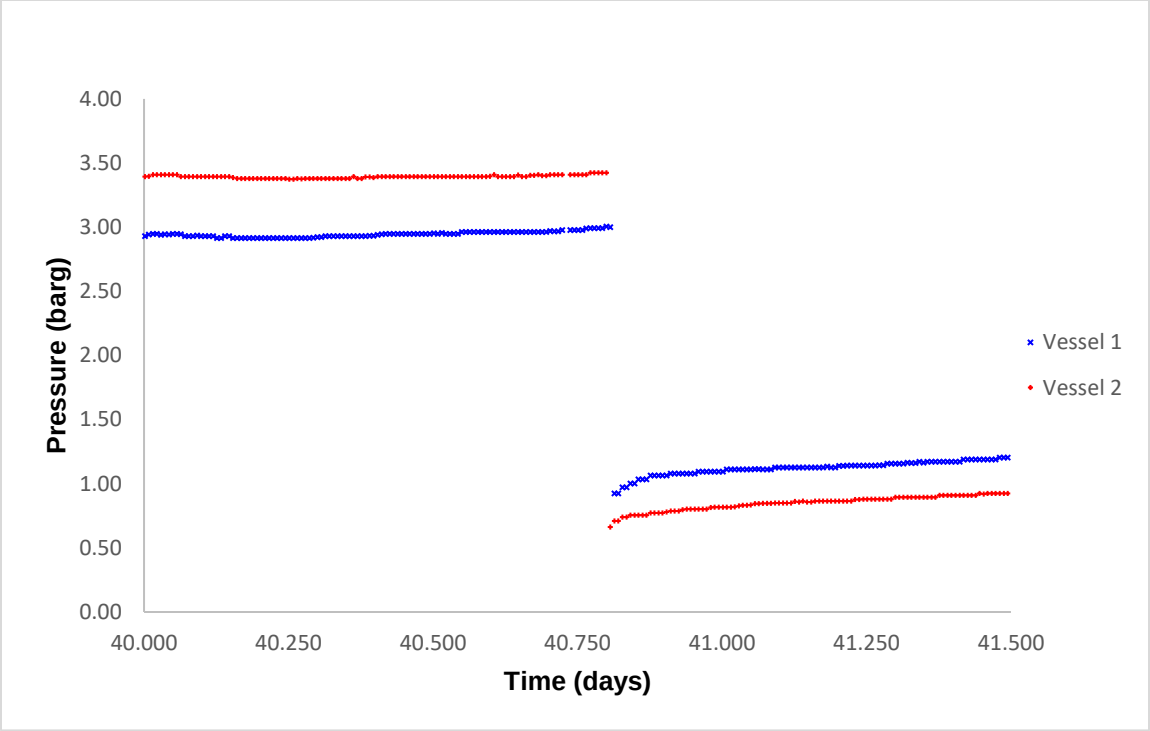

Figure 4.26 – The pressure profile of the fourth sampling and recovery of headspace pressure for vessel 1 and 2.

4.5.2. Discussion

The effects of headspace pressure on biogas composition were investigated in this experiment. The results from the first and second runs were compared. When operating at higher pressure, represented by the second run, the biogas produced from the anaerobic digestion process had a higher methane content. Biogas composition analysis from both runs also showed that, as the anaerobic digestion process continued, the production rate of methane gradually increased. The slight increase in CO_2 content from the fourth to the fifth sampling from the second run proved that as the headspace pressure increased, more CO_2 would

be dissolved in liquid because of its high solubility. Soon after the sampling, assuming not much biogas has been produced at this stage, the dissolved CO_2 in liquid was transferred back to headspace, causing the slight increase in CO_2 content.

5.*Conclusion*

5.1. Conclusion

In the last couple of decades, human activities have significantly increased the concentration of CO_2 in the atmosphere, which is the leading contributor to climate change. Energy production from combustion of fossil fuels is the principal contributor of artificial CO_2 emission (Kadam, 2002). The European Commission has deployed various strategies for its member states to tackle climate change, for instance, increasing energy efficiency by tapping into highest potential of energy saving – buildings and transport; building a pan-European integrated energy market by accurately and timely implementation of the internal market legislation; securing affordable and safe energy for citizens and businesses by making energy policies more customer friendly; driving technological shifts by launching large scale European projects to develop renewable energy production (European Commission, 2010).

Among the new large-scale projects for renewable energy production, the anaerobic digestion process has been identified as a sustainable resource for renewable energy since the feedstock it requires is biomass and waste, which can be found in the form of energy crops and inedible residues from food crops, waste oils and animal fat, manure, the organic fraction of municipal solid waste and sewage sludge (Apples, *et al*., 2011). Furthermore, a study (Chisti, 2007) suggested that microalgae are more likely to be the primary source for renewable biodiesel with the capability of meeting global demand for transport fuels. This

leaves an abundant supply of residues of microalgae as feedstocks for anaerobic digestion (Ehimen, Sun, Carrington, Brich, & Eaton-Rye, 2011). Different techniques of the anaerobic digestion process with various feedstocks have been investigated for decades (Chelliapan & Sallis, 2010; Jewell, *et al*., 1981; Gómez, *et al*., 2006; Chan, *et al*., 2009; Callaghan, *et al*., 2002). Typical biogas produced by anaerobic digestion process contains 53 to 70% CH_4, 30 to 47% CO_2, moisture and other trace gases (Persson, Jönsson & Wellinger, 2006). For applications such as vehicle fuel and injection into the natural gas grid, the biogas needs to be upgraded to meet the standard (Ryckebosch, *et al*., 2011). On one hand, current well-developed upgrading technologies such as absorption, pressure swing adsorption and membrane separation, as well as developing technologies such as cryogenic separation and ecological lung, require a lot of process equipment and the procedures are normally designed for large scale plants in order to achieve economic benefits. On the other hand, *in situ* methane enrichment has the potential to be economical for smaller plants (Persson, *et al*., 2006).

This project is the first systematic study into the variation of biogas production with self-generated headspace pressure. An existing computational model, known as the MAD model, was adapted and modified to investigate the effect headspace pressure has on biogas production. Measuring the weight difference of sealed reactors before and after venting as a method of calculating biogas production had proven to be effective. Experiments on the anaerobic digestion of pondweed proved that the biogas production rate decreases as the headspace

pressure increases. The modified model yielded similar results and showed a matching trend.

The modified model was then used as a parameter estimation tool to determine the maximum specific growth rate of the bacteria used in anaerobic digestion of microalgae, but the results were not close.

Glucose and yeast fermentation demonstrated that the CO_2 production rate declines as the headspace pressure rises in a manner that is similar to anaerobic digestion.

Pressurised anaerobic digestion of seaweed showed a smooth biogas production over a two-week period when the biogas was not vented at all. The biogas production rate slowed down towards the end of two-week period as well. Pressurised anaerobic digestion of pondweed with twin bioreactor proved that anaerobic digestion at higher pressure produced biogas with higher CH_4 content. A mass balance analysis of the biogas sampling showed that CO_2 has a much lower solubility in digestate than in pure water, as given in Henry's law.

The hypothesis of this project is that pressurised anaerobic digestion process can produce biogas with higher methane content than conventional processes operating at atmospheric pressure. Therefore, the need for upgrading process can be reduced or possibly even removed. Due to the fact that CO_2 is much more soluble than CH_4 in water at atmospheric pressure, if the anaerobic digestion process is performed in a pressure vessel with increased headspace pressure, according to Henry's Law, more CO_2 would be dissolved in the liquid fraction and

would consequently bring about an increase in the CH_4 content of the biogas. The effects of added pressure on biogas content from the anaerobic digestion process were examined. The advantage of introducing pressure to anaerobic digestion process is that it can combine the production and upgrading process, which is essentially a form of *in situ* methane enrichment. As a result, the methane content in the end product would be higher compared to a conventional anaerobic digestion process.

As aforementioned in section 2.2.3 and section 2.2.4, there is no information available about how the performance of *in situ* biogas upgrading technology in commercial applications compares to other well-established technologies. This project aimed to develop a fully functional pressurised anaerobic digestion process that could produce high methane content biogas without the need for additional biogas upgrading processes. Once the laboratory-scale experiment produces meaningful results, it can be up scaled to a pilot scale project to obtain the necessary information and fill in those gaps.

In addition, this work shows that substantial pressures can be self-generated without a large reduction in the rate of biogas production. This means that increased headspace pressure could provide the motive force for gas sparging or liquid injection to give mixing without the need for agitation.

Finally, pursuing the engineering aims in this work has uncovered two interesting observations which are worthy of further study. Firstly, the solubility of carbon dioxide in the digestate appears to be at least an order of magnitude less than that for carbon dioxide in pure water. Secondly, the rate at which carbon dioxide

is produced by fermenting yeast cells appears to be controlled to some extent by the rate at which dissolved carbon dioxide diffuses across the cell membrane.

5.2. Future Work

For the modified model, a more comprehensive parameter estimation exercise could be carried out in which the model is exported from CellDesigner into Copasi, then Copasi's parameter estimation tools used to fit more parameters than just the maximum specific growth rate for the bacteria involved in the laboratory-scale experiments.

For glucose and yeast fermentation, it would be of considerable interest to run more fermentations with higher target pressures between 1.2 barg and 5.4 barg so a better data trend can be calculated with the help of those extra data points.

Finally, the twin reactor system could be used to rerun the laboratory-scale experiments over a period of several weeks with periodic feeding to demonstrate continuous operation at elevated pressures and sustained enhancement of methane fraction and hence energy content of the biogas. The effect on biogas production of periodic sparging from one headspace to the other could also be assessed.

6.*References*

Abdelgadir, A., Chen, X., Liu, J., Xie, X., Zhang, J., Zhang, K., . . . Liu, N. (2014). Current Biotechnological Advancements on Sustainable Metal and Nutrient Removal. *BioMed Research International, 2014*, 10-19. doi:10.1155/2014/841573

Abbasi, T., Tauseef, S. M., & Abbasi, S. A. (2012). A Brief History of Anaerobic Digestion and "Biogas". In T. Abbasi, S. M. Tauseef, & S. A. Abbasi, *Biogas Energy* (p. 11). New York: Springer.

Abdelgadir, A., Chen, X., Liu, J., Xie, X., Zhang, J., Zhang, K., . . . Liu, N. (2014). Characteristics, Process Parameters, and Inner Components of Anaerobic Bioreactors. *BioMed Research International, 2014*. doi:10.1155/2014/841573

Al-mashhadani, M. K., Wilkinson, S. J., & Zimmerman, W. B. (2016). Carbon Dioxide Rich Microbubble Acceleration of Biogas Production in Anaerobic Digestion. *Chemical Engineering Science, 156*, 24-35. doi:10.1016/j.ces.2016.09.011

Altschul, S. F., Madden, T. L., Schäffer, A. A., Zhang, J., Zhang, Z., Miller, W., & Lipman, D. J. (1997). Gapped BLAST and PSI-BLAST: A New Generation

of Protein Database Search Programs. *Nucleic Acids Research, 25*(17), 3389-3402. doi:10.1093/nar/25.17.3389

Angenent, L. T., & Sung, S. (2001). Development of Anaerobic Migrating Blanket Reactor (AMBR), a Novel Anaerobic Treatment System. *Water Research, 35*(7), 1739-1747. doi:10.1016/S0043-1354(00)00447-4

Appels, L., Lauwers, J., Degrève, J., Helsen, L., Lievens, B., Willems, K., . . . Dewil, R. (2011). Anaerobic Digestion in Global Bio-Energy Production: Potential and Research Challenges. *Renewable and Sustainable Energy Reviews, 15*(9), 4295-4301. doi:10.1016/j.rser.2011.07.121

Arroyo-López, F. N., Orlić, S., Querol, A., & Barrio, E. (2009). Effects of Temperature, pH and Sugar Concentration on the Growth Parameters of Saccharomyces cerevisiae, S. kudriavzevii and Their Interspecific Hybrid. *International Journal of Food Microbiology, 131*(2-3), 120–127. doi:10.1016/j.ijfoodmicro.2009.01.035

Barber, W. P., & Stuckey, D. C. (1999). The Use of the Anaerobic Baffled Reactor (ABR) for Wastewater Treatment: A Review. *Water Research, 33*(7), 1559-1578. doi:10.1016/S0043-1354(98)00371-6

Basha, H. (2011, December 15). *Anaerobic Treatment and Biogas (Short)*. Retrieved July 26, 2017, from SlideShare: https://www.slideshare.net/skhumayunbasha/anaerobic-treatment-and-biogas-short

Batstone, D. J., Keller, J., & Steyer, J.-P. (2006). A Review of ADM1 Extensions, Applications, and Analysis: 2002–2005. *Water Science & Technology, 54*(4), 1-10. doi:10.2166/wst.2006.520

Batstone, D. J., Keller, J., Angelidaki, R., Kalyuzhnyi, S., Pavlostathis, S., Rozzi, A., . . . Vavilin, V. (2002). *Anaerobic Digestion Model No. 1 : IWA Task Group for Mathematical Modelling of Anaerobic Digestion Processes.* London: IWA Publishing.

Bernard, O., Hadj-Sadok, Z., Dochain, D., Genovesi, A., & Steyer, J.-P. (2001). Dynamical Model Development and Parameter Identification for an Anaerobic Wastewater Treatment Process. *Biotechnology and Bioengineering, 75*(4), 424-438. doi:10.1002/bit.10036

Blue Sky Bio Ltd. (2018, May 20). Retrieved from BLUESKYBIO: https://www.blueskybio.co.uk/

Bond, T., & Templeton, M. R. (2011). History and Future of Domestic Biogas Plants in the Developing World. *Energy for Sustainable Development, 15*(4), 347-354. doi:10.1016/j.esd.2011.09.003

Boopathy, R., & Sievers, D. M. (1991). Performance of a Modified Anaerobic Baffled Reactor to Treat Swine Waste. *Transactions of the ASAE, 34*(6), 2573-2578. doi:10.13031/2013.31908

Bowen, B. H., & Irwin, M. W. (2008). *Coal Characteristic CCTR Basic Facts File #8*. Retrieved July 9, 2018, from

https://www.purdue.edu/discoverypark/energy/assets/pdfs/cctr/outreach/Basics8-CoalCharacteristics-Oct08.pdf

Bożym, M., Florczak, I., Zdanowska, P., Wojdalski, J., & Klimkiewicz, M. (2015). An Analysis of Metal Concentrations in Food Wastes for Biogas Production. *Renewable Energy, 77*, 467-472. doi:10.1016/j.renene.2014.11.010

Braber, K. (1995). Anaerobic digestion of Municipal Solid Waste: A Modern waste Disposal option on the Verge of Breakthrough. *Biomass and Bioenergy, 9*(1-5), 365-376. doi:10.1016/0961-9534(95)00103-4

Brander, M. (2012, August). *Greenhouse Gases, CO2, CO2e, and Carbon: What Do All These Terms Mean?* Retrieved January 14, 2019, from Eecometrica: https://ecometrica.com/assets/GHGs-CO2-CO2e-and-Carbon-What-Do-These-Mean-v2.1.pdf

Braz, G. H., Fernandez-Gonzalez, N., Lema, J. M., & Carballa, M. (2019). Organic Overloading Affects the Microbial Interactions During Anaerobic Digestion in Sewage Sludge Reactors. *Chemosphere, 222*, 323-332. doi:10.1016/j.chemosphere.2019.01.124

Brindle, K., & Stephenson, T. (1996). The Application of Membrane Biological Reactors for the Treatment of Wastewaters. *Biotechnology and Bioengineering, 49*(6), 601-610. doi:10.1002/(SICI)1097-0290(19960320)49:6<601::AID-BIT1>3.0.CO;2-S

British Petroleum and BP Amoco. (2018). *BP Statistical Review of World Energy.* London: BP p.l.c.

Callaghan, F. J., Wase, D. A., Thayanithy, K., & Forster, C. F. (2002). Continuous Co-Design of Cattle Slurry with Fruit and Vegetable Waste and Chicken Manure. *Biomass & Bioenergy, 27*, 71-77. doi:10.1016/S0961-9534(01)00057-5

Chan, Y., Chong, M., Law, C., & Hassell, D. G. (2009). A Review on Anaerobic–Aerobic Treatment of Industrial and Municipal Wastewater. *Chemical Engineering Journal, 155*(1-2), 1-18. doi:10.1016/j.cej.2009.06.041

Charoenchai, C., Fleet, G. H., & Henschke, P. A. (1998). Effects of Temperature, pH, and Sugar Concentration on the Growth Rates and Cell Biomass of Wine Yeasts. *American Journal of Enology and Viticulture, 49*(3), 283-288.

Chelliapan, S., & Sallis, P. J. (2010). Performance of an Up-Flow Anaerobic Packed Bed Reactor System Treating Pharmaceutical Wastewater. *Proceedings of International Conference on Biology, Environment and Chemistry (ICBEC 2010).* Singapore: IACSIT Press.

Chen, L.-Y., Chen, J.-M., Gituru, R. W., & Wang, Q.-F. (2012). Generic Phylogeny, Historical Biogeography and Character Evolution of the Cosmopolitan Aquatic Plant Family Hydrocharitaceae. *BMC Evolutionary Biology, 12*. doi:10.1186/1471-2148-12-30

Chen, Y., Rößler, B., Zielonka, S., Lemmer, A., Wonneberger, A.-M., & Jungbluth, T. (2014). The Pressure Effects on Two-Phase Anaerobic

Digestion. *Applied Energy, 116*, 409-415. doi:10.1016/j.apenergy.2013.11.012

Chisti, Y. (2007). Biodiesel from Microalgae. *Biotechnology Advances, 25*(3), 294-306. doi:10.1016/j.biotechadv.2007.02.001

Chong, S., Sen, T. K., Kayaalp, A., & Ang, H. (2012). The Performance Enhancements of Upflow Anaerobic Sludge Blanket (UASB) Reactors for Domestic Sludge Treatment – A State-of-the-art Review. *Water Research, 46*(11), 3434-3470. doi:10.1016/j.watres.2012.03.066

Cook, C. D., & Urmi-König, K. (1984). A Revision of the Genus Egeria (Hydrocharitaceae). *Aquatic Botany, 19*(1-2), 73-96. doi:10.1016/0304-3770(84)90009-3

Cook, C. D., & Urmi-König, K. (1985). A Revision of the Genus Elodea (Hydrocharitaceae). *Aquatic Botany, 21*(2), 111-156. doi:10.1016/0304-3770(85)90084-1

Cozma, P., Ghinea, C., Mămăligă, I., Wukovits, W., Friedl, A., & Gavrilescu, M. (2013). Environmental Impact Assessment of High Pressure Water Scrubbing Biogas Upgrading Technology. *Clean Soil Air Water, 41*(9), 917-927. doi:10.1002/clen.201200303

Dague, R. R., McKinney, R. E., & Pfeffer, J. T. (1966). Anaerobic Activated Sludge. *Water Pollution Control Federation, 38*(2), 220-226.

Dague, R. R., McKinney, R. E., & Pfeffer, J. T. (1970). Solids Retention in Anaerobic Waste Treatment Systems. *Journal (Water Pollution Control Federation), 42*(2), R29-R46.

D'Amore, T., Russell, I., & Stewart, G. G. (1989). Sugar Utilization by Yeast During Fermentation. *Journal of Industrial Microbiology & Biotechnology, 4*(4), 315–323. doi:10.1007/BF01577355

Daud, M. K., Rizvi, H., Akram, M. F., Ali, S., Rizwan, M., Nafees, M., & Zhu, S. (2018). Review of Upflow Anaerobic Sludge Blanket Reactor Technology: Effect of Different Parameters and Developments for Domestic Wastewater Treatment. *Journal of Chemistry, 2018*, 13. doi:10.1155/2018/1596319

De Dobbelaere, A., De Keulenaere, B., De Mey, J., Lebuf, V., Meers, E., Ryckaert, B., . . . Van Driessche, J. (2015). *Small-Scale Anaerobic Digestion : Case Studies in Western Europe.* Rumbeke: Inagro.

De Schamphelaire, L., & Verstraete, W. (2009). Revival of the Biological Sunlight-to-Biogas Energy Conversion System. *Biotechnology and Bioengineering, 103*(2), 296-304. doi:10.1002/bit.22257

Dobson, P. D., & Kell, D. B. (2008). Carrier-Mediated Cellular Uptake of Pharmaceutical Drugs: An Exception or the Rule? *Nature Reviews Drug Discovery, 7*, 205-220. doi:10.1038/nrd2438

Eckert, J. S. (1966). *United States Patent No. 326678A.* Retrieved from https://patents.google.com/patent/US3266787A/en#patentCitations

Ehimen, E. A., Sun, Z. F., Carrington, C. G., Brich, E. J., & Eaton-Rye, J. J. (2011). Anaerobic Digestion of Microalgae Residues Resulting from the Biodiesel Production Process. *Applied Energy, 88*(10), 3454-3463. doi:10.1016/j.apenergy.2010.10.020

European Commission. (2010). *Energy 2020 A strategy for Competitive, Sustainable and Secure Energy .* Brussels: European Commission.

Everett, B., Boyle, G., Peake, S., & Ramage, J. (2012). *Energy Systems and Sustainability: Power for a Sustainable Future* (2nd ed.). Oxford: Oxford University Press.

Funahashi, A., Matsuoka, Y., Jouraku, A., Morohashi, M., Kikuchi, N., & Kitano, H. (2008). CellDesigner 3.5: A Versatile Modeling Tool for Biochemical Networks. *Proceedings of the IEEE, 96*(8), 1254-1265. doi:10.1109/JPROC.2008.925458

Galanakis, C. M., Kordulis, C., Kanellaki, M., Koutinas, A. A., Bekatorou, A., & Lycourghiotis, A. (2012). Effect of Pressure and Temperature on Alcoholic Fermentation by Saccharomyces cerevisiae Immobilized on γ-alumina Pellets. *Bioresource Technology, 114*, 492-498. doi:10.1016/j.biortech.2012.03.010

Gómez, X., Cuetos, M. J., Cara, J., Morán, A., & García, A. I. (2006). Anaerobic Co-Digestion of Primary Sludge and the Fruit and Vegetable Fraction of the Municipal Solid Wastes: Conditions for Mixing and Evaluation of the

Organic Loading Rate. *Renewable Energy, 31*(12), 2017-2024. doi:10.1016/j.renene.2005.09.029

Goswami, R., Chattopadhyay, P., Shome, A., Banerjee, S. N., Chakraborty, A. K., Mathew, A. K., & Chaudhury, S. (2016). An Overview of Physico-Chemical Mechanisms of Biogas Production by Microbial Communities: a Step Towards Sustainable. *3 Biotech, 6*(72). doi:10.1007/s13205-016-0395-9

Grande, C. A. (2012). Advances in Pressure Swing Adsorption for Gas Separation. *ISRN Chemical Engineering, 2012*, 1-13. doi:10.5402/2012/982934

Gros, J. B., Dussap, C. G., & Catté, M. (1999). Estimation of O2 and CO2 Solubility in Microbial Culture Media. *Biotechnology Progress, 15*(5), 923−927. doi:10.1021/bp990074i

Han, Y., & Dague, R. (1997). Laboratory Studies on the Temperature-Phased Anaerobic Digestion of Domestic Primary Sludge. *Water Environment Research, 69*(6-7), 1139-1143. doi:10.2175/106143097X125885

Hayes, T. D., Isaacson, H. R., Pfeffer, J. T., & Liu, Y. M. (1990). *In Situ* Methane Enrichment in Anaerobic Digestion. *Biotechnology and Bioengineering, 35*(1), 73-86. doi:10.1002/bit.260350111

He, G., Liu, T., Sadiq, F. A., Gu, J., & Zhang, G. (2017). Insights into the Microbial Diversity and Community Dynamics of Chinese Traditional Fermented Foods from Using High-Throughput Sequencing Approaches.

Journal of Zhejiang University-SCIENCE B (Biomedicine & Biotechnology), 18, 289-302. doi:10.1631/jzus.B1600148

Heard, G. M., & Fleet, G. H. (1988). The Effects of Temperature and pH on the Growth of Yeast Species During the Fermentation of Grape Juice. *Journal of Applied Bacteriology, 65*(1), 23-28. doi:10.1111/j.1365-2672.1988.tb04312.x

Hidaka, T., Takabe, Y., Tsumori, J., & Minamiyama, M. (2017). Characterization of Microalgae Cultivated in Continuous Operation Combined with Anaerobic Co-Digestion of Sewage Sludge and Microalgae. *Biomass and Bioenergy, 99*, 139-146. doi:10.1016/j.biombioe.2017.02.019

Hjorth, M., Nielsen, A. M., Nyord, T., Hansen, M. N., Nissen, P., & Sommer, S. G. (2009). Nutrient Value, Odour Emission and Energy Production of Manure as Influenced by Anaerobic Digestion and Separation. *Agronomy for Sustainable Development, 29*(2), 329-338. doi:10.1051/agro:2008047

Hu, Y., Kobayashi, T., Qi, W., Oshibe, H., & Xu, K.-Q. (2018). Effect of Temperature and Organic Loading Rate on Siphon-Driven Self-Agitated Anaerobic Digestion Performance for Food Waste Treatment. *Waste Management, 74*, 150-157. doi:10.1016/j.wasman.2017.12.016

Intergovernmental Panel on Climate Change. (2014). *Climate Change 2014 Mitigation of Climate Change.* New York: Cambridge University Press.

Inyang, M., Gao, B., Pullammanappallil, P., Ding, W., & Zimmerman, A. R. (2010). Biochar from Anaerobically Digested Sugarcane Bagasse.

Bioresource Technology, 101(22), 8868-8872. doi:10.1016/j.biortech.2010.06.088

Irwin, R., Surapaneni, A., Smith, D., Schmidt, J., Rigby, H., & Smith, S. R. (2017). Verification of an Alternative Sludge Treatment Process for Pathogen Reduction at Two Wastewater Treatment Plants in Victoria, Australia. *Water & Health, 15*(4), 626–637. doi:10.2166/wh.2017.316

Jacobson, M. Z. (2005). Correction to ‘‘Control of Fossil-Fuel Particulate Black Carbon Andorganic Matter, Possibly the Most Effective Method of Slowing Global Warming’’. *Journal of Geophysical Research, 110*(D14). doi:10.1029/2005JD005888

Jewell, W. J., Switzenbaum, M. S., & Morris, J. W. (1981). Municipal Wastewater Treatment with the Anaerobic Attached Microbial Film Expanded Bed Process. *Water Pollution Control Federation, 53*(4), 482-490.

Johansen, A., Nielsen, H. B., Hansen, C. M., Andreasen, C., Carlsgart, J., Hauggard-Nielsen, H., & Roepstorff, A. (2013). Survival of Weed Seeds and Animal Parasites as Affected by Anaerobic Digestion at Meso- and Thermophilic Conditions. *Waste Management, 33*(4), 807-812. doi:10.1016/j.wasman.2012.11.001

Johansson, T. B., Reddy, A. K., Kelly, H., William, R. H., & Burnham, L. (1993). *Renewable Energy: Sources for Fuels and Electricity.* Washington, D.C.: Island Press.

Jones, R. C., & Hough, J. S. (1970). The Effect of Temperature on the Metabolism of Baker's Yeast growing on Continuous Culture. *Microbiology, 60*, 107-116. doi:10.1099/00221287-60-1-107

Kadam, K. L. (2002). Environmental Implications of Power Generation Via Coal-Microalgae Cofiring. *Energy, 27*(10), 905-922. doi:10.1016/S0360-5442(02)00025-7

Kangle, K. M., Kore, S. V., Kore, V. S., & Kulkarni, G. S. (2012). Recent Trends in Anaerobic Codigestion: A Review. *Universal Journal of Environmental Research and Technology, 2*(4), 210-219.

Kapdi, S. S., Vijay, V. K., Rajesh, S. K., & Prasad, R. (2005). Biogas Scrubbing, Compression and Storage: Perspective and Prospectus in Indian Context. *Renewable Energy, 30*(8), 1195-1202. doi:10.1016/j.renene.2004.09.012

Kariyama, I. D., Zhai, X., & Wu, B. (2018). Influence of Mixing on Anaerobic Digestion Digestion Efficiency in Stirred Tank Digester: A Review. *Water Research, 143*, 503-517. doi:10.1016/j.watres.2018.06.065

Kim, M., Ahn, Y.-H., & Speece, R. E. (2002). Comparative Process Stability and Efficiency of Anaerobic Digestion; Mesophilic vs. Thermophilic. *Water Research, 36*(17), 4369-4385. doi:10.1016/S0043-1354(02)00147-1

Kinyua, M. N., Rowse, L. E., & Ergas, S. J. (2016). Review of Small-Scale Tubular Anaerobic Digesters Treating Livestock Waste in the Developing World. *Renewable and Sustainable Energy Reviews, 58*, 896-910. doi:10.1016/j.rser.2015.12.324

Konings, W., Lolkema, J., Bolhuis, H., van Veen, H., Poolman, B., & Driessen, A. (1997). The Role of Transport Processes in Survival of Lactic Acid Bacteria. *Antonie van Leeuwenhoek, 71*(1), 117-128. doi:10.1023/A:100014352

Koyama, M., Yamamoto, S., Ishikawa, K., Ban, S., & Toda, T. (2014). Anaerobic Digestion of Submerged Macrophytes: Chemical Composition and Anaerobic Digestibility. *Ecological Engineering, 69*, 304–309. doi:10.1016/j.ecoleng.2014.05.013

Latif, M. A., Mehta, C. M., & Batstone, D. J. (2018). Enhancing Soluble PhosphateConcentration in Sludge Liquor by Pressurised Anaerobic Digestion. *Water Research, 145*, 660-666. doi:10.1016/j.watres.2018.08.069

Lemmer, A., Merkle, W., Baer, K., & Graf, F. (2017). Effects of High-Pressure Anaerobic Digestion up to 30 Bar on pH-Value, Production Kinetics and Specific Methane Yield. *Energy, 138*, 659-667. doi:10.1016/j.energy.2017.07.095

Lettinga, G. (1995). Anaerobic Digestion and Wastewater Treatment Systems. *Antonie van Leeuwenhoek, 67*(1), 3-28. doi:10.1007/BF00872193

Lettinga, G., van Velsen, A., Hobma, S., de Zeeuw, W., & Klapwijk, A. (1980). Use of the Upflow Sludge Blanket (USB) Reactor Concept for Biological Wastewater Treatment, Especially for Anaerobic Treatment.

Biotechnology and Bioengineering, 22(4), 699-734. doi:10.1002/bit.260220402

Levén, L., Nyberg, K., Korkea-aho, L., & Schnürer, A. (2006). Phenols in Anaerobic Digestion Processes and Inhibition of Ammonia Oxidising Bacteria (AOB) in Soil. *Science of The Total Environment, 364*(1-3), 229-238. doi:10.1016/j.scitotenv.2005.06.003

Li, H., Jin, C., Zhang, Z., O'Hara, I., & Mundree, S. (2017). Environmental and Economic Life Cycle Assessment of Energy Recovery from Sewage Sludge Through Different Anaerobic Digestion Pathways. *Energy, 126*, 649-657. doi:10.1016/j.energy.2017.03.068

Li, Y., Yang, G., Li, L., & Sun, Y. (2018). Bioaugmentation for Overloaded Anaerobic Digestion Recovery with Acid-Tolerant Methanogenic Enrichment. *Waste Management, 79*, 744-751. doi:10.1016/j.wasman.2018.08.043

Ligero, P., de Vega, A., & Soto, M. (2001). Influence of HRT (Hydraulic Retention Time) and SRT (Solid Retention Time) on the Hydrolytic Pre-Treatment of Urban Wastewater. *Water Science and Technology, 44*(4), 7-14. doi:10.2166/wst.2001.0163

Lin, K. C., & Pearce, M. E. (1991). Effects of Mixing on Anaerobic Treatment of Potato-Processing Wastewater. *Canadian Journal of Civil Engineering, 18*(3), 504-514. doi:10.1139/l91-061

Lin, Y., Zhang, W., Li, C., Sakakibara, K., Tanaka, S., & Kong, H. (2012). Factors Affecting Ethanol Fermentation Using Saccharomyces cerevisiae BY4742. *Biomass and Bioenergy, 47*, 395-401. doi:10.1016/j.biombioe.2012.09.019

Lindmark, J., Thorin, E., Fdhila, R. B., & Dahlquist, E. (2014). Effects of Mixing on the Result of Anaerobic Digestion: Review. *Renewable and Sustainable Energy Reviews, 40*, 1030-1047. doi:10.1016/j.rser.2014.07.182

Liu, Y., Xu, H.-L., Yang, S.-F., & Tay, J.-H. (2003). Mechanisms and Models for Anaerobic Granulation in Upflow Anaerobic Sludge Blanket Reactor. *Water Research, 37*(3), 661-673. doi:10.1016/S0043-1354(02)00351-2

Loganath, R., & Senophiyah-Mary, J. (2020). Critical Review on the Necessity of Bioelectricity Generation from Slaughterhouse Industry Waste and Wastewater Using Different Anaerobic Digestion Reactors. *Renewable and Sustainable Energy Reviews, 134*, 110360. doi:10.1016/j.rser.2020.110360

Lohani, S. P., & Havukainen, J. (2018). Anaerobic Digestion: Factors Affecting Anaerobic Digestion Process. In S. J. Varjani, E. Gnansounou, B. Gurunathan, D. Pant, & Z. A. Zakaria (Eds.), *Waste Bioremediation* (pp. 343-359). Singapore: Springer. doi:10.1007/978-981-10-7413-4

Lolkema, J., Speelmans, G., & Konings, W. (1994). Na+-coupled versus H+-coupled energy transduction in bacteria. *Biochimica et Biophysica Acta*

(BBA) - Bioenergetics, 1187(2), 211-215. doi:10.1016/0005-2728(94)90113-9

Longmore, W. J., Niethe, C. M., & McDaniel, M. L. (1969). Effect of CO2 Concentration on Intracellular pH and on Glycogen Synthesis from Glycerol and Glucose in Isolated Perfused Rat Liver. *The Journal of Biological Chemistry, 244*(23), 6451-6457.

Loupasaki, E., & Diamadopoulos, E. (2013). Attached Growth Systems for Wastewater Treatment in Small and Rural Communities: A Review. *Journal of Chemical Technology and Biotechnology, 88*(2), 190–204. doi:10.1002/jctb.3967

Lucero, P., Peñalver, E., Moreno, E., & Lagunas, R. (2000). Internal Trehalose Protects Endocytosis from Inhibition by Ethanol in Saccharomyces cerevisiae. *Applied and Environmental Microbiology, 66*(10), 4456–4461. doi:10.1128/AEM.66.10.4456-4461.2000

Lyberatos, G., & Pullammanappallil, P. C. (2010). Anaerobic Digestion in Suspended Growth Bioreactors. In L. K. Wang, V. Ivanov, & J.-H. Tay (Eds.), *Environmental Biotechnology* (pp. 395-438). Totowa, NJ: Humana Press.

Lyberatos, G., & Skiadas, I. V. (1999). Modelling of Anaerobic Digestion – A Review. *Global NEST Journal, 1*(2), 63-76.

Mairet, F., Bernard, O., Cameron, E., Ras, M., Lardon, L., Steyer, J.-P., & Chachuat, B. (2011). Modelling Anaerobic Digestion of Microalgae Using

ADM1. *Bioresource Technology, 102*(3), 6823-6829. doi:10.1016/j.biortech.2011.04.015

Mairet, F., Bernard, O., Cameron, E., Ras, M., Lardon, L., Steyer, J.-P., & Chachuat, B. (2012). Three-Reaction Model for Anaerobic Digestion of Microalgae. *Biotechnology and Bioengineering, 109*(2), 415-425. doi:10.1002/bit.23350

Mao, C., Feng, Y., Wang, X., & Ren, G. (2015). Review on Research Achievements of Biogas from Anaerobic Digestion. *Renewable and Sustainable Energy Reviews, 45*, 540-555. doi:10.1016/j.rser.2015.02.032

Maskow, T., Kemp, R., Buchholz, F., Schubert, T., Kiesel, B., & Harms, H. (2010). What Heat Is Telling Us about Microbial Conversions in Nature and Technology: From Chip- to Megacalorimetry. *Microbial Biotechnology, 3*(3), 269-284. doi:10.1111/j.1751-7915.2009.00121.x

Mata-Alvarez, J., Macé, S., & Llabrés, P. (2000). Anaerobic Digestion of Organic Solid Wastes. An Oerview of Research Achievements and Perspectives. *Bioresource Technology, 74*(1), 3-16. doi:10.1016/S0960-8524(00)00023-7

McCarty, P. L. (2001). The Development of Anaerobic Treatment and its Future. *Water Science & Technology, 44*(8), 149-156. doi:10.2166/wst.2001.0487

McCormack, G. P., & Clewley, J. P. (2002). The Application of Molecular Phylogenetics to the Analysis of Viral Genome Diversity and Evolution. *Medical Virology, 12*(4), 221–238. doi:10.1002/rmv.355

Merkle, W., Baer, K., Lindner, J., Zielonka, S., Ortloff, F., Graf, F., . . . Lemmer, A. (2017). Influence of Pressuresup to 50 Bar on Two-Stage Anaerobic Digestion. *Bioresource Technology, 232*, 72-78. doi:10.1016/j.biortech.2017.02.013

Mezzullo, W. G., McManus, M. C., & Hammond, G. P. (2013). Life Cycle Assessment of a Small-Scale Anaerobic Digestion Plant from Cattle Waste. *Applied Energy, 102*, 657-664. doi:10.1016/j.apenergy.2012.08.008

Miltner, M., Makaruk, A., & Harasek, M. (2017). Review on Available Biogas Upgrading Technologies and Innovations Towards Advanced Solutions. *Journal of Cleaner Production, 161*, 1329-1337. doi:10.1016/j.jclepro.2017.06.045

Mir, M. A., Hussain, A., & Verma, C. (2016). Design Considerations and Operational Performance of Anaerobic Digester: A Review. *Cogent Engineering, 3*(1), 1-20. doi:10.1080/23311916.2016.1181696

Mirzoyan, N., Tal, Y., & Gross, A. (2010). Anaerobic Digestion of Sludge from Intensive Recirculating Aquaculture Systems: Review. *Aquaculture, 306*(1-4), 1-6. doi:10.1016/j.aquaculture.2010.05.028

Missner, A., Kügler, P., Saparov, S. M., Sommer, K., Mathai, J. C., Zeidel, M. L., & Pohl, P. (2008). Membrane Transport, Structure, Function, and Biogenesis. *The Journal of Biological Chemistry, 283*(37), 25340 –25347. doi:10.1074/jbc.M800096200

Monnet, F. (2003, Novemver). *An Introduction to Anaerobic Digestrion of Organic Wastes.* Retrieved January 20, 2019, from http://biogasmax.co.uk/media/introanaerobicdigestion__073323000_1011_24042007.pdf

Montzka, S. A., Dlugokencky, E. J., & Butler, J. H. (2011). Non-CO2 Greenhouse Gases and Climate Change. *Nature, 476*(7358), 43-50. doi:10.1038/nature10322

Mora, M., Lafuente, F. J., & Gabriel, D. (2020). Influence of Crude Glycerol Load and pH Shocks on the Granulation and Microbial Diversity of a Sulfidogenic Upflow Anaerobic Sludge Blanket Reactor. *Process Safety and Environmental Protection, 133*, 159-168. doi:10.1016/j.psep.2019.11.005

Morton, J. S. (1980). Glycolysis and Alcoholic Fermentation. *Acts & Facts, 9*(12).

Moset, V., Poulsen, M., Wahid, R., Højberg, O., & Møller, H. B. (2015). Mesophilic Versus Thermophilic Anaerobic Digestion of Cattle Manure: Methane Productivity and Microbial Ecology. *Microbial Microbiology, 8*(5), 787-800. doi:10.1111/1751-7915.12271

Müller, V. (2008). Bacterial Fermentation. *Encyclopedia of Life Sciences*. doi:10.1002/9780470015902.a0001415.pub2

Nagodawithana, T. W., Castellano, C., & Steinkraus, K. H. (1974). Effect of Dissolved Oxygen, Temperature, Initial Cell Count, and Sugar

Concentration on the Viability of Saccharomyces cerevisiae in Rapid Fermentations. *Journal of Applied Microbiology, 28*(3), 383-391.

National Small Flows Clearinghouse. (2004). The Attached Growth Process – An Old technology Takes on New Forms. *Pipeline, 15*(1), 1-8.

Nordberg, Å., Edström, M., Uusi-Penttilä, M., & Rasmuson, Å. C. (2012). Selective Desorption of Carbon Dioxide from Sewage Sludge for *InSitu* Methane Enrichment: Enrichment Experiments in Pilot Scale. *Biomass and Bioenergy, 37*, 196-204. doi:10.1016/j.biombioe.2011.12.012

Oakley, S., von Sperling, M., & Verbyla, M. (2017, March 13). *Anaerobic Sludge Blanket Reactors*. doi:10.14321/waterpathogens.61

Parker, W. J. (2005). Application of the ADM1 Model to Advanced Anaerobic Digestion. *Bioresource Technology, 96*(16), 1832-1842. doi:10.1016/j.biortech.2005.01.022

Patterson, T., Esteves, S., Dinsdale, R., & Guwy, A. (2011). An Evaluation of the Policy and Techno-Economic Factors Affecting the Potential for Biogas Upgrading for Transport Fuel Use in the UK. *Energy Policy, 39*(3), 1806-1816. doi:10.1016/j.enpol.2011.01.017

Peng, W., Lü, F., Hao, L., Zhang, H., Shao, L., & He, P. (2020). Digestate Management for High-Solid Anaerobic Digestion of Organic Wastes: A Review. *Bioresource Technology, 297*, 122485. doi:10.1016/j.biortech.2019.122485

Persson, M., Jönsson, O., & Wellinger, A. (2006). Biogas Upgrading to Vehicle Fuel Standards. *IEA Bioenergy*, 1-32.

Petersson, A., & Wellinger, A. (2009). *Biogas Upgrading Technologies-Developments and Innovations.* Retrieved July 9, 2018, from https://www.iea-biogas.net/files/daten-redaktion/download/publi-task37/upgrading_rz_low_final.pdf

RCM Digesters. (2013, June). *Complete Mix Digesters: Technical Details*. Retrieved July 7, 2017, from RCM Digesters: http://www.rcmdigesters.com/wp-content/uploads/2013/06/RCM-Complete-Mix-Technical-Details.pdf

Rico, C., Rico, J. L., Muñoz, N., Gómez, B., & Tejero, I. (2011). Effect of Mixing on Biogas Production During Mesophilic Anaerobic Digestion of Screened Dairy Manure in a Pilot Plant. *Engineering in Life Sciences, 11*(5), 476-481. doi:10.1002/elsc.201100010

Ritchie, H., & Roser, M. (2017). *Fossil Fuels*. Retrieved from Our World in Data: https://ourworldindata.org/fossil-fuels

Rivard, C. J., Himmel, M. E., Vinzant, T. B., Adney, W. S., Wyman, C. E., & Grohmann, K. (1990). Anaerobic Digestion of Processed Municiple Solid Waste Using a Novel High Solids Reactor: Maximum Solids Levels and Mixing Requirements. *Biotechnology Letters, 12*(3), 235-240. doi:10.1007/BF01026806

Ryckebosch, E., Drouillon, M., & Vervaeren, H. (2011). Techniques for Transformation of Biogas to Biomethane. *Biomass and Bioenergy, 35*(5), 1633-1645. doi:10.1016/j.biombioe.2011.02.033

Sahota, S., Shah, G., Ghosh, P., Kapoor, R., Sengupta, S., Singh, P., . . . Thakur, I. S. (2018). Review of Trends in Biogas Upgradation Technologies and Future Perspectives. *Bioresource Technology Reports, 1*, 79-88. doi:10.1016/j.biteb.2018.01.002

Singh, M., & Srivastava, R. K. (2011). Sequencing Batch Reactor Technology for Biological Wastewater Treatment: A Review. *Asia-Pacific Journal of Chemical Engineering, 6*(1), 3-13. doi:10.1002/apj.490

Sinnott, R. K. (2005). Costing and Project Evaluation. In *Chemical Engineering, Volume 6, Fourth edition* (4th ed., pp. 243-250). Oxford: Butterworth-Heinemann.

Sleator, R. D. (2011). Phylogenetics. *Archives of Microbiology, 193*(4), 235-239. doi:10.1007/s00203-011-0677-x

SSWM, Sustainable Sanitation and Water Management. (2017). *Anaerobic Baffled Reactor (ABR)*. Retrieved August 23, 2017, from http://www.sswm.info/category/implementation-tools/wastewater-treatment/hardware/semi-centralised-wastewater-treatments-8

Stamatakis, A. (2006). RAxML-VI-HPC: Maximum Likelihood-Based Phylogenetic Analyses with Thousands of Taxa and Mixed Models. *Bioinformatics, 22*(21), 2688-2690. doi:10.1093/bioinformatics/btl446

Stamatakis, A., Hoover, P., & Rougemont, J. (2008). A Rapid Bootstrap Algorithm for the RAxML Web Servers. *Systematic Biology, 57*(5), 758-771. doi:10.1080/10635150802429642

Stuart, P. (2006). The Advangages and Disadvantages of Anaerobic Digestion as a Renewable Energy Source. *Loughborough University*.

Sun, Q., Li, H., Yan, J., Liu, L., Yu, Z., & Yu, X. (2015). Selection of Appropriate Biogas Upgrading Technology-A Review of Biogas Cleaning, Upgrading and Utilisation. *Renewable and Sustainable Energy Reviews, 51*, 521-532. doi:10.1016/j.rser.2015.06.029

Sung, S., & Dague, R. (1995). Laboratory Studies on Anaerobic Sequencing Batch Reactor. *Water Environment Research, 67*(3), 294-301. doi:10.2175/106143095X131501

Switzenbaum, M. S. (1983). A Comparison of the Anaerobic Filter and Anaerobic Expanded/Fluidized Bed Processes. *Water Science and Technology, 15*(8-9), 345-358. doi:10.2166/wst.1983.0177

Tambone, F., Scaglia, S., D'Imporzano, G., Schievano, A., Orzi, V., Salati, S., & Adani, F. (2010). Assessing Amendment and Fertilizing Properties of Digestates from Anaerobic Digestion Through a Comparative Study with Digested Sludge and Compost. *Chemosphere, 81*(5), 577-583. doi:10.1016/j.chemosphere.2010.08.034

Tauseef, S. M., Abbasi, T., & Abbasi, S. A. (2013). Energy Recovery from Wastewaters with High-Rate Anaerobic Digesters. *Renewable and Sustainable Energy Review, 19*, 704-741. doi:10.1016/j.rser.2012.11.056

Tchobanoglous, G., Burton, F. L., & Stensel, H. D. (2003). *Wastewater Engineering: Treatment and Reuse* (4th ed.). New York: McGraw-Hill.

Tilley, E., Ulrich, L., Lüthi, C., Reymond, P., & Zurbrügg, C. (2014). *Compendium of Sanitation Systems and Technologies* (2nd Revised Edition ed.). Dübendorf, Switzerland: Swiss Federal Institute of Aquatic Science and Technology (Eawag).

Torija, M. J., Rozès, N., Poblet, M., Guillamón, J. M., & Mas, A. (2003). Effects of Fermentation Temperature on the Strain Population of Saccharomyces Cerevisiae. *International Journal of Food Microbiology, 80*(1), 47–53. doi:10.1016/S0168-1605(02)00144-7

Tzafriri, A. R., & Edelman, E. R. (2004). The Total Quasi-Steady-State Approximation is Valid for Reversible Enzyme Kinetics. *Journal of Theoretical Biology, 226*(3), 303-313. doi:10.1016/j.jtbi.2003.09.006

United States Environmental Protection Agency. (2015). *Appendix D—Anaerobic Digesters*. Retrieved August 7, 2017, from EPA Combined Heat and Power Partnership: https://www.epa.gov/sites/production/files/2015-07/documents/biomass_combined_heat_and_power_catalog_of_technologies_appendix_d-anaerobic_digesters.pdf

Wang, Z.-W., & Li, Y. (2014). A Theoretical Derivation of the Contois Equation for Kinetic Modeling of the Microbial Degradation of Insoluble Substrates. *Biochemical Engineering Journal, 82*, 134-138. doi:10.1016/j.bej.2013.11.002

Watanabe, K., Koyama, M., Ueda, J., Ban, S., Kurosawa, N., & Toda, T. (2017). Effect of Operating Temperature on Anaerobic Digestion of the Brazilian Waterweed Egeria densa and Its Microbial Community. *Anaerobe, 47*, 8-17. doi:10.1016/j.anaerobe.2017.03.014

Wexler, A. (1976). Vapor Pressure Formulation for Water in Range 0 to 100 °C. A Revision. *Journal of Research of the National Bureau of Standards Section A: Physics and Chemistry, 80A*(5-6), 775-785. doi:10.6028/jres.080A.071

Wiley, E. O. (2008). Phylogenetics. *Scholarpedia Journal, 3*(12), 6299. doi:10.4249/scholarpedia.6299

Yang, L., Si, B., Tan, X., Chu, H., Zhou, X., Zhang, Y., . . . Zhao, F. (2018). Integrated Anaerobic Digestion and Algae Cultivation for Energy Recovery and Nutrient Supply from Post-Hydrothermal Liquefaction Wastewater. *Bioresource Technology, 266*, 349-356. doi:10.1016/j.biortech.2018.06.083

Yang, Z., & Rannala, B. (2012). Molecular Phylogenetics: Principles and Practice. *Nature Reviews Genetics, 13*(5), 303-314. doi:10.1038/nrg3186

York, R. (212). Do Alternative Energy Sources Displace Fossil Fuels? *Nature Climate Change, 2*, 441-443. doi:10.1038/nclimate1451

Zhen, G., Kobayashi, T., Lu, X., Kumar, G., & Xu, K. (2016). Biomethane Recovery from Egeria densa in A Microbial Electrolysis Cell-Assisted Anaerobic Aystem: Performance and Stability Assessment. *Chemosphere, 149*, 121-129. doi:10.1016/j.chemosphere.2016.01.101

Appendix

Section 1 Diagrams of CellDesigner Models

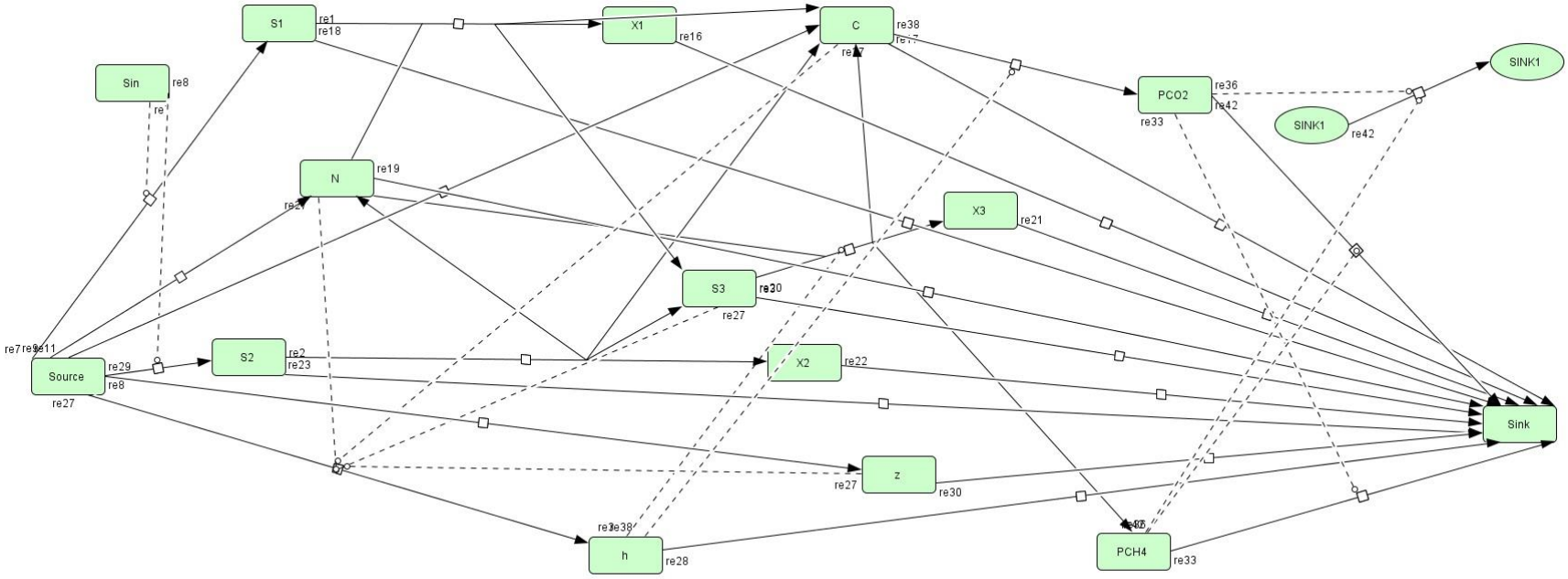

Figure 0.1– Structure of the adapted model built in CellDesigner based on the MAD model.

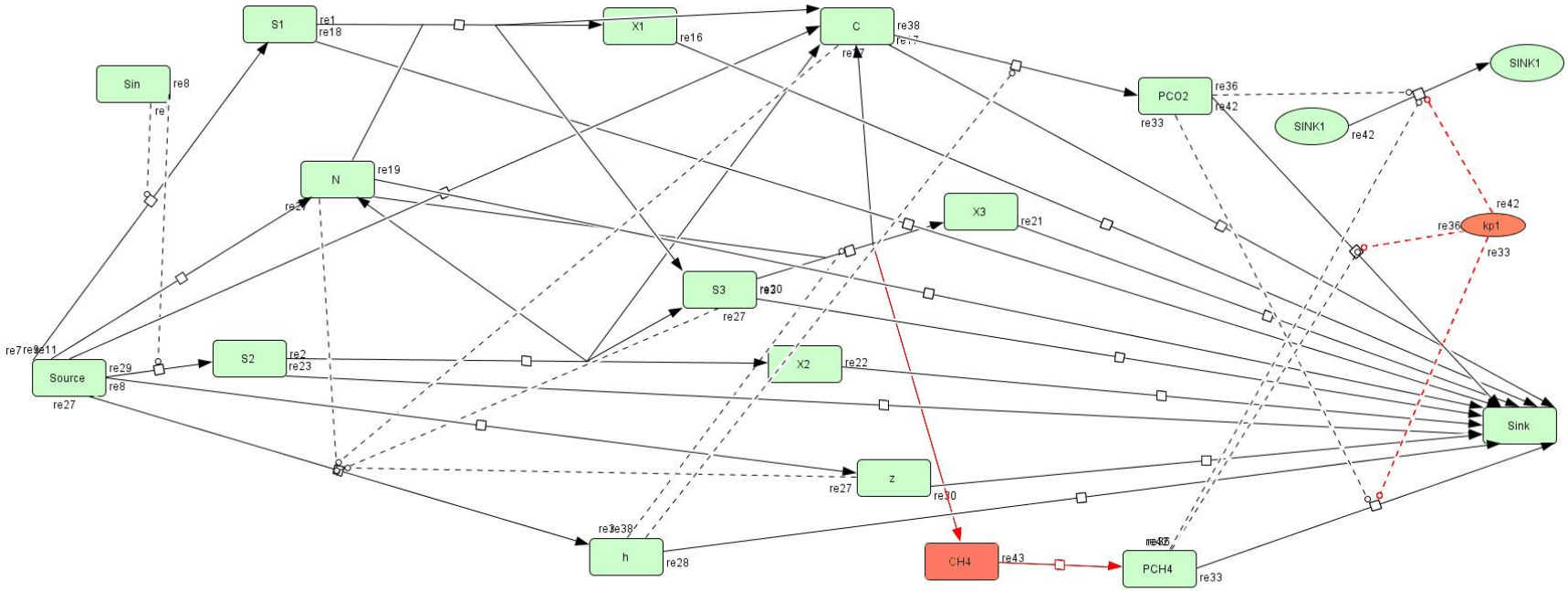

Figure 0.2– The modified model based on the experimental conditions of anaerobic digestion of microalgae performed in this study. The sections highlighted in red are the differences compared to the adapted model.

Section 2 Identifying the Biomass

DNA Extraction via PCR

The genomic DNA of the unidentified algae used in this project were extracted using AllPrep® PowerViral® DNA/RNA Kit (QIAGEN N.V., Netherlands) and following the manufacturer's protocol provided. The 18S rRNA sequence was amplified by PCR using five different pairs of primers, they are: 18S forward and reverse, Ca18S forward and reverse, Cr18S forward and reverse, EUK forward and reverse, and 18S/200S forward and reverse, all had the concentration of $10\ \mu mol/L$. The volume of the sample solutions for PCR reaction were 20 µL each, containing 10 µL 2x MyTaq™ Red Mix (includes DNA polymerase, buffer containing $MgCl_2$, dNTPs), 1 µL forward and reverse primers, 1 µL genomic DNA and 7 µL sterile distilled water. The PCR reaction was performed with an AB-2720, 96 well Thermal cycler (Applied Biosystem, UK), the reaction conditions were as follows: melting at 95°C for 1 minute, followed by 38 cycles of melting at 95°C for 15 seconds, annealing at 55°C for 15 seconds, elongation at 72°C for 45 seconds. The final step was elongation at 72°C for 5 minutes. The result of PCR reaction produced by each primer pair was determined by the visualisation as a single band on a 1% (w/v) agarose gel. The PCR products were then purified using QIAquick® Multiwell PCR Purification (QIAGEN N.V., Netherlands) using manufacturer's protocol. Then the purified PCR products were sequenced by GATC-Biotech.

Ribosomal RNA Sequencing and Phylogenetic Analysis

BLAST Program (Altschul, *et al*., 1997) was used to align the sequencing results of the algae samples from GATC-Biotech to the GenBank database by aligning with 18S-ITS nucleotide sequences to search for potential matches. This would give a list of algae species based on the similarity. Clustal Omega was then used to align the sequences of unidentified algae sample with multiple algae species with highest similarities simultaneously to produce a Multiple Sequence Alignment (MSA) diagram. Randomized Axelerated Maximum Likelihood (RAxML) (Stamatakis, 2006) was used to perform phylogenetic analysis through maximum likelihood method. Stamatakis, Hoover and Rougemont (2008) had shown that confidence in the tree architecture could be evaluated by performing 100 rapid bootstrap analysis. Sequences of closest match and unidentified algae sample were compared by Pairwise Sequence Alignment (PSA) using EMBOSS Needle and demonstrated in phylogenetic tree generated by FigTree to determine the identity of the unknown biomass sample and confirm whether there was an exact match. FigTree is a software that produces publication-ready figures of phylogenetic trees.

Identification of Biomass

The result for the DNA sequences of the unidentified algae by GATC-Biotech is demonstrated in Figure 0.3, where JP1 is the sequence of algae sample 1 and JP2 is the sequence of algae sample 2.

>JP1
TAANCCATGCATGTGCAAGTATGAACTAATTCAGATTGTGAAACTGCGAATGGCTCATTAAATCAGTTATAGTTT
GTTTGATGGTANTTACTACTCGGATAACCGTAGTAATTCTAGAGCTAATACGTGCAACAAACCCCGACTGCTGGA
AGGGATGCATTTATTAGATAAAAGGCCAATGCGGGCTTTGCTCGCTTCTCGGATGATACATGATAACTTGACGGA
TCGCACAGCCTTTGTGCTGGCGACGCATCATTCAAATTTCTGCCCTATCAACTTTCGATGGTAGGATATGGGCCT
ACCATGGTGGTGACGGGTGACGGAGAATTAGGGTTCGATTCCGGAGAGGGAGCCTGAGAAACGGCTACCACATCC
AAGGAAGGCAGCAGGCGCGCAAATTACCCAATCCTGACACGGGGAGGTAGTGACAATAAATAACAATACCGGGCT
CATCGAGTCTGGTAATTGGAATGAGTACAATCTAAATCCCTTAACGAGGATCCATTGGAGGGCAAGTCTGGTGCC
AGCAGCCGCGGTAATTCCAGCTCCAATAGCGTATATTTAAGTTGTTGCAGTTAAAAAGCTCGTAGTTGGACTTTG
GGTTGGGTCGACCGGTCCG

>JP2
GNNNCNNNGAATGGCTCATTAAATCAGTCATAGTTTGTTTGATGGTATTTACTACTCGGATAACCGTAGTAATTC
TAGAGCTAATACGTGCAACAAACCCCGACTGCTGGAAGGGATGCATTTATTAGATAAAAGGCCAATGCGGGCCTT
GCTCGCTTCTGGGATGATACATGATAACTCGACGGATCGCACAGCCTCTGTGCTGGCGACGCATCATTCAAATTT
CTGCCCTATCAACTTTCGATGGTAGGATATGGGCCTACCATGGTGGTGACGGGTGACGGAGAATTAGGGTTCGAT
TCCGGAGAGGGAGCCTGAGAAACGGCTACCACATCCAAGGAAGGCAGCAGGCGCGCAAATTACCCAATCCTGACA
CGGGGAGGTAGTGACAATAAATAACAATACCGCGCTCATCGAGTCTGGTAATTGGAATGAGTACAATCTAAATCC
CTTAACGAGGATCCATTGGAGGGCAAGTCTGGTGTCAGCAGCCGCGGTAATTCCAGCTCCAATAGCGTATATTTA
AGTTGTTGCAGTTAAAAAGCTCGTAGTTGGACTTTGGGTTGGGTCGACCGGTCCGCCTTTGGTGAGTACCGGTCG
CCTCGTCCCTTTTGCCGGTGACGTGCTCCTGGTCTTAATTGGCCGGGTCGTGCCCTCGGTGCTGTTACTTTGAAG
AAATTAGAGTGCTCAAAGCAAGCCCAAGCTCTGTATACATTAGCATGGGATAACACCACAGGATTTCGGTCCTAT
TGTGTTGGCCTTCGGGATCGGAGTAATGATTAAGAGGGACAGTCGTGGGCATTCGTATTTCATAGTCAGAGGTGA
AATTCTTGGATTTATGAAAGACGAACAACTGCGAAAGCATTTGCCAAGGATGTTTTCATTAATCAAGAACGAAAG
TTGGGGGCTCGAAGACGATCAGATACCGTCCTAGTCTCAA

Figure 0.3 – The DNA sequencing result of the unknown algae samples by GATC-Biotech. JP1 is sample 1 and JP2 is sample 2.

A section of the result of MSA for two samples of unidentified algae and some identified algae species with highest similarities can be seen in Figure 0.4.

Figure 0.4 – A section of the MSA for two algae samples and some identified algae with highest similarities produced by Clustal Omega. The hyphens '-' in the sequences are gaps added by the alignment software because some species have no nucleotides in those positions. The stars at the bottom indicate the nucleotides in that position of all aligned species is a 100% match.

The phylogenetic tree based on rRNA 18S and ITS nucleotide sequences illustrated in Figure 0.5 compares two samples of unidentified microalgae and some identified algae with highest similarity. The analysis did not identify the algae at species level because it was not available in the database. However, with bootstrap percentage values close to genera such as *Egeria densa* and *Elodea canadensis*, the tree indicated the unidentified algae belongs to *Hydrocharitaceae* family.

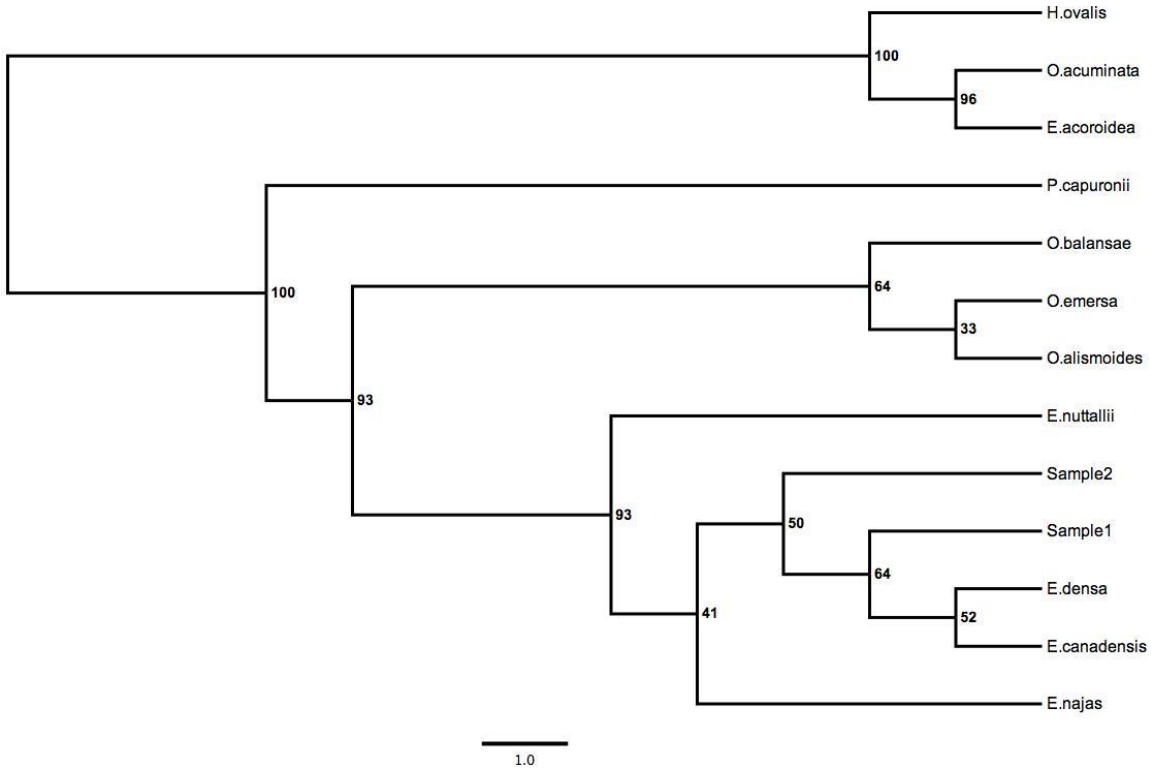

Figure 0.5 – The phylogenetic tree comparing two samples of the unknow biomass sequences with identified algae. The number to the right of the branches of each node is the bootstrap percentage value and indicates the confidence of each tree node position. The branch length scale bare at the bottom indicates evolutionary distance.

Figure 0.6 is the unidentified microalgae used in the laboratory-scale experiment at different magnifications. Figure 0.6 (a) is a photograph of the microalgae in a plastic tube. Figure 0.6 (b) and (c) are the micrographs of the microalgae at 12 times zoom and 500 times magnification respectively.

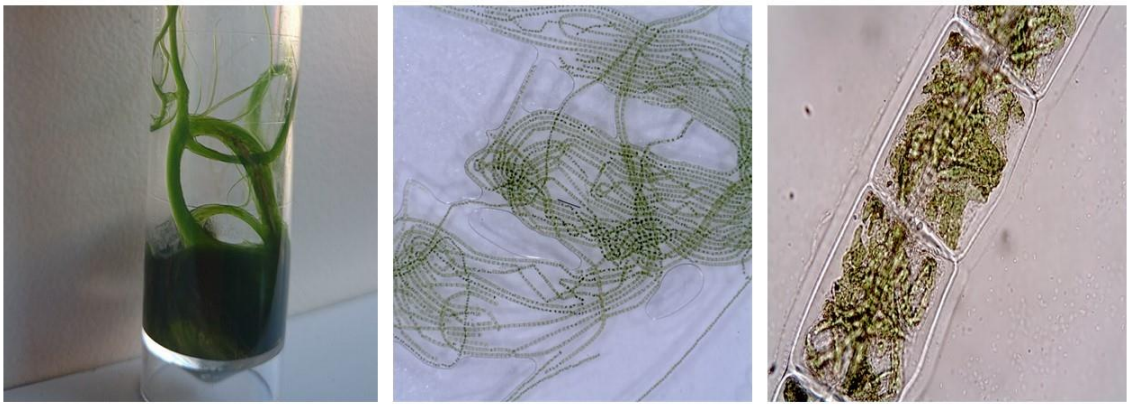

(a) (b) (c)

Figure 0.6 – Photos of the pondweed used in this project. (a) was a photo taken with a phone camera, (b) was a microscopic view at 12X magnification, (c) was a microscopic view at 500X magnification.

Discussion

The DNA of the unidentified algae species was sequenced by GATC-Biotech. Blast search was then performed to find out a list of algae species that would be potential matches. Although maximum likelihood approach was not able to identify the unknown algae at species level, it was sufficient to conclude that the pondweed belonged to the aquatic plant family Hydrocharitaceae and the closest matches were Egeria densa and Elodea canadensis. More information on the aquatic plant family Hydrocharitaceae can be found in literature by Chen *et al*., (2012), Cook and Urmi-König (1984) and Cook and Urmi-König (1985).

Previous studies have shown that Egeria densa as effective as substrate in biogas production. Watanabe, et al. (2017) reported that at 55°C the methane production rate was 220 ml per litre per day, which was double the amount at

37°C and 65°C. Another study by Zhen et al. (2016) reported an average methane yield of approximately 248.2 ± 21.0 ml per litre per day at 1.0 V, which was similar to that reported by Koyama, Yamamoto, Ishikawa, Ban and Toda (2014) at 287 ml per day per gram of VS.

It was shown that the aquatic plant used in this study has the potential to produce methane at 19.5 ml per day per gram of dry plant.